Nonlinear Force Field Resonator Tuning

Leveraging Nonlinear Force Spring Softening to Enhance MEMS Membrane Resonator Responsivity

A.J.G. Derks

Delft University of Technology

TU Delft

Nonlinear Force Field Resonator Tuning

Leveraging Nonlinear Force Spring Softening to Enhance MEMS Membrane Resonator Responsivity

by

A.J.G. Derks

Master Thesis

in partial fulfillment of the requirements for obtaining the degree of
Master of Science in Applied Physics at Delft University of Technology
to be defended publicly on Thursday 19th of June 2025 at 9:00 o'clock

Student number:	5836824
Supervisors:	Prof. dr. Richard Norte
	dr. ir. Ata Keşkekler
Project Duration:	October, 2024 - June, 2025
Faculty:	Faculty of Mechanical Engineering, Department of Precision and Microsystems Engineering, Delft
Thesis committee:	Prof. dr. Richard Norte
	Prof. dr. Gary Steele
	dr. ir. Ata Keşkekler

Cover: SEM image of the top surface of a high aspect membrane MEMS resonator with holes and a micro disc visible on the membrane, taken by M. Xu

TU Delft

Abstract

Microelectromechanical resonator sensors are crucial in the cutting-edge technologies used in our everyday communication, timekeeping and computing systems. Their extreme sensing capabilities make them ideal candidates for the innovation of future technologies. However, with our ever-growing desire for faster communication, more sensitive systems, and more advanced technologies comes the need for a new generation of resonator sensors. This next generation will have to be faster, more accurate, and just as cheap as their predecessors if they are to enable the rapid growth of our technological needs.

In this thesis, we investigate recently fabricated state-of-the-art extreme aspect ratio membrane resonators. The characteristics of extreme aspect ratio membrane resonator sensors are researched, and the effects of nonlinear forces on their operation are explored. Some of these nonlinear attractive forces, such as the Casimir effect, are common to the extreme dimensions of these resonators. Another common nonlinear attractive force in MEMS, the electrostatic force, and its effects on resonator operation and output are investigated as well. Analytical models are fashioned and a FEM model is produced and validated using experimental results, showing it reflects reality. FEM simulations show that for these extreme aspect ratio resonators, the nonlinear softening effect is solely responsible for the change in the eigenfrequency which proves to be able to boost the responsivity of these resonators by factors of hundreds to thousands. Models are investigated for both conductors and dielectric resonators with different geometries and different material parameters, which all show these results. Responsivities of $133.2\,\mathrm{kHz/kPa}$ and $1.6\,\mathrm{kHz/nm}$ are found, which exceed the state-of-the-art. The negative effects of nonlinear forces such as pull-in are considered, investigated, and models are produced which predict them to prevent device failure. Furthermore, the role of crucial resonator parameters is investigated to aid future research in leveraging this potential new technique of enhancing sensor capabilities.

Acknowledgments

In June of 2022, I had just finished my bachelor technische natuurkunde (engineering physics) at the the Hague University of Applied Sciences (THUAS), and I found myself at a crossroads. The decision between working at a company or pursuing my original dream of obtaining a university degree in the field of physics was a tough one to make. I had attempted to obtain such a degree in physics in Leiden a few years earlier, and not succeeded. I had no guarantee of success the second time around, but I decided at that time to follow my gut feeling and to pursue what I wanted most of all. I did this even though I knew that the pre-master's and the master's applied physics that would follow would be more difficult than anything I had attempted before academically. The three years at university that followed were fun, inspiring, rewarding, and eye-opening, but also beyond demanding in terms of the amount of study work that I had to perform to succeed. I can say with confidence that it is the most difficult thing I have undertaken so far in my life.

With this thesis, I have now finally reached the summit of the mountain I set out to climb nearly three years ago, and I look back on it with pride, happiness, but also with immense gratitude. First and foremost, I would like to thank the loved ones close to me. My family, Rob, Ellen and Hans, and my girlfriend Irina, for their unconditional support, their love, their advice, and their guidance during these intense years. Having people close to you to always rely on who are invariably steadfast in their belief that you have it in you, despite your disbeliefs and doubts, has been crucial to my motivation during these years. You assisted me every step of the way, and I cannot thank you enough. I could never have done it without you.

I would also like to thank my buddy Shahrukh from the THUAS, who, in the same year as I, dared the jump from the THUAS to university after getting his bachelor's. We did not know each other well at the time, but we quickly grew close. We have worked together on countless projects and homework sets at university, and I look back fondly on them. I especially remember things such as the time we decided to take on the entire course of electrodynamics in 3 weeks instead of the allocated 8 weeks due to a lack of time. We studied online together for entire days every day and succeeded with flying colours. I am grateful for your patience (I ask a lot of questions when I am confused), your friendship, and everything you taught me along the way. It seemed almost meant to be that we ended up at the same lab for our master's thesis, and I am confident that you are able to finish your project soon, despite the cleanroom setbacks you encountered.

Finally, I wish to express my gratitude to Richard and Ata for their roles in supervising my thesis project. Thank you, Richard, for your patience, your guidance, and your inspiration during this project. Meetings with you always managed to make me excited for the research I was doing, even though I sometimes felt completely different beforehand. Your knowledge, advice and ability to inspire me have been essential for this project. Thank you, Ata, for your guidance and your wisdom during this project. Your cool, calm, and almost laid-back style of supervising managed to help me to separate what was important in my research and what was not, something I often struggled with. You aided me immensely in the mathematical side of this thesis, I owe you many thanks for that.

A.J.G. Derks
Delft, June 2025

Contents

1 Introduction

Resonance for Beginners

The resonance frequency of an object is a well-defined frequency at which the object oscillates and is determined by a variety of factors such as the object's size, weight, tension and more. An oscillation is the transfer of one type of energy to another, but at the resonance frequency, this energy transfer is optimal. Because of this, the object vibrates with a much larger amplitude than it does otherwise. Other frequencies dissipate quickly and therefore affect the object or system much less. Resonance is a phenomenon which occurs in every object (even you!). A good example of this is the well-known trick of a talented singer breaking a wineglass with their voice. Anybody who has seen such a performance before will tell you that it is not about shouting the loudest, but rather, to sing at a very specific tone, or frequency. The singer applies a force to the glass by moving their vocal cords, which move the air at a certain frequency, which in turn exerts a force on the glass. In the beginning, the singer sings at frequencies which are not the resonance frequency of the wineglass. The force of the vibrating air makes the glass only move a tiny bit. The glass is not impressed as the movement is not even close enough to get it to break. However, when the sound vibrates at exactly the resonance frequency of the wineglass, the situation changes. The air now pushes at exactly the frequency at which the glass transfers the energy much more efficiently than before. The more efficient energy transfer makes the glass swing in large amplitudes back and forth, and the glass suddenly breaks.

Resonators

Resonance can be responsible for breaking objects when they have not been adequately accounted for. However, one can also leverage the fact that the amplitude of oscillation increases and use it to make sensors. These types of devices are made specifically to vibrate at their resonance frequency and are called resonators. Resonators are devices that we use every day without realising it. From the digital clocks ticking on our walls [1], to the exhaust pipes mounted under our cars which prevent the loud engine sounds from disturbing quiet neighbourhoods [2], to the musical instruments that fill the music we listen to, resonators are a part of everyday life.

Resonators play a big role in current electronics and nanotechnology [3]. As a matter of fact, you currently have a resonator in your phone which acts as a microphone [4]. These resonators are more broadly known as microelectromechanical systems (MEMS) which also have applications in energy harvesting [5], communication technologies [6], fingerprint sensors [7], accelerometers which one can use, for example, for gesture recognition [8] and even biosensing [9].

MEMS resonators are tiny structures which vibrate mechanically at very high frequencies. They are an exciting area of research as they boast extremely high resonance frequency throughput [10] and sensitivities [11], which makes them ideal sensors in many areas of science as previously mentioned. With improving fabrication techniques, it is possible these days to create resonator structures with very high aspect ratios, such as 2-dimensional membrane resonators at a very minimal scale. These resonators consist of extremely thin films suspended over wide cavities very close to the cavity bottom. With these ever-shrinking sizes and increasing aspect ratios come new challenges and new force regimes which one has to keep in mind when designing, fabricating and using these devices. These regimes do not offer only negative influences, however, and in this thesis, we will explore leveraging them to our advantage to improve resonator devices and investigate the possibilities of the next generation of MEMS sensors.

Goal and Outline of this Thesis

In this thesis, we will investigate the effects of nonlinear attractive force fields on 2 two-dimensional mechanical membrane resonators with extreme aspect ratios. Membrane resonators are the subject of much research as they offer promising new abilities to future technologies, which often coincide with nonlinear forces such as electrostatics. These nonlinear force fields occur either naturally (Casimir effect) or by design (electrostatics). Some, like electrostatics, are established techniques in MEMS actuation and detection. We will determine how these nonlinear forces have a dominant effect on their output and how they influence their operation. By attempting to model these high aspect ratio resonators within nonlinear force regimes, we hope to be able to predict, prevent, and possibly also leverage the phenomena that we encounter. We hope to provide a solid analytical and FEM simulation basis that deepens understanding of the nonlinear force effects on these extreme aspect ratio membrane resonators. We will try to assess not only the positives but also the negative aspects of these nonlinear forces. The goal is to hopefully provide future research with the knowledge on what to avoid and how to exploit the exciting opportunities that this new generation of sensors offers.

This thesis consists of five chapters, with this introduction being the first one. The second chapter will cover the necessary theory needed to understand resonators in general, after which we will cover two-dimensional membrane resonators specifically in the theory. Chapter three, the setup, presents the fabrication and operation of these membranes and introduces the experimental membrane off of which we base our FEM models. It also provides the FEM model central to our research and its validation using experimental values. We will use the FEM models extensively in the fourth chapter called the results. There, we explore a variety of sensor, force, and parameter variations and show the sensor improvements as well as new dangers that one can encounter whilst leveraging nonlinear force fields with high aspect membrane resonator sensors. We briefly give an example of a possibly improved microphone design using our previous results. We end in chapter five to share our conclusions and discuss their relevance.

2
Theory

For us to understand what makes mechanical resonators so popular in science and what makes them interesting in conjunction with nonlinear forces, we need to get to know them first. We will start with a general introduction to mechanical resonator basics and the different types of resonators that are used in science. We will cover the nonlinear forces and effects that are present in the systems of our interest and explain their influence on the resonators. Along the way, we will explore possible avenues for exploiting these nonlinear effects to improve our resonators. This is no comprehensive review on resonators, however or nonlinear resonator dynamics, as this would be too elaborate. For bigger pictures on resonators and nonlinear resonator dynamics, we refer readers to [12], [13], and [14]. Let us now start with the very definition of a mechanical resonator.

2.1. Mechanical Resonator Basics

Definition of a Resonator

Mechanical resonators are structures that oscillate at resonance, usually due to a driving force. The resonance frequency is one of the eigenfrequencies of the oscillating mechanical structure. This eigenfrequency is the specific frequency at which the exchange between the kinetic energy and the potential energy is optimal. During oscillation, the resonator continuously converts its movement (kinetic energy) to structural deformation (potential energy). This process is shown schematically in figure 2.1.

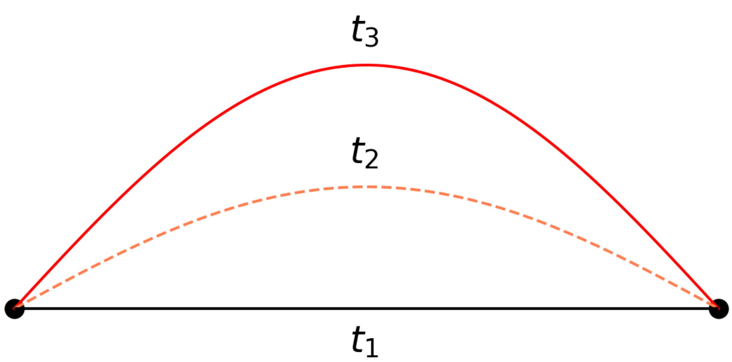

Figure 2.1: Schematic side view showing the principle of oscillating motion of a resonator. The resonator is clamped on both sides. At $t = t_1$, it is at rest, but directly after, i.e. $t > t_1$, it gets jolted upwards and the kinetic energy given to it gets converted to potential energy. At $t = t_3$, the kinetic energy is fully converted to potential energy or structural deformation. For $t > t_3$, the potential energy will convert back to kinetic energy, which will reach its maximum at the position the resonator occupied at $t = t_1$, after which it will continue downwards and repeat the oscillation motion forever.

The figure shows the simplified basics of oscillation for a doubly clamped resonator. The resonator is jolted upwards directly after $t = t_1$, at which the kinetic energy is at a maximum. It converts this energy to potential energy, and at $t = t_2$, it has converted a considerable amount of it. At $t = t_3$, the kinetic energy is fully converted into potential energy, after which the conversion is followed in reverse until the resonator reaches the position it had at $t = t_1$, at which all of the energy is kinetic energy. The resonator follows the same process but downwards until the position at $t = t_1$ is reached, after which the cycle begins anew. This continues forever if the resonator does not lose any energy.

2.1.1. Undamped Resonator

A mechanical resonator can best be modelled by a simple mass-spring system, in which a mass m moves periodically whilst attached to a spring with a linear spring constant k. The spring constant is responsible for the restoring force $F = -kx$ that flips the direction of motion periodically. The equation of motion for this system is a simple one and one that is well known:

$$m\frac{\mathrm{d}^2x}{\mathrm{d}t^2} + kx = 0. \tag{2.1}$$

The solution to this equation is found with a complex exponential as an ansatz and is a combination of sines and cosines of the form $A\sin(\omega_0 t) + B\cos(\omega_0 t)$. Here, A and B can be determined with the boundary conditions of the particular system, and ω_0 is the natural frequency or the eigenfrequency. The (angular) eigenfrequency is defined as

$$\omega_0 = \sqrt{\frac{k}{m}}. \tag{2.2}$$

2.1.2. Damped Resonator

The system shown above is a very idealised version of reality, as in this system, no energy is allowed to leak out. This would mean that our resonator would be able to resonate until the end of time, which is not the case for real resonators. In reality, a system always has some form of energy loss via damping, usually consisting of a variety of effects. These can be viscous damping due to air or liquids, heating, friction, radiation or even electronic resistance. This damping can be modelled by a linear damping ratio ζ and introduced into our equation of motion

$$m\frac{\mathrm{d}^2x}{\mathrm{d}t^2} + \zeta\frac{\mathrm{d}x}{\mathrm{d}t} + kx = 0. \tag{2.3}$$

A schematic of an undamped and a damped oscillator is shown in figure 2.2.

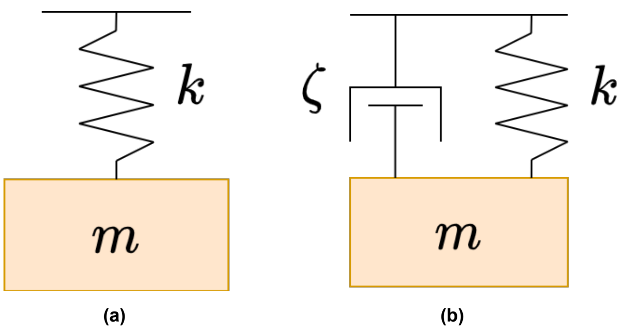

Figure 2.2: Schematics of two types of oscillators. (a) Undamped oscillator with mass m and a spring constant k. (b) Damped oscillator with the damping symbolised as a dashpot with a damping ratio ζ.

To find the solutions and eigenfrequency of this equation, we use the same ansatz as before, i.e. $e^{-\lambda t}$ with λ a complex constant. Filling in the ansatz gives us

$$m\lambda^2 + \zeta\lambda + k = 0. \tag{2.4}$$

The roots of this equation are found as

$$\lambda = \frac{-\zeta \pm \sqrt{\zeta^2 - 4mk}}{2m}. \tag{2.5}$$

The oscillation is influenced by this root depending on its sign and value. If the square root is smaller than 0, then the system is underdamped. If it is equal to 0, we call it critically damped, and if it is bigger than 0, it is called overdamped. In our case, i.e. for resonators, we are interested in the case where the oscillator is underdamped, as damping in resonators is seen as a negative effect that is to be prohibited. We therefore wish our resonators to be as underdamped as possible for them to retain their oscillation as long as possible. The solution of an underdamped harmonic oscillator is given by

$$Ae^{-\frac{\zeta}{2m}t}\sin(\omega_d t) + Be^{-\frac{\zeta}{2m}t}\cos(\omega_d t). \tag{2.6}$$

With $\omega_d = \sqrt{\frac{k}{m} - \frac{\zeta^2}{4m^2}}$. This is a more realistic representation of real-life resonators, which always have some form of damping which lessens the oscillation amplitude according to an exponential decay. A comparison between an undamped and an underdamped oscillation time versus amplitude characteristic is shown in figure 2.3.

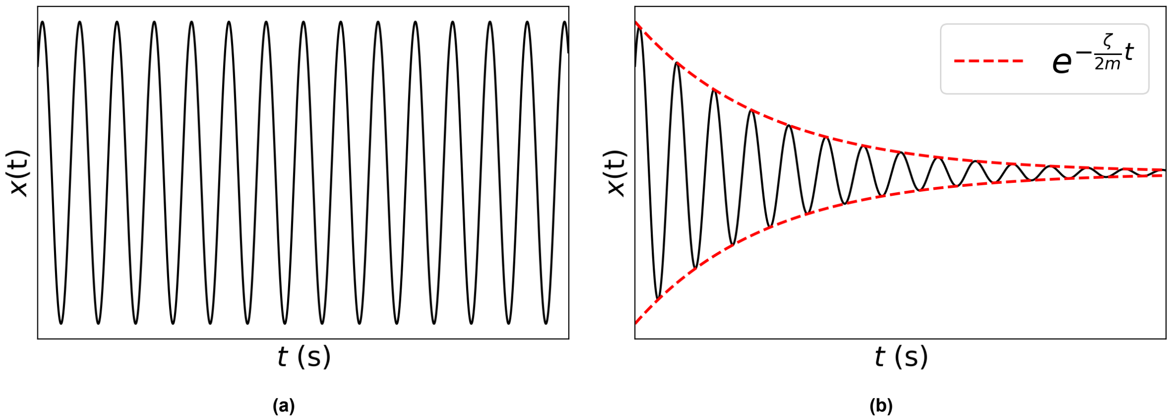

Figure 2.3: Time characteristics of two harmonic oscillators. (a) An undamped harmonic oscillator signal. The oscillation will go on forever as the energy is conserved. (b) An underdamped harmonic oscillator signal. The oscillation slowly dies out, the speed of which depends on the damping ratio ζ. The decrease in the amplitude follows the exponential decay function.

2.1.3. Driven Damped Resonators

To use these resonators as sensors, we need a parameter to measure as a response to an input. This parameter, as the name resonator implies, is the resonance frequency, which for MEMS resonators can be extremely sensitive to outside influences such as forces or adjusted mass. To achieve a measurable output, one needs to drive these resonators. This means introducing the resonator to an external force, after which the response of the resonator can be read out. Often this driving force is a harmonic one itself, the equation of motion then becomes

$$m\frac{\mathrm{d}^2x}{\mathrm{d}t^2} + \zeta\frac{\mathrm{d}x}{\mathrm{d}t} + kx = F_0\sin(\omega_d t). \tag{2.7}$$

The response of the resonator depends on the frequency of the driving force, and thus, the response can be plotted in the frequency spectrum. The magnitude of the response of the resonator to a certain drive frequency is given by [15]

$$X(\omega) = \frac{F_0/m}{\sqrt{(\omega_0^2 - \omega_d^2)^2 + \frac{\zeta^2\omega_d^2}{m^2}}}. \tag{2.8}$$

The magnitude of the response of three resonators with varying damping ratios is shown in figure 2.4.

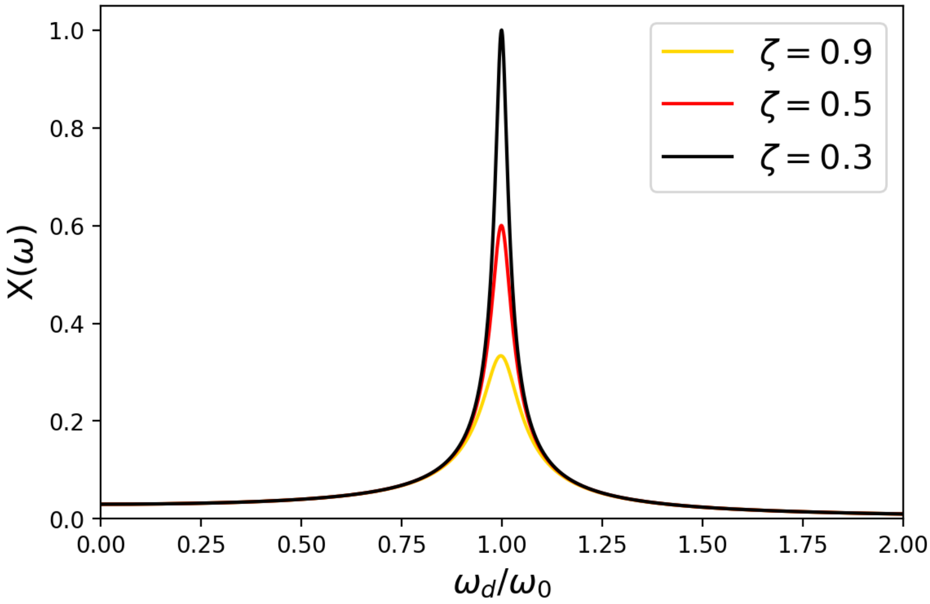

Figure 2.4: Three magnitude response characteristics of identical resonators with varying damping ratios.

The figure shows a sharp peak when the resonator is driven at the resonance frequency as it now converts the energy given by the driving force much more efficiently than before. The effect of the value of the damping is seen in the sharpness and width of the peak at the resonance frequency. If the resonator is now subjected to another effect, such as additional strain by a pressure, or a change in mass due to a particle landing on the surface, then the resonator stiffness k will change and via 2.2 the resonance too. The resonance peak shifts to the left or right, and so the resonance frequency is an output parameter that can be directly linked to the input force.

2.1.4. Quality Factor

What can immediately be noticed from figure 2.4 is the influence of the damping ratio on the sharpness and width of the response peak. This effect of the damping ratio is profound, but we will depart from using it and express it in another parameter. One that is used extensively in resonator engineering, the quality factor Q [12]. The relation between the two reads

$$Q = \frac{1}{2\zeta}. \tag{2.9}$$

This, however, is not the only definition of the quality factor. The most commonly used definition of the quality factor is the one that relates to the amount of energy loss in the system per cycle. This means that a resonator with a high quality factor is less damped and loses its oscillation less fast than one with a lower Q. The Q factor is thus a useful parameter when comparing different resonators. The definition is written as

$$Q = 2\pi \frac{\text{Total energy stored}}{\text{Energy lost per cycle}}. \tag{2.10}$$

We will give two more definitions for the quality factor. The first has connections to figure 2.3 in the fact that it is defined as a function of the so-called ringdown time τ_R:

$$Q = \frac{1}{2}\omega_0 \tau_R. \tag{2.11}$$

τ_R is an important parameter in resonator design. It shows how fast a resonator loses its magnitude, or energy, which is an undesired effect. It can be determined by following the negative trend shown in figure 2.3b. The ringdown time can then be extracted by fitting the exponential decay in the magnitude with $e^{-\tau_R/t}$ [16].

The final definition is more closely related to figure 2.4, as the quality factor can be expressed as the ratio of the so-called full width at half maximum (FWHM), being the width of the frequency peak at half the maximum magnitude, and its resonance frequency :

$$Q = \frac{\omega_0}{\Delta\omega}. \tag{2.12}$$

One might find it surprising to learn that the quality factor can be expressed by so many different definitions. It should be noted that these definitions for Q, even though they are used intermixed throughout resonator engineering, are not always the same in value numerically. They converge to one another when the quality factor of the resonator is high, i.e. the damping ratio $\zeta << 1$. In modern resonators, quality factors can be as high as a million, with the state of the art reaching tens of billions [17]. With the high quality factors being no rare occurrence, it is then no problem to use different definitions for the quality factor.

2.1.5. Types of Resonators

Resonators come in a large variety of different shapes and forms. From 1D resonators such as beams, cantilevers or bridges, to 2D resonators such as rectangular or circular plates and membranes, to even 3D bulk resonators of various shapes [18–24]. Covering this broad spectrum is not the goal of this section, rather, we provide a simple classification of various MEMS resonators based on their mode type shown by Abdolvand et. al [25] shown in table 2.1. Note that this is by no means a comprehensive classification.

Table 2.1: Simple classification of MEMS resonators by their mode type shown by Abdolvand et. al [25].

Type	Working Principle	Example
Flexural Mode	Transverse elastic deformation of a structure with at most 2 relevant dimensions.	Beam, membrane
Bulk Mode	Deformation of a three-dimensional structure by expansion and contraction using LE and WE modes.	Stiff beam, plate
Shear Mode	Three dimensional material with shear modes. The stiffness is determined by the shear modulus instead of Young's modulus.	Elastic anisotropic material
Torsional Mode	Periodic twisting motion	Paddle resonator
Coupled Mode	Multiple resonators linked by structures such as beams, influencing their resonance modes	Mechanically coupled plates

In this thesis, we will concern ourselves with a type of two-dimensional flexural mode resonators, membranes, which are clamped on all sides.

Plates and Membranes

An important difference between two types of structures, plates and membranes, has to be clarified. Plates and membranes are very similar 2D structures visually and are used extensively throughout MEMS engineering. They show the same form factor, which is why it is easy to mix them up. They are inherently different, however, due to the way they handle transverse loads. Plates handle transverse loads by bending, a large load will increase the bending stiffness as the plate bends further. Membranes sustain transverse loads by in-plane stresses. The larger the load, the larger the in-plane stress in the membrane. A test proposed by Dolleman [26] determines if a circular resonator is a plate or a membrane:

$$R^2 \frac{n_0}{D} < 1 \qquad \text{Plate} \tag{2.13}$$

$$R^2 \frac{n_0}{D} > 10^4 \qquad \text{Membrane} \tag{2.14}$$

with n_0 the in plane tension, R the radius and $D = \frac{Eh^3}{12(1-\nu^2)}$ the flexural rigidity of the resonator, with E the Young's modulus, h the thickness and ν Poisson's constant. This thesis concerns membrane resonators of the circular and square kind, with the main analysis based on an experimental setup which is later described in detail. We will then use this test to confirm that our resonators are indeed membranes according to Dolleman.

2.2. Vibration of a Mechanical Membrane Resonator

2.2.1. Clamped Circular Membrane

Having covered the basics of mechanical resonators, now it is time to dive deeper into their singularly important aspect, their oscillation at resonance. As stated before, the resonance frequency of a resonating object is the frequency at which the energy transfer is optimal between the kinetic energy and the potential energy stored as mechanical deformation. We will now derive the resonance frequencies and the associated eigenmodes of a clamped circular membrane and show what they look like. To that end, we will first find their modeshapes. We will keep close to the derivations shown in Haberman [27] and Rao [28].

We start with the 2D wave equation in which U is our displacement function:

$$\frac{\mathrm{d}^2 U}{\mathrm{d}t^2} = c^2 \nabla^2 U. \tag{2.15}$$

With c being the wave velocity in the medium and the Laplacian in polar coordinates given as

$$\nabla^2 = \frac{1}{r}\frac{\partial^2}{\partial r^2} + \frac{1}{r}\frac{\partial}{\partial r} + \frac{1}{r^2}\frac{\partial^2}{\partial \theta^2}, \tag{2.16}$$

We then assume that the solution to our 2D wave equation can be split up into independent parts and use the method of separation of variables. We thus define our displacement function $U(r,\theta)$ as

$$U(r,\theta,t) = \varphi(r)\Theta(\theta)T(t), \tag{2.17}$$

with r the radial coordinate, θ the angular coordinate, and t the time in seconds. We can then enter 2.17 into 2.15, losing the function dependent variables for brevity, we find

$$\varphi\Theta\frac{\mathrm{d}^2 T}{\mathrm{d}t^2} = c^2\left(\Theta T\frac{\mathrm{d}^2\varphi}{\mathrm{d}r^2} + \frac{1}{r}\Theta T\frac{\mathrm{d}\varphi}{\mathrm{d}r} + \frac{1}{r^2}\varphi T\frac{\mathrm{d}^2\Theta}{\mathrm{d}\theta^2}\right). \tag{2.18}$$

We divide the entirety by $c^2\varphi(r)\Theta(\theta)T(t)$ to clean up the equation. We now have

$$\frac{1}{c^2 T}\frac{\mathrm{d}^2 T}{\mathrm{d}t^2} = \frac{1}{\varphi}\frac{\mathrm{d}^2\varphi}{\mathrm{d}r^2} + \frac{1}{r\varphi}\frac{\mathrm{d}\varphi}{\mathrm{d}r} + \frac{1}{r^2\Theta}\frac{\mathrm{d}^2\Theta}{\mathrm{d}\theta^2}. \tag{2.19}$$

If we pay close attention to 2.19, we can see that both sides are completely independent of each other; we can therefore assume that both sides are equal to a constant, which we will define as $-\lambda^2$. We can now split up equation 2.19 and rewrite it into two separate equations

$$\frac{\mathrm{d}^2 T}{\mathrm{d}t^2} + c^2\lambda^2 T = 0, \tag{2.20}$$

$$\frac{1}{\varphi}\left(r^2\frac{\mathrm{d}^2\varphi}{\mathrm{d}r^2} + r\frac{\mathrm{d}\varphi}{\mathrm{d}r}\right) + \lambda^2 r^2 = -\frac{1}{r^2\Theta}\frac{\mathrm{d}^2\Theta}{\mathrm{d}\theta^2}. \tag{2.21}$$

We will repeat the same trick as just performed on equation 2.19 on 2.21, as we note that in equation 2.21, again, both sides are independent of each other. We use the separation variable κ^2 and write

$$\frac{\mathrm{d}^2\Theta}{\mathrm{d}\theta^2} + \kappa^2\Theta = 0, \tag{2.22}$$

$$\frac{\mathrm{d}^2\varphi}{\mathrm{d}r^2} + \frac{1}{r}\frac{\mathrm{d}\varphi}{\mathrm{d}r} + \left(\lambda^2 - \frac{\kappa^2}{r^2}\right)\varphi = 0. \tag{2.23}$$

To obtain a harmonic solution with a periodicity of 2π as a function of θ, κ should be defined as an integer, i.e. $0, 1, 2...$. We may now note that equations 2.20 and 2.22 are of the same form as equation 2.1 for an undamped harmonic oscillator, which was solved with a simple exponential function as an ansatz. The same ansatz delivers us the following solutions

$$T(t) = A\sin(\lambda t) + B\cos(\lambda t), \tag{2.24}$$

$$\Theta(\theta) = C\sin(\kappa\theta) + D\cos(\kappa\theta). \qquad \kappa = 0, 1, 2... \tag{2.25}$$

where A, B, C and D are scalars to be determined using boundary conditions. Now, if we rewrite equation 2.23 to the following form

$$r^2\frac{\mathrm{d}^2\varphi}{\mathrm{d}r^2} + r\frac{\mathrm{d}\varphi}{\mathrm{d}r} + \left(\lambda^2 r^2 - \kappa^2\right)\varphi = 0, \tag{2.26}$$

we don't seem to gain much of an advantage. However, we are in luck; the equation would be tough to solve on our own, but this has already been done for us. Equation 2.26 is a famous equation known as the Bessel equation of order κ with parameter λ. The solutions to this equation are given by

$$\varphi(r) = \alpha J_\kappa(\lambda r) + \beta Y_\kappa(\lambda r), \tag{2.27}$$

In which J and Y are the so-called Bessel functions of the first and second kind, respectively. One can determine α and β by using the boundary conditions of the problem at hand. We can already note β to be equal to 0 as the Bessel function of the second kind Y diverges at the middle of our membrane, i.e. $r = 0$. We are left with

$$\varphi(r) = J_\kappa(\lambda r). \tag{2.28}$$

Now, at $r = R$, meaning at the edge of our membrane, we have the boundary condition that the displacement should be 0, as it is a clamped membrane. So

$$\varphi(r) = J_\kappa(\gamma_{\kappa,n}) = 0, \tag{2.29}$$

in which we defined $\gamma_{\kappa,n} = \lambda r$ as is customary when dealing with Bessel equations. The number of solutions to 2.29 is infinite, and the values of $\gamma_{\kappa,n}$ for which this occurs, also known as the Bessel roots, have been studied for more than 100 years. For every solution belonging to an integer value of κ, an infinite number of discrete roots labeled n can be found [29]:

$\kappa = 0 \quad \& \quad J_0(\lambda r) = 0 :$ $\quad \gamma_{0,n} = 2.4048, \quad 5.5201, \quad 8.6537, \quad 11.7915, ...$

$\kappa = 1 \quad \& \quad J_1(\lambda r) = 0 :$ $\quad \gamma_{1,n} = 3.8317, \quad 7.0156, \quad 10.1735, \quad 13.3237, ...$

$\kappa = 2 \quad \& \quad J_2(\lambda r) = 0 :$ $\quad \gamma_{2,n} = 5.1356, \quad 8.4172, \quad 11.6198, \quad 14.7960, ...$

$\kappa = 3 \quad \& \quad J_3(\lambda r) = 0 :$ $\quad \gamma_{3,n} = 6.3802, \quad 9.7610, \quad 13.0152, \quad 16.2235, ...$

$\kappa = 4 \quad \& \quad J_4(\lambda r) = 0 :$ $\quad \gamma_{4,n} = 7.5883, \quad 11.0647, \quad 14.3725, \quad 17.6160, ...$

2.2.2. Eigenfrequencies of a Circular Membrane

To find an expression for the eigenfrequencies belonging to the Bessel roots, we shall make two small adjustments to our previous analysis. Firstly, the definition for c given in [28] is

$$c = \sqrt{\frac{P}{\rho}}, \tag{2.30}$$

with P the applied transverse pressure on the membrane and ρ the density. We will rewrite this to

$$\sqrt{\frac{P}{\rho}} = \sqrt{\frac{n_0}{h\rho}}. \tag{2.31}$$

With h the membrane thickness, and n_0 the 2D tension ($n0 = \sigma \cdot h$ with σ the material stress) . Secondly, we will use a harmonic function, such as $\sin(\omega t)$ for $T(t)$. This now means that equation 2.19 transforms to

$$\frac{1}{\varphi}\frac{\mathrm{d}^2\varphi}{\mathrm{d}r^2} + \frac{1}{r\varphi}\frac{\mathrm{d}\varphi}{\mathrm{d}r} + \frac{1}{r^2\Theta}\frac{\mathrm{d}^2\Theta}{\mathrm{d}\theta^2} + \frac{\rho h}{n_0}\omega^2 = 0. \tag{2.32}$$

We now see that our constant λ^2 is equal to $\frac{\rho h}{n_0}\omega^2$. If we now use the previously defined $\gamma_{\kappa,n}$ and rewrite for the eigenfrequencies of the membrane, we will arrive at

$$\omega_{\kappa,n} = \frac{\gamma_{\kappa,n}}{R}\sqrt{\frac{n_0}{\rho h}}, \tag{2.33}$$

where we used $r = R$, the radius of the membrane. The eigenfrequencies can be found for any clamped circular membrane using the values given for $\gamma_{\kappa,n}$ above.

2.2.3. Circular Eigenmodes

Finally, the general solution of the displacement function $U(r, \theta, t)$ is usually expressed using two functions labeled $W^{(1)}_{\kappa,n}$ and $W^{(2)}_{\kappa,n}$. For the sake of brevity, we will state them as given in [28] here instead of showing their full derivation

$$W^{(1)}_{\kappa,n}(r, \theta) = C_{1\kappa,n} J_\kappa(\lambda_{\kappa,n} r)\cos(\kappa\theta), \tag{2.34}$$

$$W^{(2)}_{\kappa,n}(r, \theta) = C_{2\kappa,n} J_\kappa(\lambda_{\kappa,n} r)\sin(\kappa\theta), \tag{2.35}$$

with $C_{1\kappa,n}$ and $C_{2\kappa,n}$ scalars. We include these two functions here because they have a unique and intriguing feature that will help to explain the behaviour of the membrane eigenmodes that we will demonstrate soon. These two functions only differ by a (potentially) different scalar, but more importantly, a phase of $\pi/2$. This means that for any value of κ and any n for $\kappa \neq 0$, the functions will have the same shape but an angular rotation of 90° and thus, a degenerate eigenfrequency. When plotting the eigenmodes, we will find infinite pairs of modes with degenerate eigenfrequencies that oscillate in space with a 90° rotational shift from each other.

The first ten eigenmodes of a clamped circular membrane are shown in figure 2.5 with their resonance frequencies:

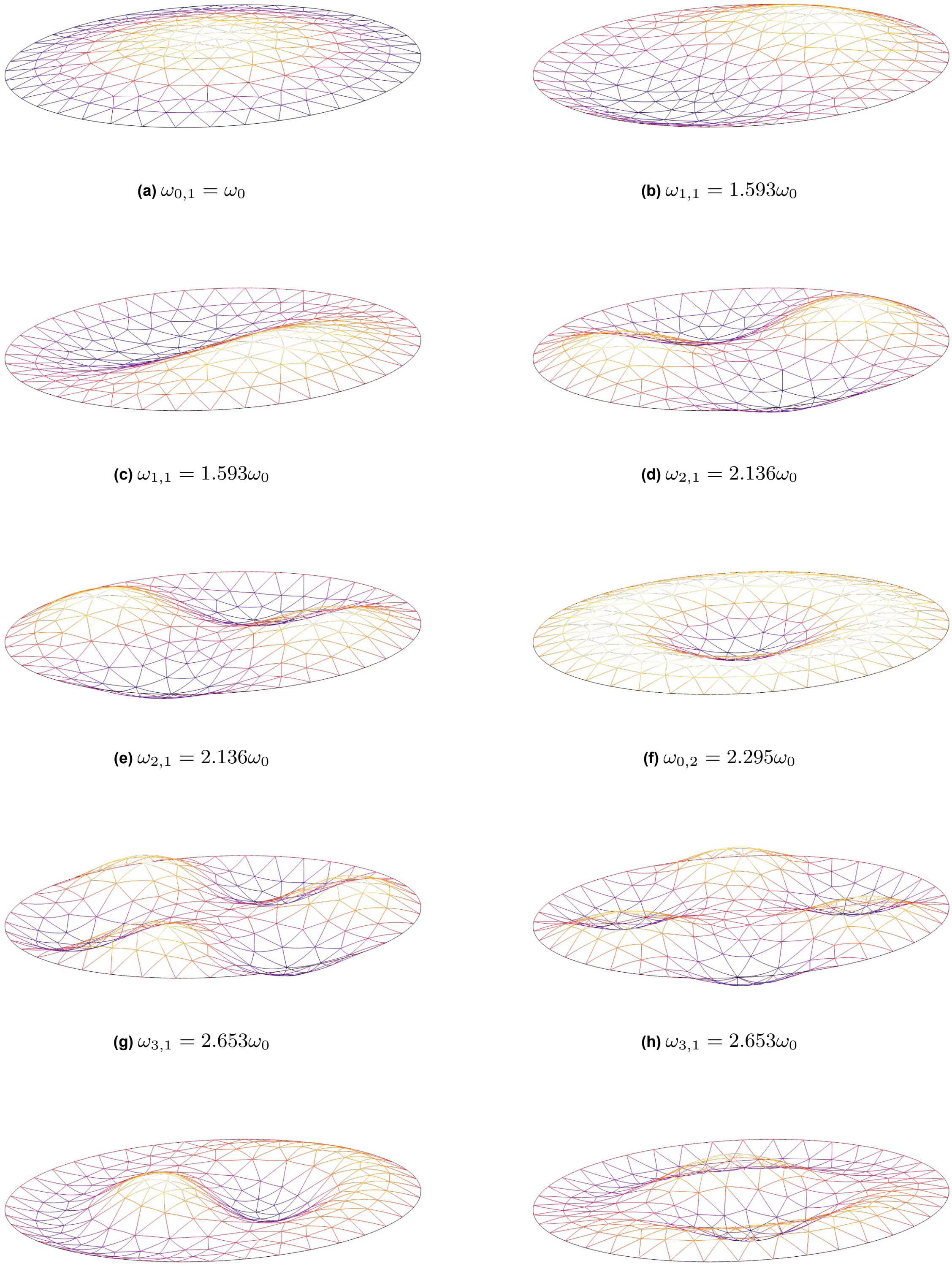

(a) $\omega_{0,1} = \omega_0$

(b) $\omega_{1,1} = 1.593\omega_0$

(c) $\omega_{1,1} = 1.593\omega_0$

(d) $\omega_{2,1} = 2.136\omega_0$

(e) $\omega_{2,1} = 2.136\omega_0$

(f) $\omega_{0,2} = 2.295\omega_0$

(g) $\omega_{3,1} = 2.653\omega_0$

(h) $\omega_{3,1} = 2.653\omega_0$

(i) $\omega_{1,2} = 2.917\omega_0$

(j) $\omega_{1,2} = 2.917\omega_0$

Figure 2.5: The modeshapes of the first ten eigenmodes of a clamped circular membrane. The degenerate modes have been included. The associated eigenfrequencies are given per mode.

2.2.4. Clamped Square Membrane

Having found the circular modeshapes, we will now turn our attention to clamped square membranes. We will show how the modeshapes are found for square membranes, which follows much of the same analysis as before, albeit in the Cartesian coordinate system rather than a polar one. We will try to keep it brief, and we only want to find the eigenfrequencies and the mode shapes of the membrane. We will therefore refrain from deriving the equations for the general solutions for rectangular membranes and refer to Haberman and Rao for interested readers [27] [28]. As done before, we will follow their derivations closely. We start at the same point as before, the 2D wave equation:

$$\frac{\mathrm{d}^2U}{\mathrm{d}t^2} = c^2\nabla^2U.$$

Where the Cartesian Laplacian is defined as

$$\nabla^2 = \frac{\mathrm{d}^2U}{\mathrm{d}x^2} + \frac{\mathrm{d}^2U}{\mathrm{d}y^2}. \tag{2.36}$$

Now, we assume our displacement function U to be splittable into independent parts, and we again try to find the mode shape by separation of variables. We define U as

$$U(x,y,t) = X(x)Y(y)T(t), \tag{2.37}$$

and enter it into the 2D wave equation:

$$XY\frac{\mathrm{d}^2T}{\mathrm{d}t^2} = c^2\left(YT\frac{\mathrm{d}^2X}{\mathrm{d}x^2} + XT\frac{\mathrm{d}^2Y}{\mathrm{d}y^2}\right). \tag{2.38}$$

Cleaning up, we have

$$\frac{1}{c^2T}\frac{\mathrm{d}^2T}{\mathrm{d}t^2} = \frac{1}{X}\frac{\mathrm{d}^2X}{\mathrm{d}x^2} + \frac{1}{Y}\frac{\mathrm{d}^2Y}{\mathrm{d}y^2}. \tag{2.39}$$

Now, as we noticed with the circular membranes, both sides are completely independent of each other, and we can thus assume them to both be equal to a constant; we again define it as $-\lambda^2$ to write

$$\frac{\mathrm{d}^2T}{\mathrm{d}t^2} + c^2\lambda^2T, \tag{2.40}$$

$$\frac{1}{X}\frac{\mathrm{d}^2X}{\mathrm{d}x^2} + \lambda^2 = -\frac{1}{Y}\frac{\mathrm{d}^2Y}{\mathrm{d}y^2}. \tag{2.41}$$

Repeating this trick on 2.41, we find two more equations using the separation constants κ

$$\frac{\mathrm{d}^2X}{\mathrm{d}x^2} + (\lambda^2 - \kappa^2)X = 0, \tag{2.42}$$

$$\frac{\mathrm{d}^2Y}{\mathrm{d}y^2} + \kappa^2Y = 0. \tag{2.43}$$

For convenience, we will rewrite 2.42 by defining $\mu^2 = \lambda^2 - \kappa^2$. Together with 2.40, we have three types of equations that we are now experienced with. Using the exponential ansatz as shown before, we find the solutions:

$$T(t) = A\sin(\lambda t) + B\cos(\lambda t), \tag{2.44}$$

$$X(x) = C\sin(\mu x) + D\cos(\mu x), \tag{2.45}$$

$$Y(y) = E\sin(\kappa y) + F\cos(\kappa y). \tag{2.46}$$

Our square membrane has sides of length L and is clamped along its boundaries. We will use the boundary conditions $X(0) = X(L) = Y(0) = Y(L) = 0$ to discover that D and F should be 0:

$$X(x) = C\sin(\mu x), \tag{2.47}$$

$$Y(y) = E\sin(\kappa y), \tag{2.48}$$

and that at $x = L$ and $y = L$, μ and κ should be integer values of π i.e.

$$\mu L = m'\pi \qquad \& \quad m' = 0, 1, 2, ...$$
$$\kappa L = n'\pi \qquad \& \quad n' = 0, 1, 2, ...$$

Using these definitions for μ and κ, and formulas 2.47 and 2.48, we find our modeshape for a clamped square membrane to be

$$\varphi_{m',n'} = \sin\left(\frac{m'\pi}{L}x\right)\sin\left(\frac{n'\pi}{L}y\right). \tag{2.49}$$

2.2.5. Eigenfrequencies of a Square Membrane

Now we turn our attention to the eigenfrequencies of this square membrane with a modeshape described by 2.49. To find the square membrane eigenfrequencies, we follow a similar approach to the one shown for circular membranes. We assume that the oscillation of the membrane is a harmonic one, and we will define the time-dependent part as $T(t) = \sin(\omega t)$. If we fill in this definition in equation 2.39 we arrive at

$$-\frac{\omega^2}{c^2} = \frac{1}{X}\frac{\mathrm{d}^2X}{\mathrm{d}x^2} + \frac{1}{Y}\frac{\mathrm{d}^2Y}{\mathrm{d}y^2}. \tag{2.50}$$

We see that this new term is equal to $\lambda^2 = \kappa^2 + \mu^2$ and so we have

$$\frac{\omega^2}{c^2} = \kappa^2 + \mu^2. \tag{2.51}$$

Using the definition of c in 2.30 together with the definitions for μ and κ found with the boundary conditions, we rewrite for our eigenfrequency and arrive at the eigenfrequency equation for a clamped square membrane

$$\omega_{m',n'} = \frac{\pi}{L}\sqrt{\frac{n_0}{\rho h}\left(m'^2 + n'^2\right)}. \tag{2.52}$$

If $L_x \neq L_y$, we have

$$\omega_{m',n'} = \pi\sqrt{\frac{n_0}{\rho h}\left[\left(\frac{m'}{L_x}\right)^2 + \left(\frac{n'}{L_y}\right)^2\right]}. \tag{2.53}$$

2.2.6. Square Eigenmodes

As stated before, we will not present the general solution of the displacement function $U(x, y, t)$. Rather, we will present the modeshapes for the square membranes graphically as done for the circular membranes. Similar to the circular membranes, for square membranes, an infinite number of degenerate modeshapes appear in pairs which differ by only a spatial rotation of $\pi/2$.

The first ten eigenmodes of a clamped square membrane are presented in figure 2.6

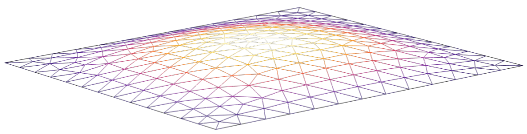

(a) $\omega_{1,1} = \omega_0$

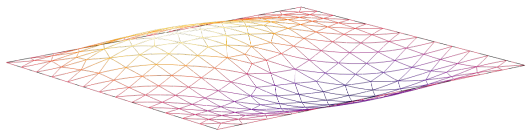

(b) $\omega_{1,2} = 1.581\omega_0$

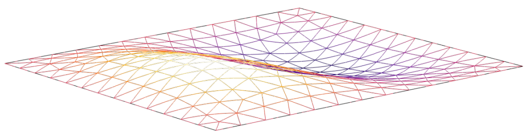

(c) $\omega_{2,1} = 1.581\omega_0$

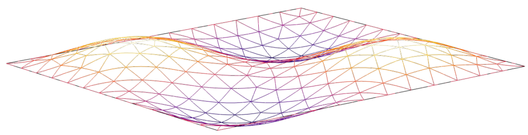

(d) $\omega_{2,2} = 2\omega_0$

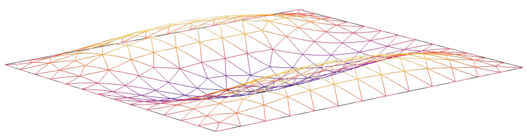

(e) $\omega_{1,3} = 2.236\omega_0$

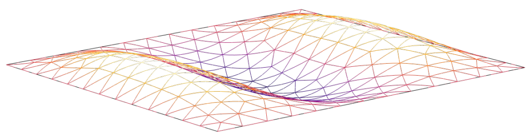

(f) $\omega_{3,1} = 2.236\omega_0$

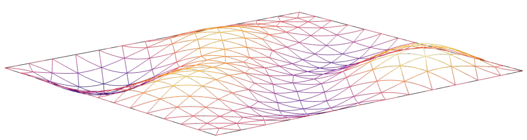

(g) $\omega_{2,3} = 2.55\omega_0$

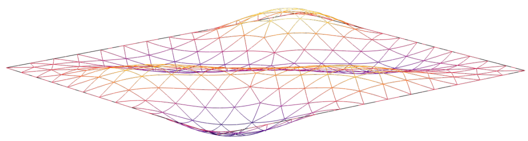

(h) $\omega_{3,2} = 2.55\omega_0$

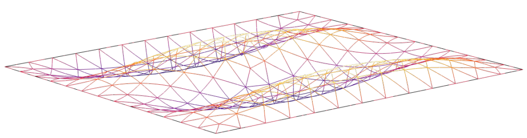

(i) $\omega_{3,3} = 2.916\omega_0$

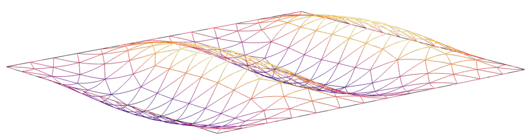

(j) $\omega_{3,3} = 2.916\omega_0$

Figure 2.6: The modeshapes of the first ten eigenmodes of a clamped square membrane. The degenerate modes have been included. The associated eigenfrequencies are given per mode.

2.2.7. Other Geometries

With the eigenfrequencies of square and circular membranes derived, we have, unbeknownst to us, solved the eigenfrequencies of the two extremes of a large set of geometric membrane shapes. Lord Rayleigh in a 1945 analysis [30] derived that regular polygon-shaped membranes and plates should have fundamental eigenfrequencies that, in terms of numerical value, should lie between square and circular ones. The formula presented by Rayleigh to find the fundamental eigenfrequencies is defined as

$$\omega = 2\pi\alpha\sqrt{\frac{n_0}{\rho A}}. \tag{2.54}$$

With α a scalar factor depending on the geometry, a short selection of some found values is shown in table 2.2, taken from [28] and [30].

Table 2.2: Value of α with which to determine the eigenfrequency of a membrane with a certain geometry [30].

Geometry	$\boldsymbol{\alpha}$
Square	4.443
Circle	4.261
Rectangle with $L_x = 2L_y$	4.967
Rectangle with $L_x = 3L_y$	5.736
Equilateral triangle	4.774
Semicircle	4.803

2.3. Nonlinear Attractive Transverse Forces

Now that we have established the necessary analytics for our 2D membrane resonators, we have completed the first half of our theoretical analysis. The second half will concern the nonlinear attractive forces that apply transverse pressures upon the membranes. We will introduce the forces and investigate the effects they have on our membrane resonators. Let us start with the Casimir force.

2.3.1. Casimir Force

Ideal Casimir Force

The Casimir effect is a quantum mechanical effect that was theoretically predicted by Hendrik Casimir in 1948 during his research into retarded van der Waals forces [31] and experimentally verified in 1997 by Steven Lamoreaux [32]. The Casimir effect is a consequence of the quantisation of the electromagnetic field. The effect manifests itself in a vacuum when two perfectly parallel reflecting objects, for example, two infinite plates, are extremely close to each other. As the distance between the plates becomes smaller, the allowed modes of the vacuum fluctuations, which appear as intermittent electromagnetic modes, are quantised. Outside of the plates, the oscillations are not quantised and are continuous. The limitation of the allowed modes between the plates results in a net force pushing the two plates together [33]. This is shown schematically in figure 2.7.

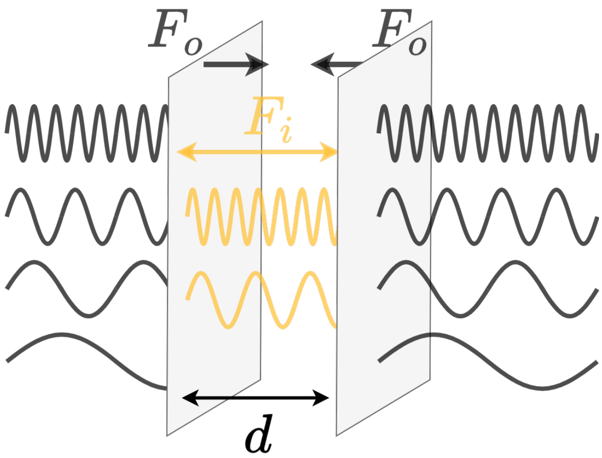

Figure 2.7: Schematic representation of the origin of the Casimir effect. The smaller d becomes, the less vacuum fluctuations fit as the allowed modes between the plates shrink. This creates a mismatch between the number of wavelengths between the plates and outside of the plates. This means that for smaller d ,$2F_o > F_i$ and that the plates are pushed towards each other, thereby increasing the effect.

The Casimir effect is thus known as an attractive pressure between two parallel objects as the plates are forced towards each other due to the mismatch between the allowed modes inside and outside the plates. The closer the two plates come together, the stronger the Casimir effect becomes, with the modes outside of the plates staying unaffected. It is therefore a nonlinear attractive force. The Casimir effect, as found by Casimir himself, the case of two infinite perfectly smooth reflecting parallel plates within a vacuum at 0K, is unfeasible in reality. However, the Casimir effect does manifest itself in other analogues in real life. One simple example is seen in the attractive movements of two parallel ships that are close to each other in a rough sea.

Real Analogues of the Casimir Force

In electromagnetism, an important analogue of the Casimir effect was found by Lifshitz in his 1956 seminal paper [34]. Lifshitz derived a formula for the Casimir effect between parallel conducting plates due to the presence of charge fluctuations at finite temperatures. These charge fluctuations manifest themselves as electromagnetic waves between and outside of the plates. This analogue, to which we will henceforth refer as just the Casimir effect, has an increasing impact in micro and nano electronics due to the ongoing miniaturisation of components, resonators included [35]. Resonators are often fabricated while suspended over a cavity, parallel to the cavity bottom, which is close to the resonator. As these two parallel objects come close to each other, the Casimir force will attempt to push the membrane and the cavity bottom together. This puts pressure on the resonator and thus changes its characteristics.

The force per unit area, i.e. the pressure exerted due to the Casimir effect for two large, parallel, conducting plates in a vacuum, is shown in equation 2.55

$$P(d) = -\eta \frac{\pi^2 \hbar c}{240} \frac{1}{d^n}. \tag{2.55}$$

With d the distance between the plates, $\hbar$ the reduced Planck's constant and c the speed of light in a vacuum. $\eta \leq 1$ is a parameter which depends on the dielectric permittivities of the two plates [36], and the exponent n is equal to 4 in the ideal case. **Both** η and n are parameters whose values are subject to the exact experimental parameters of the system. In reality, due to a multitude of factors, such as surface roughness, degree of plate parallelism, medium between the plates, dielectric constants and plate sizes, the exponent n can range in value between 3 and 4. For example, in [37], the exponent is calculated to range between 3.1 and 3.3 for a superconducting aluminium drum. Equation 2.55 is thus an idealised formula corrected with both the η parameter and the n exponent. The value of both η and n can be determined with the Lifshitz formula for the Casimir effect for finite temperatures [34] [37] :

$$P(d,T) = -\frac{k_B T}{\pi} \sum_{0}^{\infty}{}' \int dk_\perp k_\perp q_l \sum_{\alpha \in \{\text{TE,TM}\}} \left(\frac{e^{2dq_l}}{r_\alpha^{(1)} r_\alpha^{(2)}} \right)^{-1}. \tag{2.56}$$

With k_B Boltzmann's constant, $k_\perp$ the length of the in-plane projection of the electromagnetic wave and d the interplate distance. The prime denotes that the first TM term in the sum should be multiplied by half and the first TE term omitted. $r_\alpha^{(n)}$ are the nth plate Fresnel coefficients

$$r_{TE}^{(n)} = \frac{q_l - s_l}{q_l + s_l}, \tag{2.57}$$

$$r_{TM}^{(n)} = \frac{\epsilon(i\xi_l)q_l - s_l}{\epsilon(i\xi_l)q_l + s_l}, \tag{2.58}$$

in which

$$q_l = \sqrt{\frac{\xi_l^2}{c^2} + |k_\perp|^2}, \tag{2.59}$$

$$s_l = \sqrt{\epsilon(i\xi_l)\frac{\xi_l^2}{c^2} + |k_\perp|^2}, \tag{2.60}$$

$$\xi_l = \frac{2\pi k_B l T}{\hbar} \tag{2.61}$$

Where ξ_l are the Matsubara frequencies used in thermal quantum field theory. These formulas are mainly concerned with the electromagnetic properties of the media in the system. However, as stated before, surface roughness and degree of parallelism also play roles in the exact definition of **both** η and n. These two effects can be approximated using two techniques. Firstly, the Casimir force between two objects with a degree of roughness can be modelled using the proximity force approximation (PFA) [38]. The exact approximation is not universally agreed upon, with the Drude model and the Plasma model being the main candidates [39].

Secondly, in the case of resonators, one also has to take the bowing of the surface into account when considering the Casimir effect. The resonator will bow down due to the transverse force exerted by the Casimir effect. The bowing, however slight, changes the parallelism between the resonator and its cavity bottom. The effect of this can be calculated using the Derjaguin approximation [40].

We state the Lifshitz formula as it is crucial to exact Casimir force experiments and calculations. However, we will refrain from using it, the Derjaguin approximations and the PFA for the sake of simplicity. These approximations are complex calculations which, for this thesis, do not add much added value as we will be concerned with simulations in which effects such as surface roughness are difficult to include. Instead, for η, we will use the fact that Serry et. al [36] state that for metallic extremely parallel objects $\eta \approx 1$, and if only one plate is metallic then $\eta \approx 0.5$. If both are dielectrics, this value is probably close to 0. This is because metallic surfaces facilitate excellent reflection of electromagnetic waves, whereas dielectrics do not. We will assume that for the systems that we study, the parallelism is not compromised to a degree that it has significant effects on the value of η. For the exponent n, we have a different strategy in mind. As previously mentioned, in experimental setups, its value can vary in the range of 3 to 4, with 4 being the most ideal case. In our situation, it will be taken as equal to 4 and stay constant, as it has no conclusive value. Its value is never the same for different experimental setups. Later on, we will compare results from simulations with results from experiments, and we can expect these to not exactly match for $n = 4$. We will then be able to determine the value of n for the experimental setup of that measurement by equating both.

The Casimir effect is an effect that was the subject of a relatively small amount of research for a long time, but interest is building. This is because the effect used to be unattainable and therefore had no effect on sensors, as the required parallelism and distances are complex to realise. This, in addition to the very weak magnitude, makes the effect difficult to research. However, with decreasing sensor size and improving fabrication techniques, the effect is starting to play an increasing role in research. Its inverse proportionality to the fourth power of the gap size means that its magnitude is negligible except for very small distances, where it suddenly rises sharply. For example, for a gap size of $500\,\mathrm{nm}$, the Casimir effect exerts a pressure of 0.02 Pa, while for a gap of $50\,\mathrm{nm}$, the pressure reaches 206 Pa. However, these pressures can grow to be significantly larger than the ones given by formula 2.55 due to an effect known as spring softening, which we will cover later.

2.3.2. Electrostatics

Electric Field and Potential

In contrast to Casimir forces, electrostatics have been a wide area of research for a very long time and are by far the most commonly used forces to move mechanical components in MEMS [41]. From resonators, mechanical tweezers, electrofluidic sensors, charge shuttles, micropumps, micromirrors, diffraction gratings to micromotors and more, electrostatics are a valued technique in MEMS [42] [43].

The driving force behind electrostatics is, naturally, the electrostatic force itself. The electrostatic force comes about due to electrical potential differences between two objects, which are related to the electromagnetic field as

$$\vec{E} = -\nabla\phi, \tag{2.62}$$

with $\vec{E}$ the electric field between the two objects and ϕ the scalar potential. Contrary to the Casimir effect, the electrostatic effect is accompanied by so-called fringe fields. These fringe fields are stray electromagnetic field divergences necessary for the electromagnetic field lines to be completed and are visible outside the two plates in figure 2.8a. Ignoring the fringe fields and assuming the electric field points in one direction, as is the case between two parallel plates (red region in figure 2.8a), then $\phi = \frac{V}{d}$, with d the distance between the objects. For two parallel plates, like a capacitor, one can find the electrostatic force by calculating the potential energy in the electric field $U = \frac{\varepsilon_0\varepsilon_r}{2}\int|\vec{E}|^2$ in conjunction with the identity $F = -\nabla U$. For an idealised infinite parallel plate capacitor, this results in the famous relation

$$F_{ES} = -\frac{C}{2}\left(\frac{V}{d}\right)^2 = -\frac{1}{2}\frac{A\varepsilon_0\varepsilon_r V^2}{d^2}. \tag{2.63}$$

This equation, as fringing fields were ignored, is an approximation that is only valid when the size of the plates is much larger than the distance between them. When a voltage is applied to a resonator, and a ground plane is situated above or below it, the resonator will be pulled by the electrostatic force towards the grounded plane. This affects the stiffness of the resonator and thereby its resonating characteristics. Figure 2.8 shows the electric field and the voltage distribution of such a situation, with the fringing fields visible.

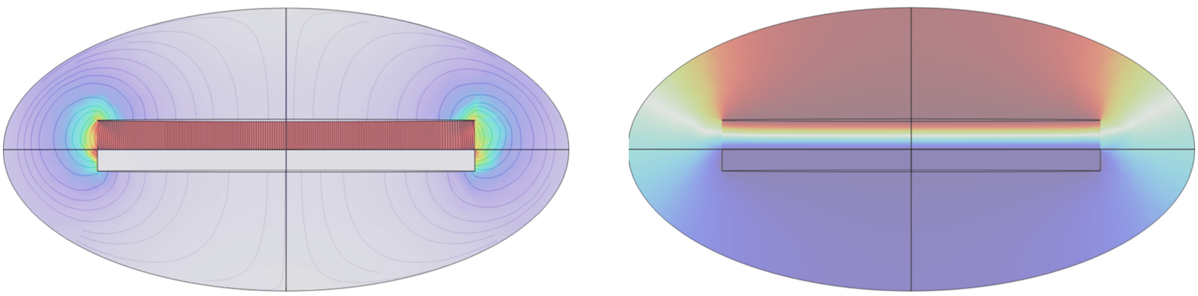

(a) (b)

Figure 2.8: Plots of a resonator subjected to a potential, with a thicker grounded base. Red is used to show high values, and blue shows low values. (a) The electric field distribution as seen from the side. (b) The electric potential distribution as seen from the side.

Shown is the side view of a resonator above a grounded base. The resonator has a voltage applied to it, and the base is grounded. The field lines indicate where the electrostatic effect is the strongest in figure 2.8a, with the space between the grounded base and the resonator showing the strongest electric field density.

An exact solution to the contribution of these fringe fields does not exist, and accurate solutions to this problem grow fast in complexity as shown analytically by Reichert et. al [44]. One can estimate the deviation by these fringing fields by using the simple approximation found by Kirchhoff [45]. This approximation of the fringing fields for a circular plate gives a more realistic indication of the impact of the fringe fields on the capacitance, and so the electrostatic effect, without being too complex.

$$C = C_0\left(1 + \frac{b}{\pi}\ln\left(\frac{16\pi}{b} - 1\right)\right), \tag{2.64}$$

with $b = d/R$ the aspect ratio between the distance between the two plates d, and the radius of a circular plate R. A plot of the percentual shift in the electrostatic force calculated between an infinite circular capacitor approximation and 2.64 is shown in figure 2.9

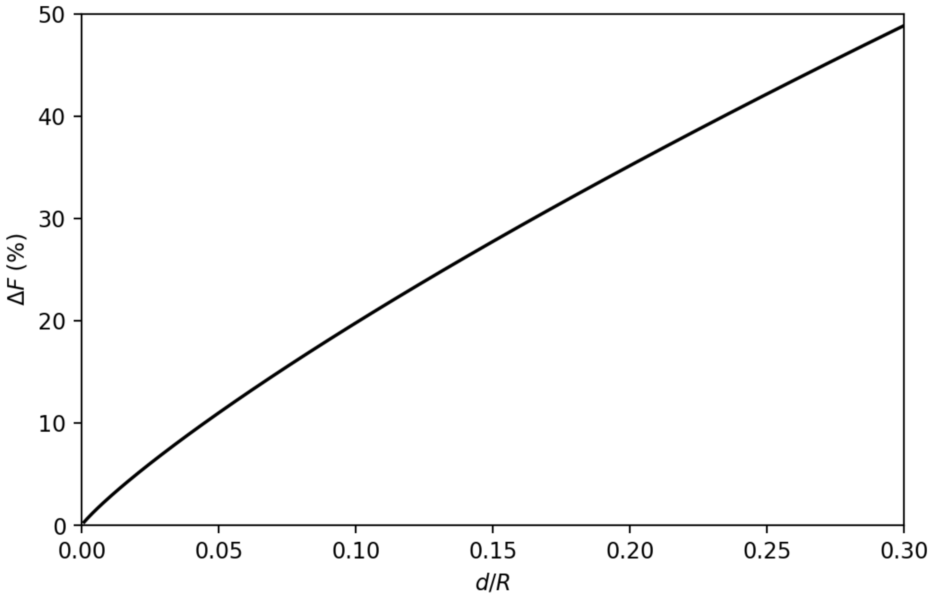

Figure 2.9: Percentual deviation between the electrostatic force as calculated by the infinite capacitor approximation and the Kirchhoff correction. Relatively small aspect ratios still lead to a sizable force error for the infinite capacitor approximation.

Figure 2.9 shows a surprisingly large error in the force calculated by the infinite capacitor approximation, even for relatively small aspect ratios. When the fringe fields are excluded, the system contains less energy. Only systems with very large aspect ratios are barely affected by the exclusion of the fringe fields, as the total energy in that case is dominated by the interplate fields, and the fringe field energy is thus negligible.

Electrostatics are not only used to move mechanical sensors; they also serve a sensing purpose in capacitive sensors. The change in the capacitance of a system can be directly linked to the change in distance between two objects with a potential between them, thereby enabling the sensing of a plethora of physical effects. Unfortunately, attractive forces such as electrostatics also introduce unwanted effects, such as pull-in.

Electrostatic Pull-in

The inherent attractive nature of electrostatics poses a problem for the design of MEMS devices. This is due to the fact that when the electrostatic force becomes too strong, an effect known as pull-in can occur, which is not exclusive to just electrostatics but any attractive distance-dependent force. If the restoring force of a resonator is unable to balance out the electrostatic force, then the resonator will deform inelastically and/or be pulled further towards the grounded electrode until it hits it (or reaches the size regime at which VanderWaals forces take over) and shorts the circuit. We would like to predict when this happens to prevent device failure by means of analytics and later on, Finite Element Analysis.

For our analytics, we choose to use a so-called lumped element model. This means that we use a simplified representation of our physical system to calculate the pull-in voltage. We do this because a full-fledged continuum model for the pull-in voltage is very complex, which in this instance is not needed. The simplified model was introduced before when discussing basic resonator theory and is shown in figure 2.10, where we model the spring constant of the membrane as a simple spring.

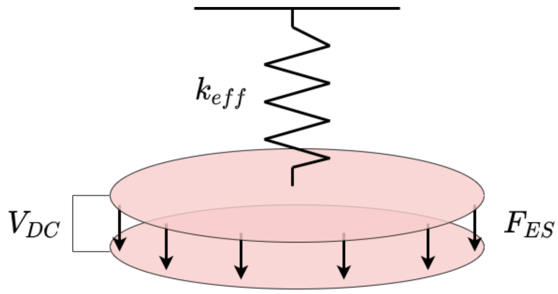

Figure 2.10: Lumped element model of a flexible membrane separated by a gap with the cavity bottom. The membrane is subjected to an electrostatic force due to a voltage difference. The membrane restoring force is modelled as a spring.

A simple calculation of the pull-in voltage will now be shown, We start by equating the opposing forces in our lumped model

$$kU = -F, \tag{2.65}$$

where k is our membrane spring constant, U is the centre deflection of the membrane, or the stretching of the spring, and F_{ES} is the electrostatic force as defined in 2.63. Pull-in occurs when the electrostatic force trumps the restoring force, and this point is known as a stability point. One determines the stability of a point by inspecting the eigenvalues of the Jacobian at that point in space [46]. For this one-dimensional system of our interest, this means linearising around the equilibrium point with a first-order Taylor expansion, i.e. equating the derivative with respect to the deflection to zero. The moment the stiffness changes sign, we know we have crossed the pull-in point. We now calculate the derivative of 2.65 with respect to U to find k:

$$k = -\frac{A\varepsilon_0\varepsilon_r V^2}{(d+U)^3}. \tag{2.66}$$

Entering this definition for k back into 2.65 and after rearranging, one finds the famous electrostatic MEMS rule of thumb:

$$U_{max} = d/3. \tag{2.67}$$

We may then use this maximum deflection distance in combination with 2.65 and 2.66 to find a maximum voltage, or the pull-in voltage for a certain gap size as

$$V_{PI} = \sqrt{\frac{8kU_{max}^3}{27\varepsilon_0\varepsilon_r A}}. \tag{2.68}$$

This quite famous relation for the pull-in voltage is an easy but also an inaccurate one. It is useful as it gives a lower bound, but more accurate models predict higher pull-in voltages and bigger maximum deflections, such as $U_{max} = 0.44d$ [47]. This is due to the fact that we have not included the nonlinear effects that occur to the spring constant of the membrane when subjected to nonlinear attractive forces such as the Casimir force, the electrostatic force or large deflections in general. These nonlinear effects, including spring softening, hardening, and an improved analytical model for the pull-in voltage, are presented in the next section.

2.4. Nonlinear Effects

Up until now, we have been limiting our analysis of resonators to the linear class. Linear resonators show the characteristic output shown in figure 2.4 when looking at their amplitude per drive frequency output. Linear in this context means that the role of the amplitude of the oscillations is linear in the equation of motion. This means that if one were to increase the amplitude of the driving force, the output response would not change. In reality, this is not the case, and the class of effects that cause this are called nonlinear and resonators that are notably affected by them nonlinear resonators. Nonlinearities are very common in nature, and linear systems are almost always approximations made in engineering to systems with negligible nonlinearities. Nonlinearities exist in a wide spectrum of different kinds, some have the effect of making the membrane softer, meaning it is more easily deflected, and some make the membrane harder [13]. Mixing of multiple nonlinear effects can also occur as shown by Samantha et. al [48]. We will start with a famous type of nonlinearity.

The most basic form of a nonlinear resonator is describable with the so-called Duffing equation of motion, which adds the so-called Duffing term β [13]

$$m\frac{\mathrm{d}^2x}{\mathrm{d}t^2} + \zeta\frac{\mathrm{d}x}{\mathrm{d}t} + kx + \beta x^3 = F_0\sin(\omega_d t). \tag{2.69}$$

Here, a new force enters the equation of motion that is proportional to the displacement cubed. The Duffing term models the behaviour of systems in which the stiffness term does not obey Hookes law. The Duffing term β can be either positive or negative, depending on the type of nonlinear effect present in the system. When the Duffing parameter is positive, i.e. $\beta > 0$, the harmonic oscillator is stiffened, or sometimes called hardened, and the restoring force of the resonator grows. If the Duffing parameter is negative, i.e. $\beta < 0$, a softening effect on the spring constant occurs and the restoring force is decreased. A softer resonator exhibits a lower resonant frequency and a stiffened one a higher resonant frequency. This effect can be seen in the output amplitude per frequency as shown in figure 2.11.

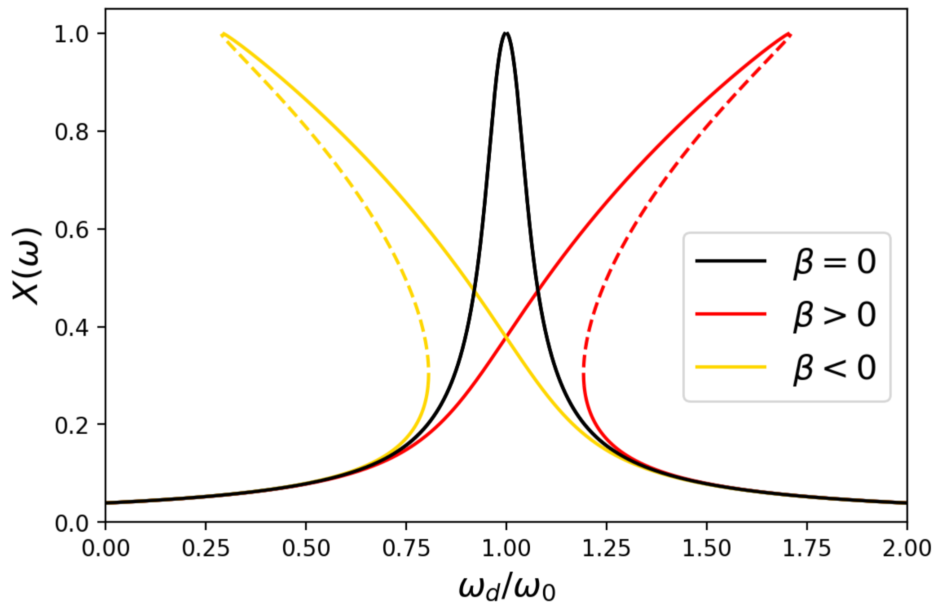

Figure 2.11: Three frequency response curves of nonlinear resonators. The three curves show the response for varying types of Duffing parameters, linear ($\beta = 0$), hardening ($\beta > 0$) and softening ($\beta < 0$). The dashed regions show the unstable regions which cause hysteresis in the frequency response. The measured value will depend on the branch taken , which depends on the direction of the drive frequency sweep.

We see that the spring softening/hardening effect pushes or bends the resonance peak to the sides and creates a dashed region, which is known as the unstable region [14]. The resonator will not stay in this region and will snap back to either the top or the bottom branch of the output. This means that the Duffing resonator exhibits hysteresis as an approach in drive frequency from the left will follow a different trajectory compared to an approach in drive frequency from the right.

2.4.1. Types of Nonlinearities

As mentioned before, there exists a wide variety of nonlinearities in MEMS resonators. These vary from nonlinearities found in the damping, to ones found due to actuation, detection, or the materials of the resonators themselves. We will cover the two most important ones for the 2 two-dimensional resonators of our interest. The first being the softening effect caused by external attractive nonlinear force fields that act upon the resonator, such as an electrostatic force or the Casimir force. The second is a nonlinearity caused by the geometry of the resonator when subjected to large deflections, known as geometrical nonlinearity. We will also show how these nonlinearities can be used to potentially improve these resonators.

2.4.2. Nonlinear Force Field Frequency Softening

The nonlinear force field softening effect is a counterintuitive one, as one would expect the stiffness to increase when a resonator is pulled by a nonlinear force, but the opposite occurs. It is an effect that has been well known for decades, as electrostatic actuation and detection are one of the most popular tools in MEMS technology. It is, however, not exclusive to the electrostatic effect and occurs for any sort of distance dependent force field pulling on the resonator as we will now show based on a calculation given by [13]. Let us consider a general nonlinear attractive force field that pulls on a membrane and is dependent on the distance between the membrane and a backplate parallel to it. We will define it as

$$F(U) = -\frac{C}{(d+U)^q}, \tag{2.70}$$

in which U is the centre deflection of the circular membrane from its equilibrium point and d is the distance between the membrane and the backplate, and C is a force-dependent constant. If the force would not be present, then the equilibrium position would be a distance d from the backplate, but with the force pulling on the membrane, the equilibrium position shifts to $d+U$, note ($U<0$). The opposing forces in the system are then

$$kU = -\frac{C}{(d+U)^q}. \tag{2.71}$$

We now take the force term on the left-hand side and bring it to the right. Using the identity $F = -\nabla V$, we write

$$\frac{\mathrm{d}V}{\mathrm{d}U} = kU + \frac{C}{(d+U)^q}. \tag{2.72}$$

If the force changes slightly, then the resonator will move to a new equilibrium position U_0. We can expand the potential using a Taylor expansion around the new equilibrium point $d_0 = U + U_0$ to find

$$V(d_0) \simeq V(U_0) + \left(k/2 - \frac{qC}{(d+U_0)^{q+1}}\right)d_0^2 + \frac{1}{6}\frac{q(q+1)C}{(d+U_0)^{q+2}}d_0^3 - \frac{1}{24}\frac{q(q+1)(q+2)C}{(d+U_0)^{q+3}}d_0^4 + \mathcal{O}(d_0^5). \tag{2.73}$$

Or, equivalently,

$$V(U_0) \simeq V(U_0) + k_{eff}d_0^2 + \beta d_0^3 + \alpha d_0^4 + \mathcal{O}(d_0^5). \tag{2.74}$$

Where we have collected $\left(k/2 - qC/(d+U_0)^{q+1}\right)$ into a new parameter k_{eff} and the other terms in β and α.

We may now make two important observations. Firstly, looking at our definition of the effective spring constant, we see that it is *reduced* by the squared term resulting from the force field expansion. In other words, it is *softened* due to this attractive nonlinear force. Secondly, if this squared term were to grow larger than our original spring constant k, we would have a negative spring constant. A negative spring constant, instead of restoring the membrane, would do the opposite. This is the effect earlier described as pull-in, where the membrane would not overcome the pulling force and would snap to the backplate. The potential given in 2.74 creates the following equation of motion.

$$m\frac{\mathrm{d}^2 d_0}{\mathrm{d}t^2} + kd_0 + \beta d_0^2 + \alpha d_0^3 = 0, \tag{2.75}$$

where we have omitted any driving force. The quadratic term influences the resonance frequency but does so regardless of the direction of d_0 and β is known as an elastic constant [13]. In α we find our Duffing parameter as it is connected to the cubic term, which in this case is negative.

A nonlinear attractive force thus negatively influences the spring constant. This influence is distance-dependent, and we can expect a larger deflection to create a larger softening effect on the eigenfrequency of the membrane. This means that the shift in the eigenfrequency due to a pressure on the membrane will be bigger when softened by a nonlinear force than without it. We could see this as a potential technique to increase the responsivity/sensitivity of our resonator, as the change in eigenfrequency would be bigger with our nonlinear force present. This opportunity has been seized using magnetic fields by Karlivčič et. al [49] and with electric fields by Xiong et. al. [50] and Zhang et. al. [51] but remains an eccentric responsivity boosting technique. It would also aid the sensing of the eigenfrequency as the softened stiffness will lead to bigger deflections, which can be more easily measured. We will explore this effect in depth in theory and simulations as it promises exciting opportunities to optimize resonator sensors.

2.4.3. Softening in Circular Membranes

Electrostatic Softening

With the stiffness of the resonator softened by nonlinear effects, the resonance frequency will also change and be reduced. We will now derive the softening of the resonance frequency of a circular membrane subjected to an attractive electrostatic force field. We must note that the following derivation only has this softening effect in mind and is therefore not valid as an approximation for other nonlinear effects that might arise when the deflection distance of the membrane is no longer negligible compared to the dimensions of the membrane and the cavity bottom. We use a continuum model based on [12] and we repeat the electrostatic force between two parallel plates, when the distance between the plates is very small compared to the size of the plates, here:

$$F_{ES} = -\frac{1}{2}\frac{A\varepsilon_0\varepsilon_r V^2}{(d+U)^2}.$$

With ε_0 the permittivity of the vacuum and A the membrane area. The equation of motion of the membrane subjected to an electrostatic force field is found by equating the forces present in the system. For an infinitesimal piece of membrane area with a thickness h, the force equilibrium is

$$\rho h\frac{\mathrm{d}^2 U}{\mathrm{d}t^2} - \sigma h \nabla^2 U = F_{ES}, \tag{2.76}$$

with ∇, the Laplacian of the spherical kind. We then follow an adjusted version of a procedure shown in [12], which presents a calculation for square membranes. With some adjustments, we will find the resonance frequency of a circular membrane subjected to an attractive electrostatic potential. We will use the Galerkin method, which exploits the orthogonality of the membrane eigenmodes. We define the displacement function U of the membrane as

$$U(r) = \sum_{m'=1}^{\infty}\sum_{n'=1}^{\infty} U_{0,m',n'}\varphi_{m',n'}(r)e^{i\omega_{m',n'}t}, \tag{2.77}$$

with $U_{0,m',n'}$ the amplitude for the m', n'-th mode, $e^{i\omega_{m',n'}t}$ the time dependent oscillation term. For $\varphi(r)$, we will use the normalised first-order spherical Bessel function, which we found in an earlier deviation, as we desire to derive the eigenfrequency of the fundamental eigenmode:

$$\varphi(r)_{1,1} = \frac{R\sin\left(\frac{\alpha r}{R}\right)}{\alpha r}. \tag{2.78}$$

With $\alpha = 2.4048$, the first zero of the Bessel function of the first kind. We can linearise 2.4.3 by using a first-order Taylor expansion and write

$$F_e \approx F_e(0) + \frac{\mathrm{d}F_e(0)}{\mathrm{d}U}U \approx -\frac{\varepsilon_0\varepsilon_r V^2}{2d^2} + \frac{\varepsilon_0\varepsilon_r V^2}{d^3}U. \tag{2.79}$$

The first electrostatic term is a static one, as shown before, and is constant in its effect on the resonant frequency as it is independent of U. This effect is significant if geometrical nonlinearities are significant in our system, for the time being we assume that not to be the case. We consider its effect to be negligible, and we can thus ignore it. Our equation of motion then becomes

$$\rho h\frac{\mathrm{d}^2U}{\mathrm{d}t^2} - \sigma h\nabla^2 U = \frac{\varepsilon_0\varepsilon_r V^2}{d^3}U. \tag{2.80}$$

We then employ the Galerkin method to find the resonance frequency shift of the membrane due to the electrostatic field. To this end, we multiply with the mode of interest, in our case the fundamental mode $\varphi_{1,1}$ and integrate over the entire membrane surface. This gives us

$$\int_R \left(\rho h\frac{\mathrm{d}^2U}{\mathrm{d}t^2} - \sigma h\nabla^2 U - \frac{\varepsilon_0\varepsilon_r V^2}{d^3}U\right)\varphi_{1,1}dr = 0. \tag{2.81}$$

We evaluate the Laplacian of the eigenmode as:

$$\begin{aligned}\nabla^2\varphi(r)_{1,1} = r^2\left(-\frac{a\sin\left(\frac{ar}{R}\right)}{Rr} + \frac{2R\sin\left(\frac{ar}{R}\right)}{ar^3} - \frac{2\cos\left(\frac{ar}{R}\right)}{r^2}\right) + 2r\left(\frac{\cos\left(\frac{ar}{R}\right)}{r} - \frac{R\sin\left(\frac{ar}{R}\right)}{ar^2}\right)\\ = -\frac{\alpha\sin(\frac{\alpha r}{R})}{rR}\end{aligned} \tag{2.82}$$

and after calculating the other terms, we arrive at

$$\int_R \left(-\rho h\omega_{1,1}^2\varphi_{m',n'} + \sigma h\frac{\alpha^2}{R^2}\frac{R\sin(\frac{\alpha r}{R})}{\alpha r} - \frac{\varepsilon_0\varepsilon_r V^2}{d^3}\varphi_{m',n'}\right)\varphi_{m',n'}dr = 0. \tag{2.83}$$

We then rewrite the second term and collect the r dependent terms to find

$$-\rho h\omega_{1,1}^2\int_R \varphi_{1,1}^2 dr + \sigma h\frac{\alpha^2}{R^2}\int_R \varphi_{1,1}^2 dr - \frac{\varepsilon_0\varepsilon_r V^2}{d^3}\int_R \varphi_{1,1}^2 dr = 0, \tag{2.84}$$

note that due to the eigenmodes being orthogonal, the only eigenmode that is nonzero when multiplied with $\varphi_{1,1}$ is $\varphi_{1,1}$ itself. Losing the integral terms, the eigenfrequency is then isolated and becomes

$$\omega_{1,1}^2(V) = \frac{\alpha^2}{R^2}\frac{\sigma}{\rho} - \frac{\varepsilon_0\varepsilon_r V^2}{\rho h d^3}. \tag{2.85}$$

If no voltage is present, then the eigenfrequency is just

$$\omega_{1,1}^2(0) = \frac{\alpha^2}{R^2}\frac{\sigma}{\rho}. \tag{2.86}$$

Using 2.85 and 2.86, the first-order Taylor approximation of the fundamental eigenfrequency of the membrane in an electrostatic field can be written as

$$\omega_{1,1}^2(V) = \omega_{1,1}^2(0)\left(1 - \frac{R^2}{\alpha^2}\frac{\varepsilon_0\varepsilon_r}{\sigma h d^3}V^2\right). \tag{2.87}$$

Casimir Softening

The frequency softening of a circular membrane subjected to the Casimir force field can be found in a similar fashion, with the only difference being the nonlinear force itself. The Casimir force for an infinitesimal piece of membrane is again linearised with a first-order Taylor approximation:

$$F_{Cas} \approx F_{Cas}(0) + \frac{\mathrm{d}F_{Cas}(0)}{\mathrm{d}U}U \approx -\eta\frac{\pi^2\hbar c}{240d^4} + \eta\frac{\pi^2\hbar c}{60d^5}U. \tag{2.88}$$

Again, ignoring the static term, the same procedure as above is followed. The first-order Taylor approximation of the fundamental eigenfrequency is then found as

$$\omega_{1,1}^2(\eta) = \omega_{1,1}^2(0,0)\left(1 - \frac{R^2}{\alpha^2}\frac{\eta\pi^2\hbar c}{60\sigma h d^5}\right), \tag{2.89}$$

where $\omega_{1,1}^2(0)$ is equal to 2.86. The Casimir effect will always be present in the sensors covered in this thesis, the electrostatic effect is one that can be manually turned on or off. The combination of both effects is therefore always the case if electrostatics are chosen to play a role in future sensors. The combined effect on the resonance frequency will therefore be given here. The procedure is again equivalent to those given above, and therefore, we only show the resulting eigenfrequency:

$$\omega_{1,1}^2(V,\eta) = \omega_{1,1}^2(0,0)\left(1 - \frac{R^2}{\alpha^2\sigma h}\left(\frac{\varepsilon_0\varepsilon_r}{d^3}V^2 + \eta\frac{\pi^2\hbar c}{60d^5}\right)\right) \tag{2.90}$$

With $\omega_{1,1}^2(0,0)$ given in 2.86.

General Nonlinear Force Field Softening

As mentioned before, the Casimir force and the electrostatic force are never exactly equal to their analytical formulas. This is due to non-perfect geometries, fringe fields, and/or non-ideal conductors. The exponent in the interplate distance term is therefore rarely equal to 2, in the case of electrostatics, or 4 in the case of the Casimir effect. We therefore present the frequency softening for a general attractive nonlinear force field here.

We define our general attractive nonlinear force, with C as the distance independent term as

$$F_{Gen} = -\frac{C}{(d+U)^q}. \tag{2.91}$$

Using the first order Taylor expansion we are given

$$F_{Gen}(U) \approx F_{Gen}(0) + \frac{\mathrm{d}F_{Gen}(0)}{\mathrm{d}U}U = -\frac{C}{d^q} + \frac{qC}{d^{q+1}}U \tag{2.92}$$

It must again be noted that we need to assume that the membrane deflects only a small amount due to this force, such that the geometric nonlinearity is negligible. This nonlinear force, therefore, should not be too strong to pull it out of this regime. Using the now well-known procedure, we find for the resonance frequency

$$\omega_{1,1}^2(C) = \omega_{1,1}^2(0)\left(1 - \frac{R^2}{\alpha^2}\frac{qC}{\sigma h d^{q+1}}\right). \tag{2.93}$$

With $\omega_{1,1}^2(0)$ again equal to 2.86.

2.4.4. Softening in Square Membranes

The calculation of the frequency of the fundamental eigenmode is performed in much the same way as the circular one. The main difference is that we use a different modeshape, we found it before and it was defined as

$$\varphi_{m,n} = \sin\left(\frac{m'\pi}{L}x\right)\sin\left(\frac{n'\pi}{L}y\right).$$

The eigenfrequency softening for a square membrane is shown for an electrostatic potential in [12], and we will not repeat it here. We will give the derivation of the combination of the electrostatic effect and the Casimir effect briefly. We shall use the starting equation given in 2.76 with a Cartesian Laplacian, and the displacement function given in 2.77 with φ as above. We linearise the electrostatic and the Casimir effects using the first-order Taylor expansions

$$F_e \approx F_e(0) + F_c(0) + \frac{\mathrm{d}F_e(0)}{\mathrm{d}U}U + \frac{\mathrm{d}F_c(0)}{\mathrm{d}U}U \approx -\frac{\varepsilon_0\varepsilon_r V^2}{2d^2} - \eta\frac{\pi^2\hbar c}{240d^4} + \frac{\varepsilon_0\varepsilon_r V^2}{d^3}U + \eta\frac{\pi^2\hbar c}{60d^5}U, \qquad (2.94)$$

and as before, only keep the non-static terms. We integrate over the entire membrane surface and multiply with the desired modeshape, i.e. $\varphi_{1,1}$

$$\int\int_A \left(\rho h\frac{\mathrm{d}^2U}{\mathrm{d}t^2} - \sigma h\nabla^2 U - \left(\frac{\varepsilon_0\varepsilon_r V^2}{d^3} + \eta\frac{\pi^2\hbar c}{60d^5}\right)U\right)\varphi_{1,1}dxdy = 0. \qquad (2.95)$$

After we work out the double time derivative and the Cartesian Laplacian, we multiply with the fundamental mode, and divide out the x and y dependent terms, we can rewrite the equation and find the softened eigenfrequency

$$\omega_{1,1}^2(V,\eta) = \omega_{1,1}^2(0,0)\left(1 - \frac{1}{2}\frac{L^2}{\pi^2\sigma h}\left(\frac{\varepsilon_0\varepsilon_r}{d^3}V^2 + \eta\frac{\pi^2\hbar c}{60d^5}\right)\right), \qquad (2.96)$$

with $\omega_{1,1}^2(0,0) = 2\frac{\pi^2}{L^2}\frac{\sigma}{\rho}$.

2.4.5. Pull-in with Stiffness Softening

With our softened eigenfrequencies found for circular and square membranes, we are ready to tackle the pull-in problem, which we attempted before. We have now derived the softening effect and will use it to find a better approximation for the pull-in voltage and pull-in distance than $d/3$.

As discussed before, 'pull-in' in MEMS and NEMS design occurs when using attractive forces such as electrostatics. Pull-in occurs when a structure's restoring force is not able to balance out the displacing force. This results in the structure elastically deforming, snapping or becoming stuck to another part.

The case of membrane pull-in in the case of electrostatics has been extensively explored in recent years [52–54]. The case of an additional Casimir force field has also been explored by various authors [55–57], but one for circular membranes remains rare. A full, in-depth analysis of the pull-in effect for a continuum structure strained by multiple nonlinear distance-dependent attractive force fields can be complex, and an elaborate exploration deserves a thesis in itself. We will therefore again opt for a lumped order model with the softening effect included in order to find the voltage at which our structures fail for a given gap size. This method follows the derivation presented by [58], with numerous adjustments to fit our specific situations.

Pull-in Voltage for Circular Membranes

A lumped element model of two circular plates is shown in figure 2.10. The top plate is pulled towards the bottom one with an electrostatic force, and now also by the Casimir force. These forces are balanced out by the spring constant k_{eff}. We are under the assumption that the membrane deflection is very minute compared to its own size. This means that we can ignore the geometric nonlinear hardening effects and that we can effectively model voltage pull-in using this simplified model with spring softening. When we include the Casimir effect, we have for our force equation.

$$kU = -\frac{1}{2}\frac{A\varepsilon_0\varepsilon_r V^2}{(d+U)^2} - \frac{A\pi^2\hbar c}{240(d+U)^4}. \tag{2.97}$$

We would ideally like to find the maximum deflection U_{max} like we did before as a good starting point. We follow our previous method and calculate the derivative of 2.97 with respect to U,

$$k = \frac{A\varepsilon_0\varepsilon_r V^2}{(d+U)^3} + \frac{A\pi^2\hbar c}{60(d+U)^5}. \tag{2.98}$$

Filling in k using its newfound definition into 2.97, we find

$$\left(\frac{A\varepsilon_0\varepsilon_r V^2}{(d+U)^3} + \frac{A\pi^2\hbar c}{60(d+U)^5}\right)U = -\frac{1}{2}\frac{A\varepsilon_0\varepsilon_r V^2}{(d+U)^2} - \frac{A\pi^2\hbar c}{240(d+U)^4}. \tag{2.99}$$

Now, we have an equation in which we cannot isolate U, find U_{max} and by extension, also not V_{max}. One could use root-finding algorithms, although finding the correct roots of equations like these proves to be surprisingly difficult. We will therefore keep U as a free variable, and we will later find its perfect value by fitting and find the pull-in voltage via a different technique.

We want to write the spring constant, affected by the spring softening, as a function of the maximum deflection and the voltage. We will re-use 2.90, in which we linearised the force fields around the centre deflection as our starting point, as we assumed our deflections to be small compared to the membrane itself. We take 2.90 and use 2.86 to write

$$\omega_{1,1}^2(V,\eta) = \frac{\alpha^2}{R^2}\frac{\sigma}{\rho} - \frac{\varepsilon_0\varepsilon_r}{\rho h}\frac{V^2}{d^3} - \eta\frac{\pi^2\hbar c}{60\rho h}\frac{1}{d^5}. \tag{2.100}$$

Via the definition of the resonance frequency, we write:

$$\omega^2 = \frac{k_{eff}}{m_{eff}} = \frac{k - k_{soft}}{m_{eff}}, \tag{2.101}$$

we may then use the effective mass of a circular membrane, which is dependent on the eigenmode, $m_{eff} = 0.2695\rho\pi R^2 h = \gamma\rho\pi R^2 h$ [59], to write for k_{eff}:

$$k_{eff} = k - k_{soft} = \left(\frac{\alpha^2}{R^2}\sigma - \frac{\varepsilon_0\varepsilon_r}{h}\frac{V^2}{d^3} - \eta\frac{\pi^2\hbar c}{60h}\frac{1}{d^5}\right)\gamma\pi R^2 h. \tag{2.102}$$

We now define the following:

$$k = \frac{\alpha^2\sigma}{R^2}\gamma\pi R^2 h \qquad \text{and} \qquad k_{soft} = \left(\frac{\varepsilon_0\varepsilon_r}{h}\frac{V^2}{d^3} + \eta\frac{\pi^2\hbar c}{60h}\frac{1}{d^5}\right)\gamma\pi R^2 h. \tag{2.103}$$

With these definitions made, we can now substitute k_{eff} in 2.97 for k:

$$\left(k - \left(\frac{\varepsilon_0\varepsilon_r}{h}\frac{V^2}{d^3} + \eta\frac{\pi^2\hbar c}{60h}\frac{1}{d^5}\right)\gamma\pi R^2 h\right)U = \frac{1}{2}\frac{A\varepsilon_0\varepsilon_r V^2}{(d+U)^2} + \eta\frac{A\pi^2\hbar c}{240(d+U)^4}. \tag{2.104}$$

As said previously, when deriving the softening terms, the deflections are assumed to be very small compared to the size of the membrane. We can therefore use parallel plate approximation ($d + U \approx d$) on the right-hand side of 2.104 around the equilibrium position $U = 0$ without introducing a significant error. Reshuffling terms gives us

$$kU = \frac{1}{2}\frac{A\varepsilon_0\varepsilon_r V^2}{d^2} + \eta\frac{A\pi^2\hbar c}{240}\frac{1}{d^4} + \left(\frac{\varepsilon_0\varepsilon_r}{h}\frac{V^2}{d^3} + \eta\frac{\pi^2\hbar c}{60h}\frac{1}{d^5}\right)\gamma\pi R^2 hU. \tag{2.105}$$

2.105 is similar in form to 2.97. The right-hand side of 2.105 describes a force that can be used to find the pull-in voltage. To that end, we will use formula 26a given by Sarafraz et. al [60] which relates the pressure on a circular membrane to its centre displacement. We first use the definition $P = F/A$ to transform 2.105 into a formula for the pressure, and equate its right-hand side to formula 26a by Sarafraz et. al:

$$\mathscr{A}\frac{n_0}{R^2}U + \mathscr{B}\frac{Eh}{R^4}U^3 = \frac{1}{2}\frac{\varepsilon_0\varepsilon_r V^2}{d^2} + \eta\frac{\pi^2\hbar c}{240}\frac{1}{d^4} + \left(\frac{\varepsilon_0\varepsilon_r}{h}\frac{V^2}{d^3} + \eta\frac{\pi^2\hbar c}{60h}\frac{1}{d^5}\right)\gamma h U. \tag{2.106}$$

Here, $\mathscr{A}$ and $\mathscr{B}$ are values that can be found in the paper, in our case, they are equal to 3.61 and 2.2837, respectively. Finally, we can now collect the voltage-dependent terms and rewrite 2.106 to find the voltage as a function of U, where we will fill in U_{max} for the pull-in voltage:

$$V_{PI}(\eta, V) = \sqrt{\frac{\mathscr{A}\frac{n_0}{R^2}U_{max} + \mathscr{B}\frac{Eh}{R^4}U_{max}^3 - \eta\frac{\pi^2\hbar c}{240}\left(\frac{1}{d^4} + \frac{4\gamma U_{max}}{d^5}\right)}{\varepsilon_0\varepsilon_r\left(\frac{1}{2d^2} + \frac{\gamma U_{max}}{d^3}\right)}}. \tag{2.107}$$

In the results, this function will be plotted for various values of U and compared to the pull-in voltage values given by the COMSOL model. The best fit for U_{max} can then be found and the according pull-in voltages determined analytically.

Circular Deflection Distance

In equation 2.107, we have entered the yet to be determined U_{max} as our parameter for when the pull-in phenomenon occurs. We may also forego U_{max} and instead want to find the deflected distance of the centre of our membrane for a given voltage with the Casimir effect present for a certain gap size. To this end, we re-state equation 2.106 again

$$\mathscr{A}\frac{n_0}{R^2}U + \mathscr{B}\frac{Eh}{R^4}U^3 = \frac{1}{2}\frac{\varepsilon_0\varepsilon_r V^2}{d^2} + \frac{\pi^2\hbar c}{240}\frac{1}{d^4} + \left(\frac{\varepsilon_0\varepsilon_r}{h}\frac{V^2}{d^3} + \frac{\pi^2\hbar c}{60h}\frac{1}{d^5}\right)\gamma U.$$

To find our deflection distance, we will again perform an approximation. Looking at the left-hand side, we may notice that the term proportional to U^3 is significantly lower in magnitude than the term proportional to U. For example, if we assume our deflection to be $100\,\mathrm{nm}$ and our radius to be $0.4\,\mathrm{mm}$, then the term proportional to U is more than 6000 times larger in magnitude. We shall thus discard the U^3 term to simplify our equation. If we now collect our U dependent terms and rewrite for U, we find

$$U = \frac{\frac{1}{2}\frac{\varepsilon_0\varepsilon_r V^2}{d^2} + \frac{\pi^2\hbar c}{240}\frac{1}{d^4}}{\mathscr{A}\frac{n_0}{R^2} - \left(\varepsilon_0\varepsilon_r\frac{V^2}{d^3} + \frac{\pi^2\hbar c}{60}\frac{1}{d^5}\right)\gamma}. \tag{2.108}$$

This equation will give us the approximate deflection of the centre of the membrane due to the electrostatic and Casimir forces. We should be wary of using this approximation for situations where the deflections grow large. The higher order Taylor terms in the softening of the resonance frequency, which in our formula are absent, might play a significant role the further the membrane deflects, and the neglected term proportional to U^3 will impact the accuracy increasingly for larger deflections. We can expect to see larger deviations from FEM results in these situations. Note that this equation does not tell us when pull-in occurs in itself, as it will give an arbitrary deflection distance even if $U > U_{max}$. U_{max} will have to be determined from FEM simulations and will provide a bound for the usefulness of this formula.

Pull-in Voltage for Square Membranes

As with the derivations shown for the eigenfrequencies and the frequency softening, the pull-in voltage calculations for square membranes are very similar to those for circular ones, with some subtle differences. Chowdury et. al performed a pull-in calculation for only the electrostatic effect for a square membrane [58], which served as a guideline for our derivation. We adjusted it to accommodate the

Casimir effect for our circular membranes, and we could, in principle, repeat their full calculation for a square membrane with the added Casimir effect, but we will refrain from doing so. Instead, we will state the differences and present the results here. Our starting point is naturally different as we will use 2.96 instead of 2.87. We are then able to follow the same steps as in the circular case, remembering that the effective mass of a square membrane is $m_{eff} = m/4$. We have one further change to our procedure, which is the pressure-deflection formula. We used one for circular membranes presented by Sarafraz et. al [60] and shall now use the one for square membranes presented by Maier et. al [61], which is defined as

$$P(U) = C_1 \frac{n_0}{(L/2)^2} U + C_2(\nu) \frac{Eh}{(L/2)^4} U^3, \tag{2.109}$$

with $C_1 = 3.45$ and $C_2 = \frac{1.994(1-0.271\nu)}{(1-\nu)}$.

Following the above described procedure with these adjustments, for the pull-in voltage for a clamped square membrane we then have

$$V_{PI} = \sqrt{\frac{C_1 \frac{n_0}{(L/2)^2} U_{max} + C_2 \frac{Eh}{(L/4)^4} U_{max}^3 - \eta \frac{\pi^2 \hbar c}{240} \left(\frac{1}{d^4} + \frac{U_{max}}{d^5} \right)}{\varepsilon_0 \varepsilon_r \left(\frac{1}{2d^2} + \frac{U_{max}}{4d^3} \right)}}. \tag{2.110}$$

For its centre deflection distance, we find

$$U = \frac{\frac{1}{2} \frac{\varepsilon_0 \varepsilon_r V^2}{d^2} + \frac{\pi^2 \hbar c}{240} \frac{1}{d^4}}{C_1 \frac{n_0}{(L/2)^2} - \frac{1}{4} \left(\varepsilon_0 \varepsilon_r \frac{V^2}{d^3} + \frac{\pi^2 \hbar c}{60} \frac{1}{d^5} \right)}. \tag{2.111}$$

Note that the factor $\gamma = 0.2695$ is very close to $1/4$ for the effective mass of the circular and square membranes, respectively.

2.4.6. Geometric Nonlinearity

In our previous derivations, we assumed the membrane deflections to be negligible enough to exclude hardening effects due to geometric nonlinearities. Geometrical nonlinearities are common in MEMS resonators, as resonators often are driven into the high-amplitude regime. It is, however, not necessary for the resonator to be pushed to extremely high amplitudes for the geometric nonlinearity to take hold and affect its dynamics noticeably. Geometric nonlinearity is a consequence of the boundary conditions of a resonator [13]. In the systems of our interest, namely clamped membranes, the boundary conditions prevent the structures from moving at the boundaries. This means that if the membrane is to oscillate transversely, it is inescapable for the membrane material to not deform slightly by means of flexural bending or stretching. When the membrane deflects from its equilibrium position, it stretches and compresses longitudinally. For a circular MEMS, this stretching, for the base frequency mode as shown in figure 2.5a, is radially symmetric. A schematic side view of a deflected circular membrane is shown in figure 2.12.

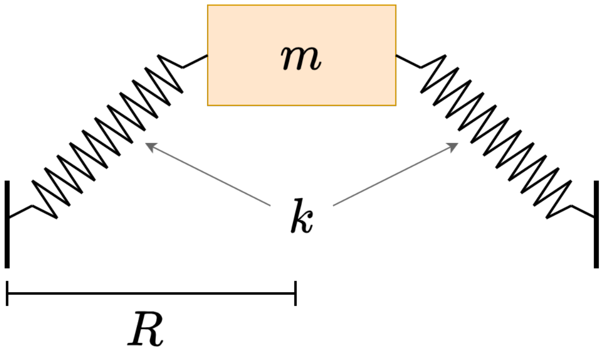

Figure 2.12: Side view schematic of a circular membrane resonator during oscillation with a high amplitude. The high amplitude causes radially symmetric elongation and increases the longitudinal strain. This triggers the rise of the geometric nonlinearity, which has a hardening effect on the stiffness of the resonator, making its resonance frequency rise.

Figure 2.12 shows the membrane material as springs. The stiffness of these springs is directly related to the elongation along their radial coordinate according to Hooke's law. If the length of the springs at rest is equal to R, and the height of an arbitrary amplitude is H, then the length of the spring at this amplitude is equal to $R_2 = \sqrt{R^2 + H^2}$. Using Hooke's law $F = -kx$ we write $F = -k(R - R_2)$. The force component parallel to the direction of the oscillation can be found by multiplying by the sine of the angle between the equilibrium position and the new position of the spring, which is equal to the opposite divided by the hypotenuse: We then write for the total force in the transverse direction, i.e. the direction of oscillation for the two springs [14]:

$$F = 2k(R - R_2)\frac{H}{\sqrt{R^2 + H^2}} = 2\left(\frac{kHR}{\sqrt{R^2 + H^2}} - kH\right). \tag{2.112}$$

Already, a linear and a nonlinear part can be identified from this relation. Taylor expanding this equation will result in the appearance of a Duffing parameter.

As this elongation changes periodically during oscillation, the spring stiffnesses of both springs do too and the change to the frequency as a result as well. For higher order modes and square membrane configurations, shown in figures 2.5 and 2.6, this elongation is not necessarily radially symmetric any more. These varying spring constants can have a hardening or softening effect on the resonance frequency depending on the situation, with influence from variables such as the drive frequency, stiffness, clamping type, geometry of the resonator, and more [14] [62].

An accurate calculation of geometric nonlinearity is quite cumbersome to perform and we refrained from doing so up until this point. However, for our high aspect ratio systems, it might be justifiable to omit it. As mentioned before, the geometric nonlinearity is generally associated but not exclusive to resonators driving at large amplitudes. The geometry of the devices of our interest means that the ratio of the oscillation amplitudes compared to the radius of the membrane at rest will be on the order of $d/R < 1/10000$. Still, we would like to prove that this geometric nonlinearity is negligible and for that we will use a formula given in Steeneken et. al [63]. The range of the gaps between the membrane and the backplate will be approximately $200\,\mathrm{nm}$ - $800\,\mathrm{nm}$. Steeneken et. al derive an approximate formula for the exact centre deviation of a circular membrane drum, for which the nonlinear stiffness is 10% of the magnitude of the linear stiffness. They define the onset of the nonlinear regime beyond this deflection. This choice is arbitrary, as there is no real, recognisable well-defined regime. We will follow this choice of ratio between the linear and nonlinear stiffnesses, with the onset of the nonlinear regime where one has to account for nonlinear effects, the moment that the nonlinear stiffness exceeds 10% of the linear stiffness in magnitude. It is given as

$$U_{\text{non linear}} = \sqrt{\alpha\frac{3n_oR^2(1-\nu)}{2Eh}}, \tag{2.113}$$

where n_0 is the initial material stress, E the Young's modulus, α is the ratio between the nonlinear stiffness and the linear stiffness, in this case equal to 0.1, h the membrane thickness and ν the Poisson ratio. Using the experimentally obtained values of one of our systems which we use in our simulations prematurely, which one can find in tables 3.1 and 3.2 in the next chapter, we find a center deviation of $\approx 7.7\,\mu\mathrm{m}$ for which the nonlinear stiffness reaches 10% of the linear stiffness in magnitude. Beyond this deviation, we consider the resonator to enter the nonlinear regime.

A deflection of $7.7\,\mu\mathrm{m}$ is beyond any deviation that will be possible in our systems as the maximum gap size that we will consider is $800\,\mathrm{nm}$, a deflection of that size will lead to the membrane colliding with the backplate due to Casimir and or electrostatic forces. As mentioned before, according to [47], U_{max} is approximately equal to $0.44d$ for a system with only an electrostatic force. Incorporating the Casimir force into this model will undoubtedly reduce this distance, meaning we can expect a $U_{max} < 0.44 \cdot 800 = 350\,\mathrm{nm}$, which is far below our nonlinear regime threshold. We can flip 2.113 around and solve for α to discover that the influence of the nonlinear stiffness in our system will always be $<< 1\%$ of the linear stiffness, justifying its omission from our analytics.

3

Setup and Finite Element Model

We have now shown the fundamentals of resonators and explored the analytics behind the mode-shapes and eigenfrequencies of square and circular membranes. We found that nonlinear forces such as the Casimir effect and electrostatics offer a surprising potential opportunity due to their softening effect, with the flip side being a possible pull-in occurrence. After determining other nonlinearities to be negligible, we are now ready to take a look at the experimentally fabricated resonators, off of which our simulations will be based. We hinted at some of their features earlier on, but we will now highlight the key characteristics that distinguish these resonators and what makes them worthwhile investigating. These insights will provide a deeper understanding of their fabrication, operation and important parameter values crucial to their unique characteristics.

We will then continue by diving into simulating these resonators and the steps that were taken to validate those computer models. At the end of this chapter, we will be ready to explore the opportunity of improving the responsivity of our resonators using nonlinear force field effects.

3.1. General Overview

Our 2-dimensional resonators consist of a membrane clamped on all sides, suspended above a parallel cavity bottom, equal in shape. Schematics of both the circular and the square type, which have not been drawn to scale, are shown in figures 3.1 and 3.2.

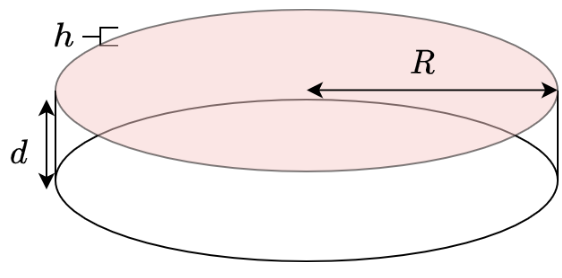

Figure 3.1: Schematic representation of a clamped circular membrane resonator. The image is not to scale. Shown are important resonator parameters such as the radius R, thickness h and the size of the gap, or the cavity, between the membrane and the cavity bottom d.

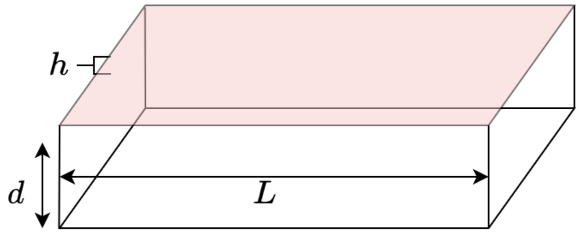

Figure 3.2: Schematic representation of a clamped square membrane resonator. The image is not to scale. Shown are important resonator parameters such as the length L, thickness h and the size of the gap, or cavity, between the membrane and the cavity bottom d.

Important parameters are the area defining lengths: R and L, the membrane thickness h and the size of the gap between the suspended membrane and the bottom of the cavity below it d. The cavity bottom is carefully fabricated to be as smooth as possible, as is the resonator, to enable an extremely parallel surface to act as a parallel plate setup for electrostatics and Casimir forces. The signature feature of these sensors is their extreme aspect ratio between the cavity gap d and the size of the resonator, whilst maintaining a small membrane thickness h.

The resonators subject to our research are based on experimental resonators fabricated by Xu. et al, featured in [64] and [65]. These concerned square membranes with a lengths L of up to $0.7\,\mathrm{mm}$, or radius R up to $0.4\,\mathrm{mm}$, suspended above cavity gaps ranging from $200\,\mathrm{nm}$ to $1500\,\mathrm{nm}$, and with a maximum membrane thickness of $150\,\mathrm{nm}$. These sizes result in a maximal aspect ratio of 1/3500 between the cavity depth and the membrane side length. To put that into perspective, the average size of a football field (or soccer as named by some) is 100 meters. A sensor of that ratio at that scale would consist of two perfectly parallel square 100 by 100 meter football fields separated by a 2 euro coin. The thicknesses of these square football fields would be thinner than the gap between them, highlighting the extremes of this sensor, the materials and the great lengths Xu et. al had to go to to fabricate such devices.

3.2. Fabrication and Operation

The fabrication of these sensors is extremely difficult without having the two plates stick to each other during fabrication, making the technology state-of-the-art. These extreme aspect ratios allow the resonator to stay within the softening regime and not enter the realm where geometric nonlinearity plays a large influence, as the membrane deflection during oscillation is negligible compared to its other dimensions. The state-of-the-art aspect ratio also increases the Casimir force and the electrostatic force due to the extreme parallelism combined with a large surface area.

3.2.1. Membrane Materials

The membrane material can vary in principle, but requires several important properties to be considered for these kinds of devices. These properties are

- High stiffness due to high material stress to be able to withstand falling onto the cavity bottom during fabrication or during oscillation. It should be able to withstand additional transverse forces created by external pressures or nonlinear force fields.
- Possible to fabricate using existing nanofabrication techniques and machinery. Especially its resistance to certain etching techniques to facilitate the removal of layers below it, to suspend it without any damage to the cavity bottom or membrane.
- Metals in general are preferred as these boast high reflectivities, which facilitate Casimir forces and electrostatics, although dielectrics might still be of interest if they boast any reflective properties. Non-reflective insulators can be used, but not in conjunction with electrostatics and or Casimir forces.

The fabrication of these resonators naturally differs for different materials, as aspects such as etchant, exposure times, and deposition techniques might vary. We mean to provide a general overview of how the membranes are fashioned on a silicon substrate. This will thus inescapably exclude many details and intermediate steps. For a highly detailed approach on NbTiN membranes, we refer the reader to [64], an aluminium recipe is shown in [37], and information on the SiC membranes device is given by [65].

NbTiN is a type II superconductor [66], giving it ideal electromagnetic reflective and conductive properties below T_c, meaning we can expect $\eta = 1$ and electrostatics to work well. SiC is an insulator [67] in its pure form, but can be doped to create a semiconductor [68]. It therefore boasts low reflective properties $\eta << 0.5$, with $\eta = 0.5$ if the cavity bottom is coated with a conductor. It will not respond to voltages in its pure form but can be actuated by them when coated with conducting films, as shown in [69].

3.2.2. Fabrication Steps

We start, as with almost every electronic device in the world, with a silicon base. Silicon is a preferred base due to its abundance, but it is also highly adaptable due to the availability of highly selective etching techniques. This also makes silicon a preferred so-called 'sacrificial layer'. This is a layer which plays a role early on in fabrication but is removed later [70]. This use of silicon is also the case when fabricating these membranes. The very first step in fabrication is the deposition of the desired cavity bottom material. This is often the same material as the membrane itself, but can be varied if so desired. Important is an extremely smooth surface to facilitate conditions for Casimir forces and electrostatics. The fabrication step is shown schematically, not to scale, in figure 3.3.

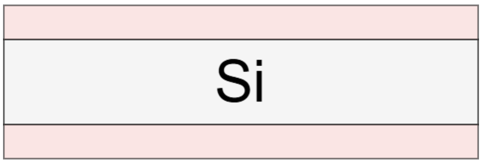

Figure 3.3: Schematic side view of the first fabrication step. Shown is a slice of a much larger wafer. The image is not to scale and simplified. Shown in grey is the silicon wafer acting as a base. The wafer is then coated in a thin equilateral layer of material, which is usually the same material out of which the membrane will be fabricated. This does not have to be the case, however.

The deposition is usually performed using techniques such as LPCVD or ICPECVD to accommodate the parallelism between the cavity bottom and the membrane later on. As the material builds wherever it comes in contact with silicon, the entirety of the chip, including the bottom, will be layered with it even though this is not necessary. A sacrificial layer has to be deposited next onto the top of the chip as shown in figure 3.4.

Figure 3.4: Schematic side view of the second fabrication step. Shown is a slice of a much larger wafer. The image is not to scale and simplified. Shown in blue is the sacrificial layer. The sacrificial layer is usually silicon, just as the base shown in grey.

The sacrificial layer is shown in blue, it is usually silicon, the same material as the base shown in grey, but this does not have to be the case, which is why we differentiate it. It will later be removed, but for now aids in the fabrication of the membrane structure. Fabrication step 3 is the step where the membrane is created, and a repetition of fabrication step 1. The entire chip is covered using the material that the membrane consists of. We display it using the same colour as the cavity bottom in figure 3.5.

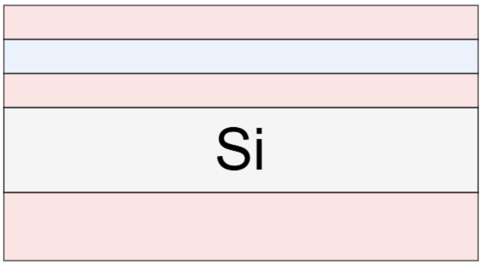

Figure 3.5: Schematic side view of the third fabrication step. Shown is a slice of a much larger wafer. The image is not to scale and simplified. The chip is again covered fully in the material the membrane is fashioned of, in this case the same as the cavity bottom.

The membrane has been fabricated but is stuck to the sacrificial layer, which has to be removed. This process is known as 'lift-off' [71]. This is not possible in in the current situation as there is no way to get at this sacrificial layer. In order to remove it, we have to go through the membrane itself. Using a mix of resist spinning, optical lithography and washing techniques, a layer of resist with little holes in them is applied on the membrane top. Using an anisotropic etching process, meaning directional, the holes in the resist are elongated by etching the membrane material away until the sacrificial layer is reached. After cleaning of the resist, the situation is as the one shown in figure 3.6.

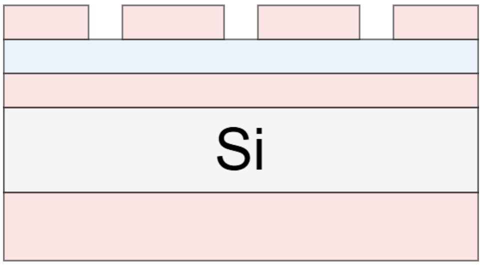

Figure 3.6: Schematic side view of the situation after the membrane has been patterned. Shown is a slice of a much larger wafer. The image is not to scale and simplified. The membrane has been patterned with little holes by means of resist spinning and optical lithography techniques.

Due to the membrane now being patterned with holes, there is a way to reach the sacrificial layer. The holes lower the parallel plate effects such as the Casimir effect and electrostatics somewhat, as these are directly linked to the surface areas that the two plates share. The holes are patterned with intervals. Important being the distance between the holes, which should be large compared to the membrane gap d. Now, to remove the sacrificial layer, one has to be careful. The etch needs to be extremely selective, as the etch should only etch away the sacrificial layer and ideally not harm the membrane and the bottom of the cavity in order to conserve the parallelism. The etch, due to the sacrificial layer being present everywhere under the membrane, has to be an isotropic one, meaning it etches in all directions. One should not make the mistake of using a wet etch, as the narrow cavity will trap some etchant irreversibly, which will lead to capillary forces pulling the membrane down, causing the membrane to stick to the cavity bottom and the sensor failing. An isotropic plasma etch is therefore among the preferred methods. Once the sacrificial layer has been etched away, the membrane is suspended above the cavity. The final situation is shown in figure 3.7. Note that the sides which clamp the membrane have not been sketched.

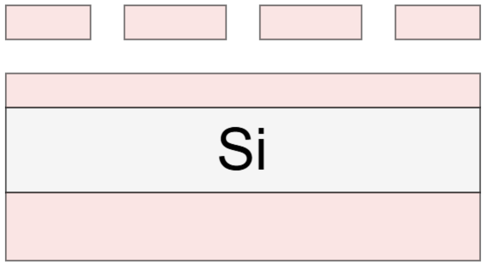

Figure 3.7: Schematic side view of the situation after the membrane has been suspended in a process called 'lift off'. Shown is a slice of a much larger wafer. The image is not to scale and simplified. The membrane hangs above the cavity bottom freely and is clamped on its sides (not shown) by removing the intermediate sacrificial layer.

3.2.3. Actuation and Detection

As shown in oscillator theory earlier on, in order to obtain an output signal which can be related to exterior influences such as force or mass, one usually needs to drive the resonator. Although for resonators of extremely high Q's, one can read out the resonance peak from the Brownian thermal noise alone, as shown by Davidovikj et. al in [72], an actuation mechanism is usually still needed. Electrostatic actuation is a method used to actuate a membrane [73]. One can ground one of the plates in the parallel plate configuration and put an AC voltage on the flexible sensor in order to make it oscillate. Detection using electrostatics is a tried and tested method used in MEMS microphones, where the change in the capacitance due to the change in distance between the flexible plate and the static ground plane can be read out [74]. A second method for both actuation and detection is thermoelastics [14]. Thermoelastic actuation is performed by using local heating with pulses from, for example, a laser. The local heating in the membrane creates stress in the material due to the local thermal expansion of the material. If this heating is performed with pulses with the right timing, the resonator will start to oscillate. It can also be used to detect the motion of a resonator by pointing a low-energy laser at the resonator to prevent too much heating. One can then find the resonator's amplitude or frequency by reading out the reflected light using a Fabry-Perot interferometer in combination with conversion algorithms [75].

As the field of mechanical resonators is broad, other varieties of transduction and detection techniques exist [12] such as electrodynamics [76], capacitive actuation [77], piezoresistivity [78], piezoelectrics [79] and optical actuation [80].

3.3. Finite Element Modeling

Analytics are insightful but limited in their applications. As one will have noticed, with the derivations shown in the theory, approximations are quickly made to decrease the rapidly growing complexity of equations, even for relatively simple systems such as the resonators of our study. In order to analyze our systems to a deeper extent we will use the finite element method (FEM). For the finite element model of the membrane resonators, we will use the commercially available COMSOL Multiphysics as it boasts numerous MEMS-related multiphysics packages that specialise in membranes, electrostatics, nonlinear analyses and more.

The membranes experimentally fabricated, characterised and used for measurements„ which we will attempt to replicate directly, were fashioned out of NbTiN [64] and SiC [65] as mentioned before. The parameter values given in these papers for our materials will be used in our simulations. In our simulations, we do not go for bigger gaps than $800\,\mathrm{nm}$. Casimir forces at distances larger than this play no significant role in the membrane oscillation, electrostatics, in principle, can be investigated with higher voltages, but to investigate the interplay between the two, the cavity size is kept within the Casimir regime.

3.3.1. Model Parameter Values

In our prospective simulations, we will use the two earlier-mentioned materials to generate results. The parameter values for these three materials have been collected, in table 3.1. All of the system parameters for circular and square membranes are collected and presented in table 3.2.

Table 3.1: Film material parameters used in COMSOL and analytical models [64][65].

Parameter	Symbol	Unit	NbTiN	a-SiCR3
Young's modulus	E	GPa	441	210
Density	ρ	$\mathrm{kg/m^3}$	4291	2962
Poisson's ratio	ν	-	0.252	0.199
Material stress	σ	MPa	533-566	960
Thickness	h	nm	160	81

The dimensions of the to be modelled resonators are based on the experimental square membranes fabricated in [64] with sides of $L = 0.7\,\mathrm{mm}$. Circular membranes of these dimensions were not produced. We therefore choose to simulate circular membranes with an area equal to the square ones, meaning $R = 0.4\,\mathrm{mm}$.

Table 3.2: Membrane parameter values used in COMSOL and analytical simulations.

Parameter	Symbol	Value
Radius (circle)	R	$0.4\,\mathrm{mm}$
Side length (square)	L	$0.7\,\mathrm{mm}$
Gap size	d	$200\,\mathrm{nm}$-$800\,\mathrm{nm}$
Effective mass (circle)	$m_{eff} = 0.2695m$	$0.2695\rho h\pi R^2$
Effective mass (square)	$m_{eff} = m/4$	$\rho h L^2/4$

If we now remember formula 2.14 in the theory, we may test if these resonators are plates or membranes. Using the experimental parameters for a circular resonator, we find the value of $8.4 \cdot 10^4$, meaning we are dealing with a membrane.

The reason for us limiting ourselves to a minimum gap size of $200\,\mathrm{nm}$ is twofold. First off, we base our models on the experimentally fabricated membranes mentioned earlier, and in these experiments lower gaps were never attempted. The second reason is that we want to stay in the current force regime. With gaps smaller than $200\,\mathrm{nm}$ we can expect the distance between the cavity bottom and the centre of the membrane to reach less than $100\,\mathrm{nm}$. At this size, other forces become dominant and a new force regime is entered. Especially the VanderWaals forces are of concern, which we have not considered in our analytics and which we will also not include in our simulations further on. These forces will undoubtedly influence the resonator significantly, and we therefore do not simulate gap sizes smaller than $200\,\mathrm{nm}$.

One last thing to remark is that the experimental resonators were all tested in a vacuum environment. This rules out effects such as damping due to trapped air within the cavity, which is a significant challenge in resonator engineering. It is known as squeeze film damping, which can lead to various effects which are difficult to model accurately. A comprehensive coverage is given by Bao et. al on various types of squeeze film damping models [81]. We will assume our resonators to operate in a vacuum as well and not simulate any damping forces.

3.3.2. Model Choices

An immediate challenge that arises when modelling these particular membranes is their demanding aspect ratio. Finite element simulations are expensive time-wise as is, and a membrane of this size with a mesh fine enough to accurately simulate the small gap sizes leads to COMSOL showing errors when handling the membrane physics and thus, complexity has to be reduced. As mentioned before, the resonator is a membrane rather than a plate due to it sustaining transverse loads using in-plane stresses rather than bending stresses. A simple reduction in complexity could be made by using a shell model, as a shell-type structure is significantly less computationally expensive for larger structures due to the absence of transverse shear calculations.

A second challenge lies in the implementation of the nonlinear force fields. COMSOL readily provides an in-built multiphysics package which combines the shell-type structure calculations with electrostatics. Unfortunately, due to the Casimir effect being a relatively unpopular area of scientific research compared to electrostatics, it is not provided as a base multiphysics package within COMSOL. This means that the Casimir effect has to be modelled in a different manner, such as by entering its analytical formula as a force applied to the shell structure. An analytical force formula is much less computationally taxing than a full-on multiphysics calculation, which is an advantage. However, we do not know if the implementation of a nonlinear force field by entering its analytical representation as a face load on the membrane is accurate enough compared to the multiphysics package. If this were the case, then the possibility of reducing both effects to formulas implemented as face loads would provide an exciting opportunity to simplify the simulations significantly. We therefore want to validate whether this simplified implementation of the forces is correct compared to the multiphysics packages. To accomplish this, we will build two models of a circular membrane resonator using the parameter values for NbTiN, one using the electrostatic-shell multiphysics package, and one using a force defined as 2.63. A comparison of both models will prove the validity of this approach

3.3.3. Validation

Force Calculation

We set out to validate the implementation of a nonlinear force field using its analytical representation as a face load in COMSOL. In order to do so, we will use the electrostatic effect and compare the implementation using the formula against the multiphysics package. The main differences between these two models from a physics standpoint lie in the fringe fields which are generated using the multiphysics package as they appear in reality. These fields are not captured by the analytical formula, given in 2.63. This equation, known as the infinite capacitor formula, is only valid for a system in which the distance between the plates is significantly smaller than the rest of the dimensions, which matches the description of our membrane resonator systems. We could use the Kirchoff formula instead of 2.63 in our model, but we would prefer to keep 2.63 if possible to keep the model complexity to an absolute minimum. Using equation 2.64 in conjunction with 2.63 we find our force correction factor to range from $\approx 0.18\% - 0.64\%$ for gap sizes between $200\,\mathrm{nm}$ and $800\,\mathrm{nm}$ in our circular membranes. These percentages are small enough that we have reason to believe that the fringing force fields will play little to no role in our model.

To validate the implementation of the force by formula, we sweep the voltage from ± 1 volts in both models and calculate the eigenfrequencies, using a gap size d of $250\,\mathrm{nm}$ and the parameter values for a circular NbTiN membrane. The result is shown in figure 3.8.

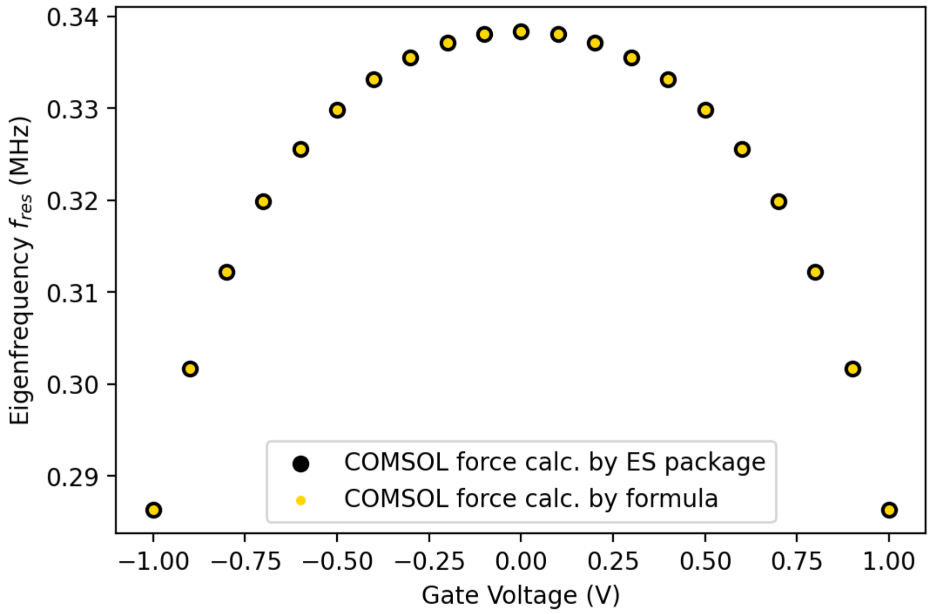

Figure 3.8: Frequency softening response of a circular nanoresonator made, from NbTiN above a $250\,\mathrm{nm}$ cavity due to an attractive nonlinear electrostatic load. Two almost identical models are shown, with one calculating the electrostatic force with an analytical formula, and the other calculating it using the built-in multiphysics engine. They show a perfect match, validating the use of a formula in order to reduce calculation time.

Figure 3.8 shows a perfect match between the models, validating the use of analytical formulas as a means to calculate nonlinear forces. This means a significant reduction of model complexity, saving on computational time. With this result in mind, we turn our attention back to the Casimir effect. The Casimir effect does not create any fringe fields as the force is exclusively between the plates. This means we can then, by extension, assume that the implementation of the Casimir effect in this manner is correct, which is good news as it was our only way of doing so. We now have a FEM model which is significantly reduced in complexity and ready to compare to our analytical models and to experimental results.

Experimental Validation of Models

With the COMSOL model having undergone significant improvements towards reducing its complexity without detriment to its accuracy, we now turn our attention to a very important test for not only the COMSOL model, but also our analytics presented in the theory. One could compare the FEM model to these analytics directly and see if they match, but we can do one better. A comparison with experimentally obtained values would determine both of their validities and could justify our assumptions, such as the negligible influence of the geometric nonlinearity.

We use data measured by Xu et. al on square membranes, fabricated from NbTiN separated, by a gap of $200\,\mathrm{nm}$ [64]. As mentioned before, NbTiN is a type 2 superconductor and thus the reflection of electromagnetic waves is maximised under the critical temperature within the cavity, i.e. $\eta \approx 1$. Xu et. al performed voltage sweeps from $\pm 0.3\mathrm{V}$ and measured the softened resonance frequency of the membrane per voltage. As mentioned in the theory, we can expect the simulations not to line up with the experimental data straight away, as the exponent n, which we set equal to 4 in the simulations, in reality often varies between 3 and 4. We can find the value of n for which the simulations match the experimental results. If this is within the range of possible values and the values match well, then we can conclude that the models are correct. We show the experimental data with results given by COMSOL and equation 2.96 in figure 3.9.

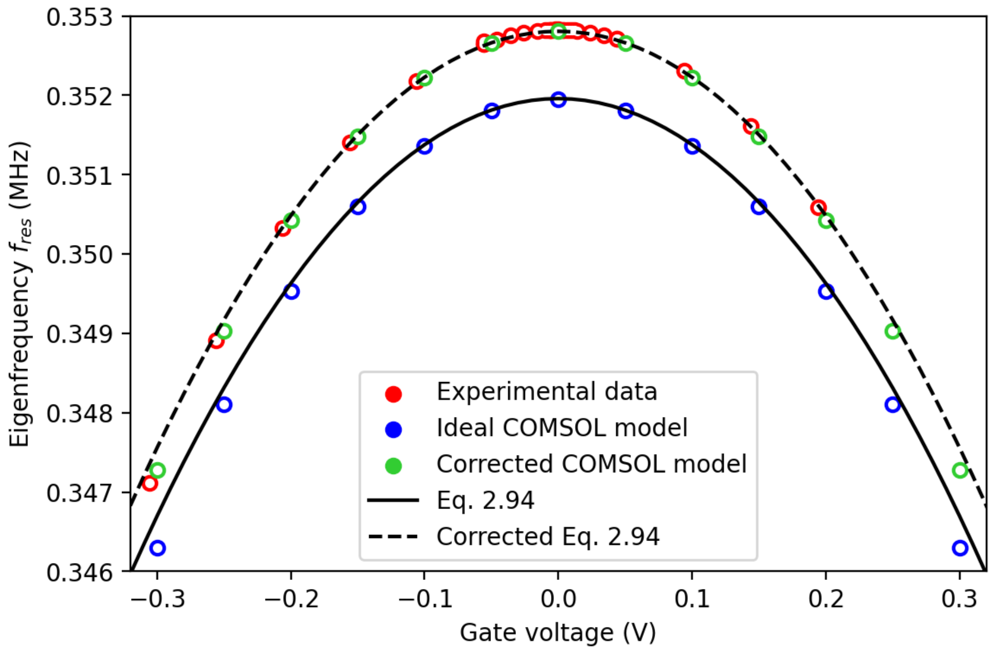

Figure 3.9: Comparison of analytical model and FEM model of a square NbTiN membrane with a cavity gap of $200\,\mathrm{nm}$ to experimental results measured by Xu et. al. The softening effect caused by electrostatics is visible and the comparison validates the analytical model and FEM model. As expected, the simulation data of the ideal situation $n = 4$ does not exactly match the experimental data. Using $n = 3.65$, we find the two models perfectly match experimental results.

We can be content, as figure 3.9 validates our analytical model and our COMSOL model of the membrane resonators. As we expected beforehand, the ideal case of $n = 4$ deviates from the experiments. A value of $n = 3.65$ does fit the experimental values perfectly, which is well within the range of possible exponent values. The analytical model does start to deviate from the values given by COMSOL and the experiment at larger voltages, an effect likely caused by the fact that we opted to only use first-order Taylor expansions instead of second or third-order ones. The COMSOL model does not suffer from this and proves accurate compared to the experimental values, even for the larger voltages. The deviation between the COMSOL model and the analytical formula grows significantly for even larger voltages, demonstrating the limited use of the analytics due to the approximations made. This deviation is shown in more detail and discussed in Appendix A. Note that the experimental data is shifted to the left as the voltage values were not exactly the same as the ones in our simulations.

We have now, next to the validation for the implementation of the force calculation, also validated that our COMSOL model can accurately model reality. We thus have a correctly functioning FEM model on our hands with which we will explore the interesting aspects of resonators in nonlinear force fields such as the possibility of increasing their responsivity as we imagined in the theory. We will continue to use $n = 4$ in our simulations going forward, as the parameter is highly dependent on the experimental setup and is thereby unique to every situation. We thus stick to the generalized ideal case of $n = 4$ for simplicity and generality, where we also note that this value gives the maximum force that can be created by the Casimir effect. The results should be appreciated with this in mind.

4 Results

With the theoretical knowledge of mechanical resonators under our belt we created an additional valuable tool in the form of a FEM model in the previous chapter. We simplified the model, validated it and are now ready to start our analysis of these nonlinearly strained mechanical resonators. We will first explore how the nonlinear forces change the eigenfrequency characteristics of these membranes and show their magnitudes. Afterwards, we will dive into the earlier-mentioned exciting potential avenue to increase the responsivity of our membrane resonators when using nonlinear force fields. We will set out to provide a full picture, and not merely sugarcoat the results. To that end, we will follow up on the increases in responsivity with analyses on pull-in voltages, pull-in deflections, and we will finish with potential applications and parameter sweeps to gain insight into the viability of fabricating these types of membranes for practical purposes. We will use the FEM COMSOL model throughout this chapter.

The reader might already have questioned our reasons for calling the sensor enhancement 'responsivity' and not 'sensitivity', sensitivity sounds much more exciting after all! Some authors [82] state that these are two terms that mean the same thing when it comes to resonators. The difference can be slight, however, and the truth is that it is difficult to determine if the potential enhancement to the resonators can be defined as sensitivity or responsivity definitively. Both sensitivity and responsivity are dependent on more than just this simulated system. They are influenced by the measurement apparatus, the 'perfectness' of the resonator, the environment of the experiment and many other variables. Sensitivity is the minimally measurable change in the output parameter compared to the noise floor. Noise is something that is completely missing in our simulations altogether. Responsivity is the swing in the output compared to the input, and that is something that we can easily determine with our simulations. The boost is therefore more easily justified as one in responsivity. We will thus refrain from naming the sensor enhancement an enhancement in sensitivity, as we have no proper way of confirming that it, too, is improved. Further research, especially experimental, could determine if this responsivity boost is also one in sensitivity.

4.1. Nonlinear Force Field Influence on Resonator Eigenfrequency

Earlier on in the theory, we found that nonlinear attractive forces affect the spring constants negatively of mechanical resonators. In other words, they reduce them or *soften* them. This means that the resonator is more easily pulled down and a further distance than it would with forces such as a static pressure. The spring constant is directly linked to the eigenfrequency of a resonator by $\omega = \sqrt{k/m}$, meaning that we can expect the eigenfrequency to reduce as well. We encountered this already in figure 3.9. The eigenfrequency is the defining output characteristic of a resonator, which is why the influence of nonlinear forces is a major player in resonator sensor applications. In our sensors, it is the dominating effect as the geometric nonlinearity is barely present for these geometries, as we determined in the theory.

We saw the minor softening influence of nonlinear forces such as the Casimir effect and electrostatics on the eigenfrequency already in figure 3.9. However, the frequency shifts can be more drastic than the one shown there. As an example, lets set the electrostatic voltage to $0.75\,\mathrm{V}$ in our COMSOL model and add the Casimir force with $\eta = 1$ for a circular NbTiN resonator using the parameter values given in tables 3.1 and 3.2, choosing $\sigma = 533\,\mathrm{MPa}$. We then sweep the gap size distance d from $200\,\mathrm{nm}$ to $800\,\mathrm{nm}$ and calculate for the eigenfrequency. The result is shown in figure 4.1.

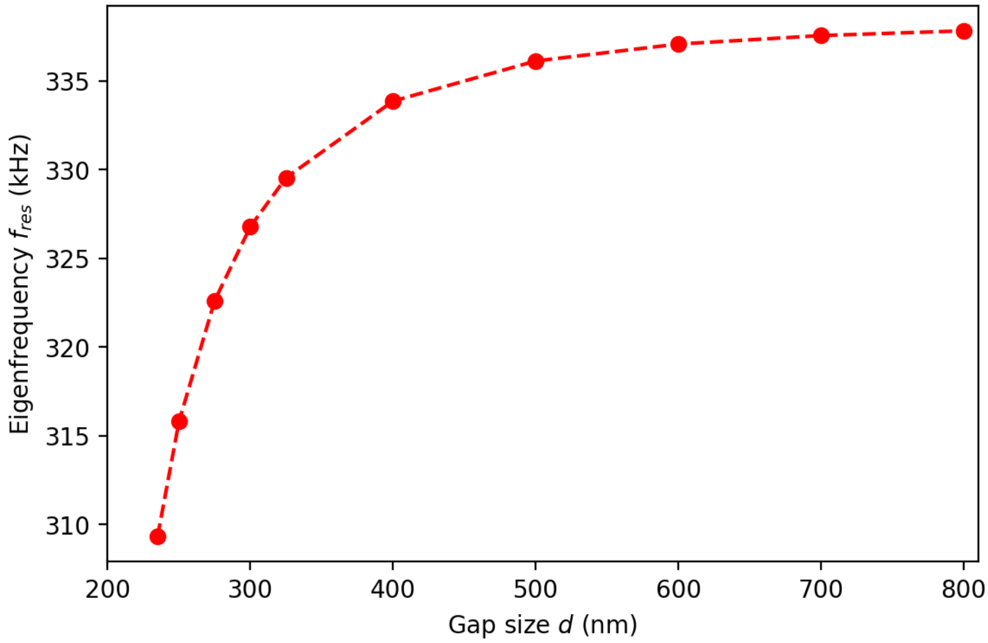

Figure 4.1: Simulated eigenfrequencies of a circular NbTiN resonator subjected to the Casimir force and electrostatics using the parameters given in tables 3.1 and 3.2 with the lower value of σ chosen. The voltage is set to $0.75\,\mathrm{V}$ and $\eta = 1$. The eigenfrequency changes dramatically for a changing gap size due to the nonlinear force fields growing in strength, thereby softening the spring constant.

We see that the eigenfrequency is dramatically softened by the combination of the Casimir and electrostatic forces. The softening is more dramatic the smaller the gap becomes, as lower gaps mean larger nonlinear forces. The difference between the eigenfrequency for $d = 235\,\mathrm{nm}$ and $d = 800\,\mathrm{nm}$ is $28.5\,\mathrm{kHz}$. The change in the eigenfrequency becomes more extreme the larger the force grows. This effect signals the dangerous side of the use of nonlinear attractive forces. If the force is increased, then the eigenfrequency dips more severely to lower values, due to the restoring force of the membrane becoming softer and softer. At some point, this restoring force loses the battle against the attractive forces, and a pull-in occurs. This is the reason why the gap distance in the softening curve in figure 4.1 does not reach $200\,\mathrm{nm}$ as we set out to do. COMSOL shows an error for this gap size with these nonlinear force magnitudes, as it finds no way to calculate an eigenfrequency, meaning pull-in happened. We will revisit this pull-in extensively and show how to prevent it later.

The influence of the nonlinear forces is considerable, and that might be surprising considering how minimal the pressures in principle are. For example, for a gap size of $235\,\mathrm{nm}$, the Casimir effect and a voltage of $0.75\,\mathrm{V}$ exert pressures of $0.43\,\mathrm{Pa}$ and $45.1\,\mathrm{Pa}$ respectively if one only uses the standard formulas. The influence of the spring softening must therefore be considerable to be able to make the membrane collapse, even if its aspect ratio is extreme. To demonstrate this, we plot the magnitudes of both effects, with or without the spring softening considered, and their resultant magnitudes for a circular membrane in figure 4.2 by using equation 2.106.

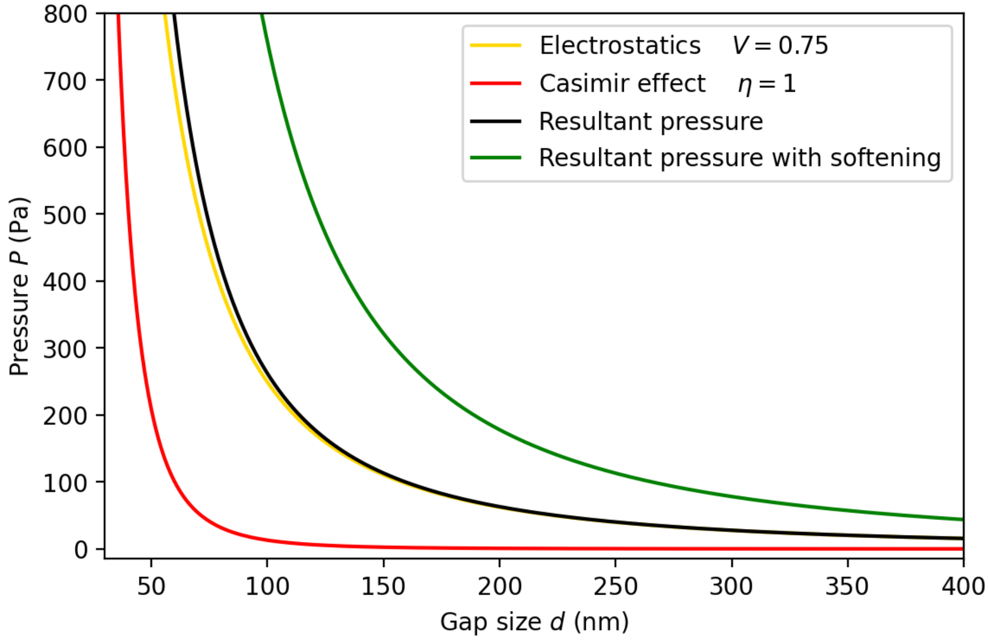

Figure 4.2: Magnitudes of the Casimir force and electrostatic force with V = $0.75\,\mathrm{V}$ for a circular membrane with and without the softening effect. The resultant pressures show the immense influence of the softening effect on the force magnitude.

The magnitude of the softening effect has been approximated using COMSOL simulations to determine U for equation 2.106. We see that the softening effect increases the force magnitude considerably. Still, we should remember that our analytical expression is a first-order approximation, and that is shown in figure 3.9 to underestimate the strength of the forces when they grow larger. This mismatch grows quickly and we can therefore expect the actual magnitude of the nonlinear forces to be considerably more than the $\approx 200\,\mathrm{Pa}$ given by our approximation to the softened situation for $d = 200\,\mathrm{nm}$, which explains the pull in occurrence.

Another aspect which can be noted from figure 4.2 is how the Casimir effect plays little to no role for a long time until it rises sharply due to its proportionality with $1/d^4$. This means that if we use a low voltage value combined with the Casimir effect in our simulations that we can expect a sudden sharp softening effect that quickly leads to pull-in as the Casimir effect lies dormant for a long time until it suddenly grows in size.

The membrane deflection and the softening of the stiffness have a recursive relationship as they increase each other's magnitude. The further the membrane deflects, the softer the eigenfrequency becomes due to the smaller gap. The softened stiffness makes the deflection grow, and the cycle goes on. This means that an increase in the membrane deflection by any means will enlarge the softening effect. Now, imagine if we were to apply a static force on top of these nonlinear forces, such as a static pressure. We would expect the membrane to deflect further than normal when subjected to this static pressure due to the stiffness being reduced. This could be any pressure, for example, sound. The static pressure would worsen the softening of the eigenfrequency, and with it, a larger Δf would be read out due to this pressure than if we had omitted the nonlinear forces.

The nonlinear forces thus make our output parameter, i.e. the eigenfrequency, change significantly more when subjected to the same static pressure. We can therefore see this effect as an opportunity to increase the responsivity of our sensor. Pressures would result in a higher output swing, i.e. a bigger shift in eigenfrequency than without the nonlinear force present. To explore if this is the case, we model two versions of the circular NbTiN membrane, one with an electrostatic potential of $0.5\,\mathrm{V}$ and one without it. We omit the Casimir effect for simplicity and keep the gap size at $350\,\mathrm{nm}$ and sweep over a variety of static pressures which push the membrane towards the cavity bottom. The resulting eigenfrequencies are shown in figure 4.3.

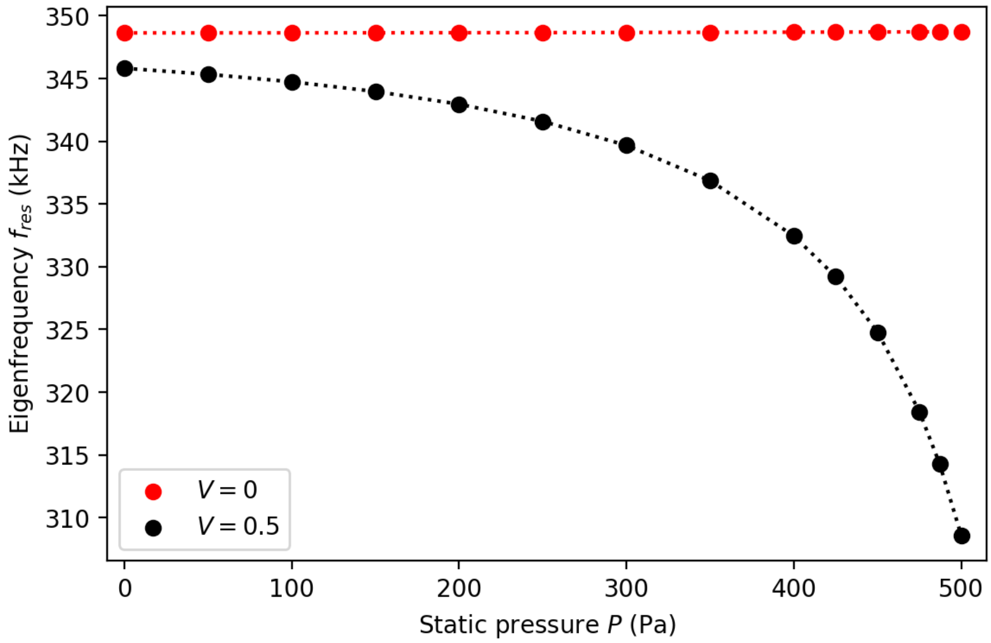

Figure 4.3: Eigenfrequencies of a circular NbTiN membrane with parameters given in tables 3.1 and 3.2 with $\sigma = 566\,\mathrm{MPa}$. The membrane eigenfrequency is shown for a case with and without an electrostatic voltage applied to it for a gap size of $350\,\mathrm{nm}$ when sweeping over static pressures. The influence of a nonlinear force field when a static pressure is applied is visible.

Our suspicion was correct, the membrane eigenfrequency is influenced more greatly due to a static pressure when influenced by an attractive nonlinear force field, which is an exciting result. The red line, indicating the case without the voltage, shows an eigenfrequency increase of $92\,\mathrm{Hz}$ due to the geometric nonlinearity. The black line, which includes the voltage of $0.5\,\mathrm{V}$, trumps this with a decrease in eigenfrequency of $37\,360\,\mathrm{Hz}$. One could imagine using this to amplify the output swing of a microphone in which the pressure from the sound waves applies a transverse pressure on the membrane, for example. We can plot the absolute value of the difference in the eigenfrequency to determine the responsivity for this range of pressures, as we do in figure 4.4.

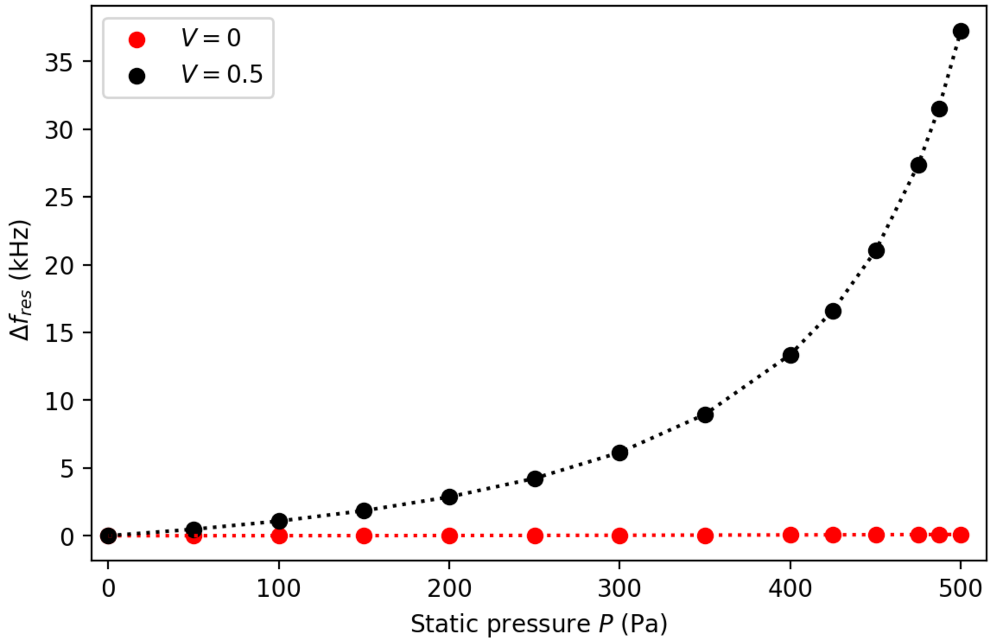

Figure 4.4: Absolute value of the change in eigenfrequency, or responsivity, of a circular NbTiN membrane with parameters given in tables 3.1 and 3.2 with $\sigma = 566\,\mathrm{MPa}$. The membrane eigenfrequency is shown for a case with and without an electrostatic voltage applied to it for a gap size of $350\,\mathrm{nm}$ when sweeping over static pressures. The influence of a nonlinear force field when a static pressure is applied is visible.

We see the responsivity skyrocket to the earlier mentioned 37360 times the original shift in the frequency. We can thus extract a responsivity of $37\,360\,\mathrm{Hz}/500\,\mathrm{Pa}$ for this particular sensor setup.

Having seen the effect of nonlinear forces on the eigenfrequency first-hand, we shall now dive deeper into the two earlier-mentioned resonator setups. A circular NbTiN membrane and a square SiC membrane. We will explore the eigenfrequency characteristics for different situations in which we vary the gap size d, electrostatic voltage V and the Casimir parameter η. We will first quantify a standard way to explore the responsivity boost. We aim not to show similar simulations twice and will explain the differences between them along the way. Let's start with the circular NbTiN membrane.

4.2. Circular NbTiN Resonator

The parameters which we use in our COMSOL model can be found in the setup chapter, namely in tables 3.1 and 3.2, for these simulations, we use $\sigma = 533\,\mathrm{MPa}$. We mentioned the definition of responsivity before, the ratio of the output to the change in the input. In order to make our research into the responsivity boost of nonlinear force fields simpler, we will need to define a way to quantify it. The responsivity in [12] is given as

$$\mathscr{R} = \frac{\partial \omega_0}{\partial x}\frac{1}{\omega_0}, \tag{4.1}$$

Where ω_0 is the resonance frequency and x is the change in an observable, such as the mass or the force on the membrane. In engineering, the responsivity is often expressed as the output swing in the measured voltage. This method does not apply to our simulations, as we do not use an electric circuit to obtain our results. Therefore, we shall use a custom definition which is tailored to be easy to obtain using our simulations.

We define the responsivity increase as the scalar change in the resonance frequency ω_0 when subjected to a pressure $\mathbf{P_0}$. The pressure $\mathbf{P_0}$ is the pressure which shifts the resonance frequency of the membrane by 1 Hz when there are no other forces present. So if our resonator eigenfrequency changes $1\,\mathrm{Hz}$ when only under a static pressure P_0, and, for example, changes $20\,\mathrm{Hz}$

when subjected to the same pressure with nonlinear forces present, then the responsivity is increased by 20 times. For the case of the circular NbTiN resonator, the resonance frequency shifts by $1\,\mathrm{Hz}$ when the membrane is subjected to $P_0 = 50\,\mathrm{Pa}$.

4.2.1. Casimir Responsivity Boosting

We will start with only the Casimir effect present. By doing so, we will determine what we can achieve by only using parallelism before we consider effects which require other types of parameters, such as input voltage. We calculate the eigenfrequency for two distinct cases, one for $\eta = 1$, i.e. both the membrane and the cavity bottom are conductive, and $\eta = 0.5$, meaning only the membrane or only the cavity bottom is conductive. In these two circumstances, we again sweep over various gap sizes and calculate the eigenfrequency for 2 separate cases. One for static pressures of $P = 0\,\mathrm{Pa}$ and one for $P = P_0 = 50\,\mathrm{Pa}$ in order to determine the responsivity increase. The eigenfrequencies are shown in figure 4.5.

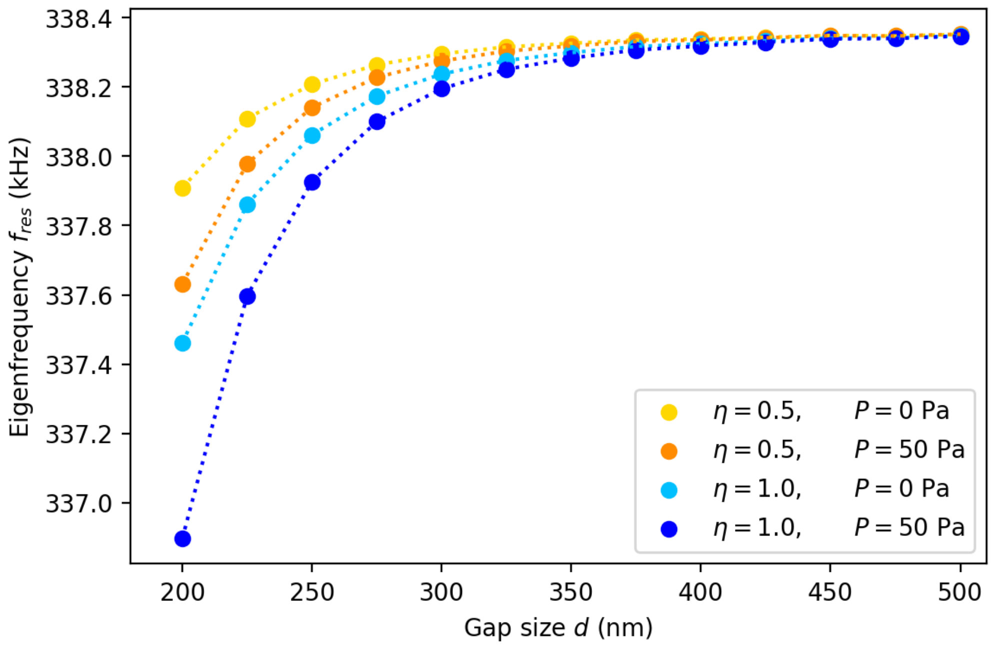

Figure 4.5: Eigenfrequencies of a circular NbTiN resonator subjected to the Casimir effect for two distinct cases. One for $\eta = 1$, and one for $\eta = 0.5$. For each case, two simulations, which are grouped by colours, have been performed. One for a static pressure of $P = 0\,\mathrm{Pa}$ and one for $P = 50\,\mathrm{Pa}$. The eigenfrequencies are calculated for different gap sizes.

The two cases per value of η have been grouped by colour. We can see the softening effect due to the Casimir force. Its effect increases for higher values of η, which is to be expected. Let's now plot the differences in the eigenfrequencies for the two different pressures to determine the absolute value of the shift per gap size for each value of η. We present these values in figure 4.6

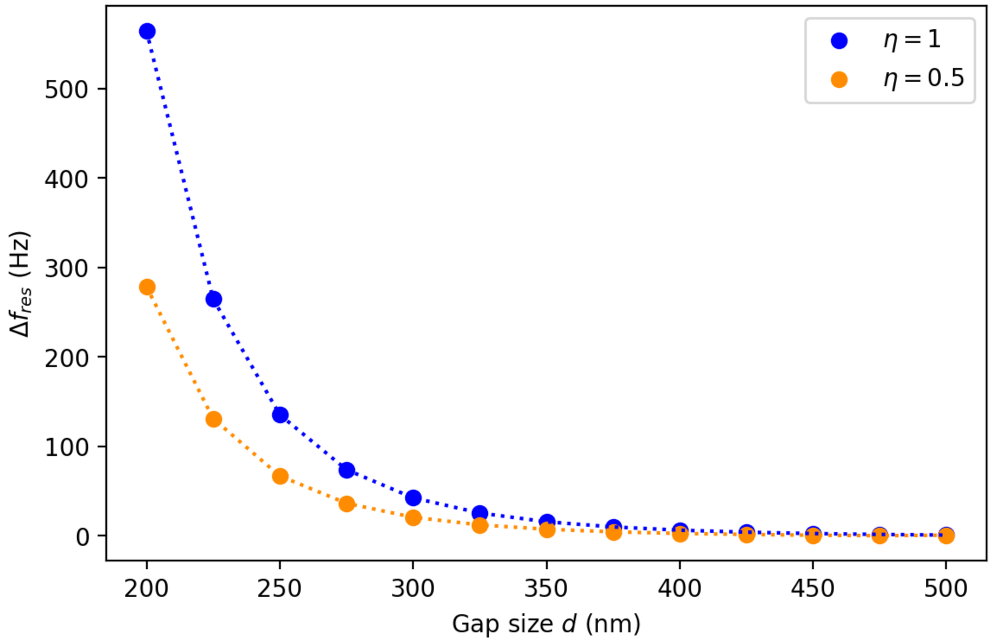

Figure 4.6: Absolute value of the change in eigenfrequency of a circular NbTiN membrane subjected to the Casimir effect for two values of η per gap size when put under a pressure P_0. The higher value of η shows a larger increase in responsivity due to the magnitude of the force being larger.

We see the absolute values of the differences between the eigenfrequencies for the two situations per value of η. They show an exciting result, the responsivity increase can be on the order of a hundred times from merely the Casimir effect alone, with a peak of 570 times the original responsivity reached with the full force Casimir effect. The reduced Casimir effect still manages to boost the responsivity by a factor of 280 for the smallest gap size. This is a promising result for multiple reasons. The first is that the Casimir force, despite its weaker magnitude compared to the electrostatic effect for these gap sizes, is still able to show a sizable responsivity boost. The second is seen when one considers the fact that the Casimir force, in a way, is a 'free' force. No voltage has to be applied, nor any other outside parameters or methods have to be implemented. The only needed parameters are a big surface area and high parallelism. Even when using only one conducting layer, the responsivity increases to more than a hundredfold for gaps lower than $225\,\mathrm{nm}$. The downside is the very narrow gap sizes required to do this, especially if only the membrane itself is conducting. Nonetheless, this is very promising, and we want to determine what effect the electrostatic effect will add to this, considering its larger magnitude.

Combined Responsivity Boosting

We now turn on the electrostatic effect in our simulations. With both effects now in effect, the pull-in phenomenon is more likely to occur than before, and we will shortly see how this affects the possible gap sizes for some voltages. The minimum gap size that we investigate is $200\,\mathrm{nm}$ as stated before. With a gap this small, we will not consider voltages that are bigger than $1.2\,\mathrm{V}$. This voltage leads to an electric field strength of 6 million volts per meter. We set the Casimir parameter $\eta = 1$ for this experiment; sweeps using $\eta = 0.5$ can be found in the appendices. We then perform similar gap size sweeps as before, but instead of varying the Casimir parameter η, we vary V. We group the sweeps that only differ in the static pressure $P = P_0$ again by colour in figure 4.7.

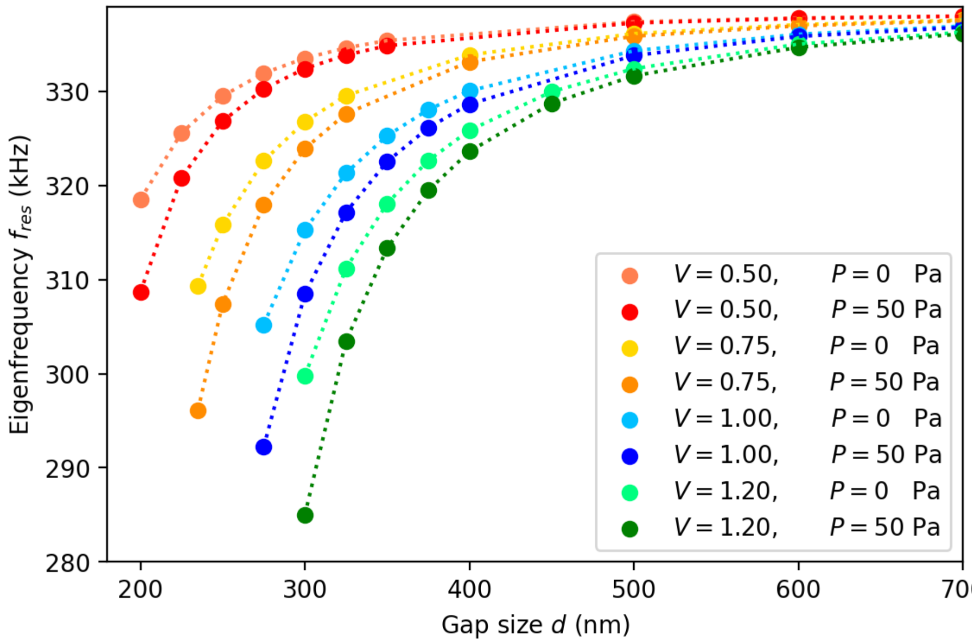

Figure 4.7: Eigenfrequencies of a circular NbTiN resonator subjected to the Casimir effect and varying electrostatic potentials. For each case, two simulations, which are grouped by colours, have been performed. One for a static pressure of $P = 0\,\mathrm{Pa}$ and one for $P = P_0 = 50\,\mathrm{Pa}$.The eigenfrequencies are calculated for different gap sizes.

Figure 4.7 shows, as we could have expected, even larger swings in the output eigenfrequency, with the biggest change seen in the $1.2\,\mathrm{V}$ $P = 50\,\mathrm{Pa}$ eigenfrequency characteristic: $\Delta f = 45\,\mathrm{kHz}$.

One thing to note is the fact that for smaller voltages, the onset of the larger softening dips starts later on. For example, for $V = 0.5\,\mathrm{V}$, the sharp downwards trend starts at approximately $d = 350\,\mathrm{nm}$. This is the case at $600\,\mathrm{nm}$ when the voltage equals $1.2\,\mathrm{V}$. So, for lower voltages, one can attain lower gap sizes at the cost of a more abrupt trend downwards, which quickly leads to pull-in. This is also seen in the fact that for larger voltages, there is no data available on the eigenfrequency for gap sizes of, for example $200\,\mathrm{nm}$. It would then seem to be easier in terms of engineering to use a larger gap in combination with a larger voltage if one were to exploit this effect, as the range of gap sizes is bigger in which the softening effect is sizable. This is, of course, only the case if this does not introduce any other unwanted effects in the phenomena that the sensor should capture.

These graphs have highlighted some key differences between using only Casimir forces and using electrostatics. Casimir forces are 'free' and do not create things such as fringe fields, which can influence other parameters. They come at the cost of a sharper drop to the pull-in point and increase the responsivity less, however.

The increase in responsivity is larger with the introduction of electrostatics. We show a graph similar to that in the Casimir sweep case, which showcases these impressive increases in figure 4.8.

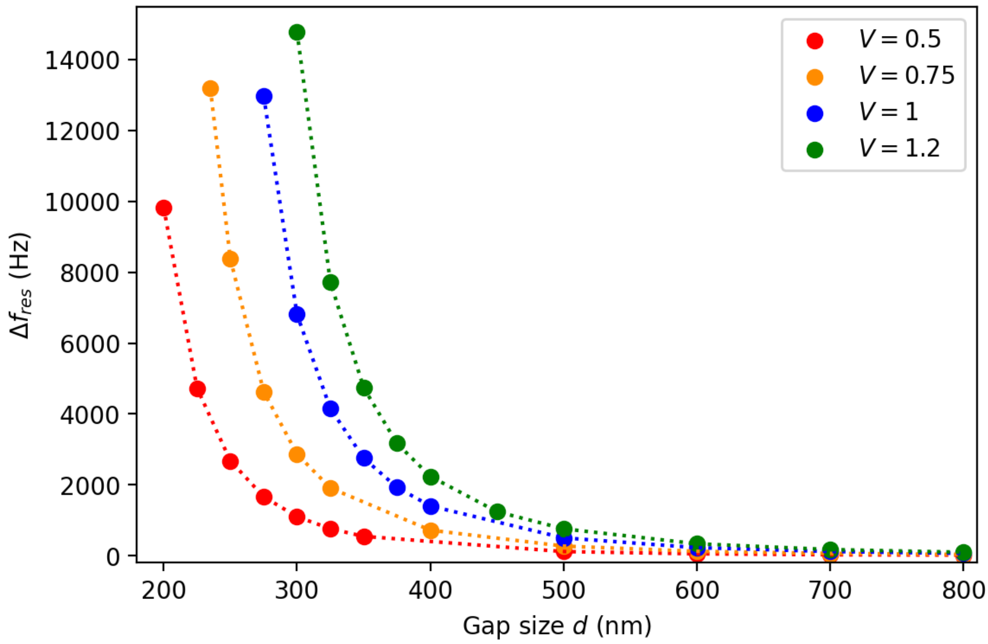

Figure 4.8: Absolute value of the change in eigenfrequency of a circular NbTiN membrane subjected to the Casimir effect and varying electric potentials per gap size d when put under a pressure P_0. The higher values of V show a larger increase in responsivity due to the magnitude of the force being larger.

Figure 4.8 presents the largest responsivity increases we have seen yet, with the largest numbers reaching orders of ten thousand, and the biggest increase found as 14782 times the original responsivity for the voltage of 1.2. The lowest voltage still manages a responsivity boost by a factor of 10000. These numbers are found in the very steep responsivity boost regions, close to pull-in. However, within the less steep 'safer' regions, we still find responsivity boosts of thousands compared to the case without any nonlinear forces. This is the case for gap sizes that are not too small, as can be seen in the green $1.2\,\mathrm{V}$ graph, as a gap of $500\,\mathrm{nm}$ shows a responsivity boost of a factor 1000. This graph shows us opportunities for big increases in sensor performance at sizes that are not at the absolute limit of current engineering.

These results are merely for circular NbTiN membranes, and ample variations can be made to the material or the geometry of the resonator, which will influence the results. We will analyse one other resonator, a square SiC membrane, in order to get a sense of the responsivity boosting possibilities using dielectrics.

4.3. Square SiC Resonator

SiC, in its pure form, is an insulator. It is possible to dope SiC to fashion a semiconductor from the material, but we will not consider this option for our simulations. In order to boost the responsivity, one could increase the reflectivity of SiC to increase the Casimir effect by adding conducting surfaces. This would enable the setup to accommodate the electrostatic effect as well, if so desired. Techniques to fashion electrostatically actuatable SiC membranes have been created as mentioned before in the setup by a variety of authors, an example being Chang et. al [69].

4.3.1. Reduced Casimir Frequency Softening

These conducting SiC resonators are promising directions for further research in responsivity boosting, but for now, we will not consider simulating them as material data is not provided, and the situation is, excluding different material parameters, the same as with the NbTiN resonator. If one obtains the material parameters for the multilayer conducting SiC membrane, then the simulations in principle can be repeated with ease. They do not provide any new insights other than different numerical values, which is why we will abstain from researching them. What we will do is determine the magnitude of the Casimir effect for more reduced values of η, however. If the bottom of the cavity is layered with a conductor, then $\eta = 0.5$ is the maximally achievable value. The value of η for two dielectrics can be determined using equation 2.56, but we can assume this to be low as η ranges from 0 to 1, with $\eta \geq 0.5$ only occurring for at least one conductive plate. We show the eigenfrequencies of the square SiC material for different gap sizes d for two values of η, 0.5 and 0.2, in figure 4.9. We include $\eta = 0.2$, which we assume to be a high value for two dielectrics. Note that this value of η has not been determined by calculations or assumptions and merely serves the purpose of showing what amount of responsivity boosting might be possible for systems with low values of η in general. Research into the exact value of η for dielectrics is not performed in this text. We omit the electrostatic effect as we are dealing with insulators. We again simulate twice per value of η for a pressure of $0\,\mathrm{Pa}$ and for $P = P_0$ which in the case of this square SiC membrane is equal to $65\,\mathrm{Pa}$ and show the results in figure 4.9.

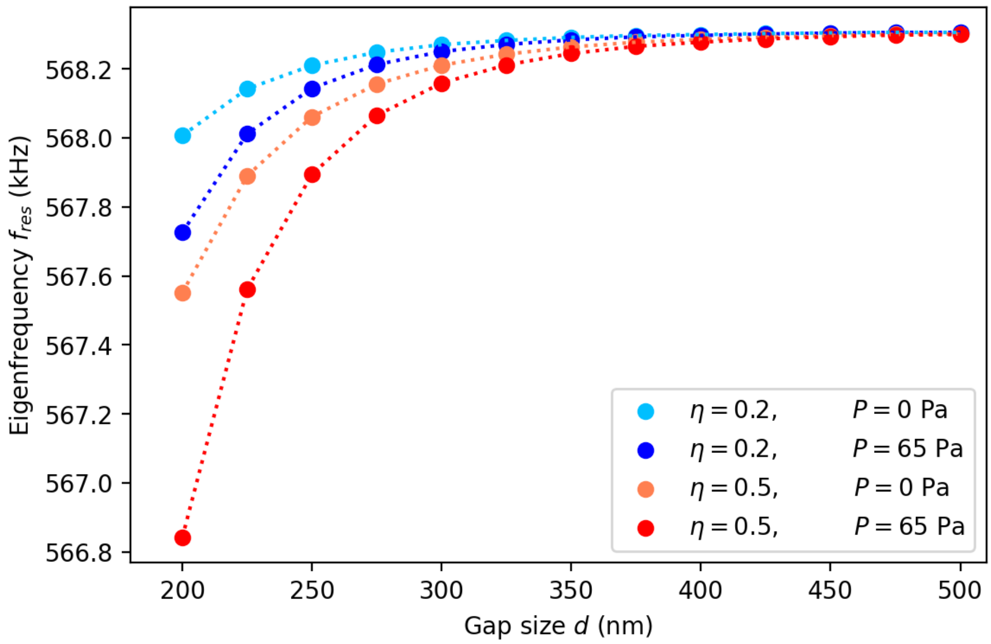

Figure 4.9: Eigenfrequencies of a square SiC resonator subjected to the Casimir effect with varying values of η. For each case, two simulations, which are grouped by colours, have been performed. One for a static pressure of $P = 0\,\mathrm{Pa}$ and one for $P = P_0 = 65\,\mathrm{Pa}$. The eigenfrequencies are calculated for different gap sizes.

Figure 4.9 shows a surprisingly large eigenfrequency change for $P = P_0$, even for reduced Casimir forces. The Casimir forces have been scaled down by a factor of 2 and 5, but we still see decreases on the order of a few hundred to almost a thousand Hertz. The eigenfrequency does not decrease as sharply as in figure 4.7 just like figure 4.5 for these gaps, the Casimir effect alone provides a safer force which does not trend towards a pull-in as fast as when combined with the electrostatic effect due to its smaller magnitude. The trend would proceed downwards sharply if we considered smaller gaps, however. If we now plot the absolute value of the frequency change as we have done twice before in other situations, we arrive at figure 4.10.

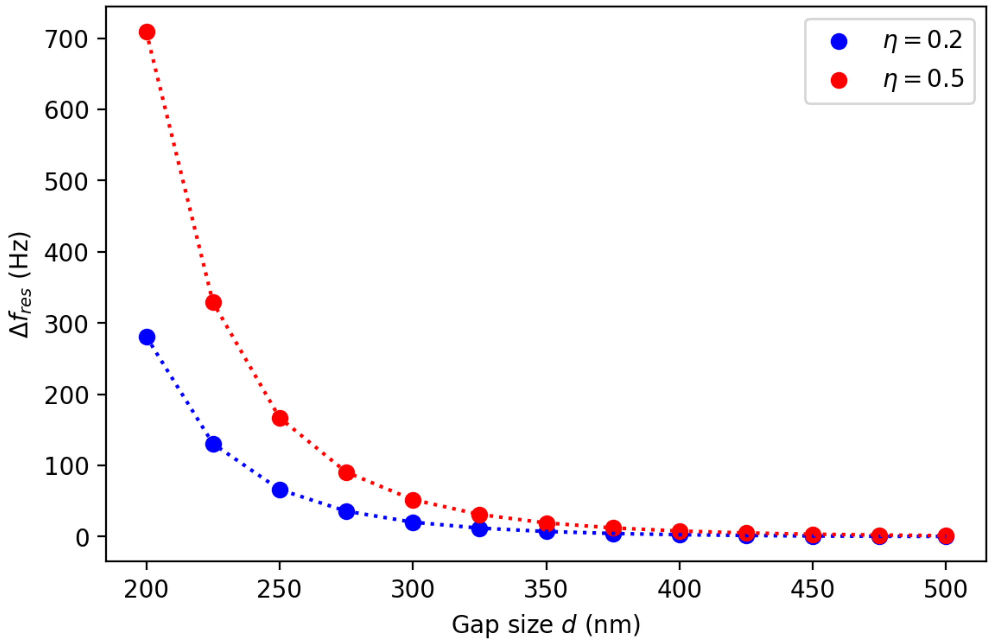

Figure 4.10: Absolute value of the change in eigenfrequency of a square SiC membrane subjected to the Casimir effect for varying values of η per gap size d when put under a pressure P_0. The higher values of η show a larger increase in responsivity due to the magnitude of the force being larger.

The change in eigenfrequency, even for these reduced Casimir forces, could still be worthwhile investigating for dielectrics, as shown by figure 4.10 where a gap size of $200\,\mathrm{nm}$ is enough to scale the responsivity by a factor of 700. When the bottom of the cavity is covered in a conductor, responsivity boosts reach the order of one hundred for gaps smaller than $275\,\mathrm{nm}$. The symbolic value $\eta = 0.2$ still shows responsivity increases for smaller gap sizes, which achieve this order of magnitude. As said before, this value of η is fictional as it is not based on anything. It merely shows the possibilities for low values of η. The red line in figure 4.10 can be directly compared to the gold line in figure 4.6 as the nonlinear force situation is the same, except for the membrane geometry. The comparison shows a more than double increase in the responsivity when using SiC for the reduced Casimir effect. We can then, by extension, assume that if one were able to produce the SiC membranes with both the membrane and the cavity bottom covered in conductors, one could achieve responsivity boosts larger than those shown in figure 4.8. The reasons for these larger boosts for SiC will be explored in a later paragraph.

4.4. Comparison to the State of the Art

With our definition for the responsivity of the membrane resonators, we have shown sizable increases which could potentially be used in future membrane resonator design. However, in order to underline the potential of this responsivity boosting technique, we shall compare it to the state of the art. In 2024, More et. al showed Graphene pressure resonator sensors to reach 'ultrahigh' responsivity ranges of $20\,\mathrm{kHz/kPa}$ over a range of $270\,\mathrm{kPa}$ [83]. To compare this to our models, we shall subject the NbTiN membrane with the same parameter values as before to a pressure of $1000\,\mathrm{Pa}$ with our responsivity boosting technique active for two situations, the first being one with only the Casimir effect present and the second one with only the electrostatic effect present. For our first case, we try three different gap sizes, and for the second case, we try three different voltages for a set gap size of $500\,\mathrm{nm}$. The simulations with their respective responsivities are shown in tables 4.1 and 4.2.

Table 4.1: Responsivities due to a static pressure of $1000\,\mathrm{Hz}$ with the Casimir effect present for the NbTiN resonator for various gap sizes.

Gap size d (nm)	Resp. ($\mathrm{kHz/kPa}$)
700	0.08
600	0.95
550	10.5

Table 4.2: Responsivities due to a static pressure of $1000\,\mathrm{Hz}$ with the electrostatic effect present for the NbTiN resonator for various voltages.

Voltage (V)	Resp. ($\mathrm{kHz/kPa}$)
0.05	3.2
0.10	18.1
0.15	133.2

We see the Casimir effect not able to hold up to the state of the art, but the electrostatic effect manages to exceed the earlier mentioned $20\,\mathrm{kHz/kPa}$ responsivity shown in [83] by a factor of 6.7. In figure 4.3, the boost to the eigenfrequency reached 40000 for a pressure of $500\,\mathrm{Pa}$, showing again that this technique offers unprecedented responsivity boosts. The exciting part of these results is found in the fact that this technique is highly tunable. Be it figure 4.3 or table 4.2, a responsivity is shown that exceeds More et. al, with two differing setups. Changing the system parameters, such as by using a smaller membrane size or a higher gap size, whilst using a higher electrostatic voltage, one can attain similar responsivities which are beyond the state of the art, with a setup fitted to one's desire. The limiting factor in design is given by the extreme aspect ratio requiring the deflection to be negligible compared to the membrane dimension.

One might be surprised to find the gap sizes of the Casimir effect experiment being as large as they are, and the voltages in the second experiment so low. This is due to the duality which we have mentioned often before, that is inherent to working with nonlinear attractive forces in conjunction with membranes of these sizes. The dynamical range, i.e. the range of a parameter value at which the sensor can perform, suffers significantly when using this effect. More et. al found a $20\,\mathrm{kHz/kPa}$ over a range of $270\,\mathrm{kPa}$. Using lower gap sizes, or higher voltages, leads to pull-in for pressures of $1\,\mathrm{kHz}$. Using these lower voltages, we can reach a pressure of $1100\,\mathrm{kPa}$ before pull-in occurs, showing the severely limited dynamical range. The responsivity is thus boosted significantly by paying the price in the dynamic range of the sensor.

These responsivity increases are exciting results as they trump the state of the art. However, we have mentioned the pull-in effect often when discussing these responsivity boosts without showing any analysis on how to prevent it. The pull-in effect poses the biggest danger for these responsivity boosted membranes, and the use of nonlinear effects means that there will always be a trade-off between them. The dynamical range of the sensor, as shown above, suffers significantly. We will discuss how we can predict the pull-in effect next in order to determine the range in which responsivity boosted membranes can operate safely.

4.5. Pull-in and Membrane Deflection

We explored the mathematics behind the pull-in effect in the theory. We considered the Casimir effect and the electrostatic effect together, with the possibility of removing them from the equation by setting either η or V to 0. By using the first-order Taylor terms for the softening effects, for a circular membrane, we arrived at

$$V_{PI}(\eta, V) = \sqrt{\frac{\mathscr{A}\dfrac{n_0}{R^2}U_{max} + \mathscr{B}\dfrac{Eh}{R^4}U_{max}^3 - \eta\dfrac{\pi^2\hbar c}{240}\left(\dfrac{1}{d^4} + \dfrac{4\gamma U_{max}}{d^5}\right)}{\varepsilon_0\varepsilon_r\left(\dfrac{1}{2d^2} + \dfrac{\gamma U_{max}}{d^3}\right)}},$$

In which U_{max} was a free variable to be determined using FEM simulations. The square membrane variant was given in 2.110. We saw the effect of static pressures on the eigenfrequencies of membranes in figure 4.3. With the static pressure adding to the softening effect, it can directly contribute to the pull-in effect. This can easily be modelled by adding a ΔP to the right side of equation 2.106. This changes our pull-in equation to

$$V_{PI}(\eta, V, \Delta P) = \sqrt{\frac{\mathscr{A}\frac{n_0}{R^2}U_{max} + \mathscr{B}\frac{Eh}{R^4}U_{max}^3 - \eta\frac{\pi^2\hbar c}{240}\left(\frac{1}{d^4} + \frac{4\gamma U_{max}}{d^5}\right) - \Delta P}{\varepsilon_0\varepsilon_r\left(\frac{1}{2d^2} + \frac{\gamma U_{max}}{d^3}\right)}}. \tag{4.2}$$

There are a lot of variables which one could explore to determine its critical value in certain situations before pull-in occurs, such as the material parameters $E, n_0, \mathscr{B}, \varepsilon_r$, the geometric parameters R, h, d, γ, L and the external force parameters $\eta, V, \Delta P$. To keep it brief, we will again use the parameters for a circular NbTiN resonator given before, use $\eta = 1$ and set $\Delta P = 0$. We will use the voltage V as our independent variable and show how to determine the pull-in voltage using a combination of FEM and analytics.

4.5.1. Voltage

Our method to determine the pull-in voltage uses a combination of FEM and equation 2.107. First, we use equation 2.107. We can, in principle, calculate the pull-in voltage if we have the right value of U_{max}, but at the moment we do not know its exact value. Let us first examine the values of the pull-in voltages per gap size for different values of U_{max}. They are shown in figure 4.11.

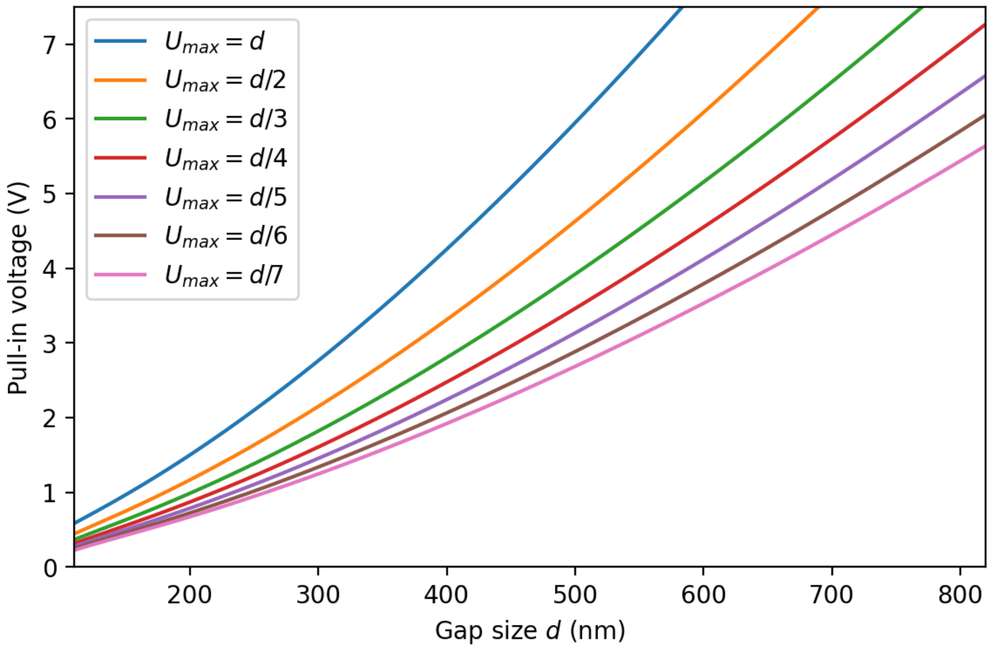

Figure 4.11: Analytically determined pull-in voltages per gap size per value of U_{max} for a circular NbTiN membrane calculated by equation 2.107. The parameters used are given in tables 3.1 and 3.2. Note that $U_{max} \leq d$ as the membrane can never deflect further than the gap size itself.

We have defined U_{max} as the scaled gap distance: $U_{max} = d/m$, as the membrane can, of course, never deflect further than the gap size itself.

Now, to find the correct value of m to determine which of the lines shown above is correct, we use COMSOL. We try to calculate the eigenfrequencies of the membrane for a gap size range of $d =$

$120\,\mathrm{nm} - 800\,\mathrm{nm}$ with the Casimir effect and the electrostatic effect pulling on the membrane. Per gap size, we increase the voltage until the simulation is unable to find the eigenfrequency any longer. COMSOL gives an error the moment this occurs, as it is unable to find an eigenfrequency. We interpret the voltage at which this happens as the pull-in voltage.

Now, we combine the data we found with COMSOL and the pull-in equation. We vary the value of m until we find the line that provides an optimal fit to the COMSOL data, and the best match will give the optimal value of U_{max}. Note that this value of U_{max} does not necessarily have to be the maximum deviation of the centre of the membrane. We must remember that we are only using the first Taylor terms, and that U_{max} does not have to be a constant fraction of the gap size, either, as other effects such as geometric nonlinearity can change the stiffness more positively for larger deflections. The value we find will be a good fit to be used for our specific NbTiN membrane, which we can use to determine the safe operating region. We fit the data found with COMSOL and find what is shown in figure 4.12.

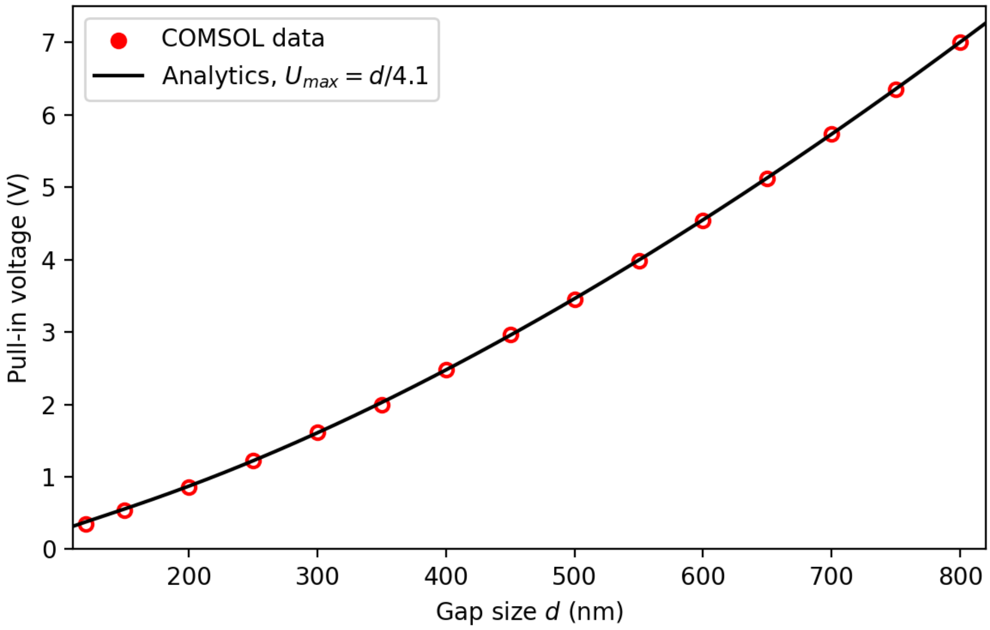

Figure 4.12: Pull-in voltages per gap size per value of U_{max} for a circular NbTiN membrane calculated by equation 2.107 using $U_{max} = d/m = d/4.1$. The parameters used are given in tables 3.1 and 3.2. The optimal value $m = 4.1$ was found by fitting the curves with the pull-in data from COMSOL.

Figure 4.12 shows an excellent match with the data provided by COMSOL for the pull-in voltage for our circular NbTiN membrane. The value of m at which this fit matches optimally was found to be 4.1, meaning that for a gap size d, according to our analytics, $U_{max} = d/4.1$. The analytical solution provides a surprisingly good match with COMSOL, considering we used only first-order Taylor terms for the softening. For lower gap sizes, it overestimates the pull-in voltage slightly. We must mention that the data we obtained using COMSOL was found by increasing the voltage ever so slightly until a crash occurs. This is a long iterative process with no distinctive end, and some values of V_{PI} might be closer to the real V_{PI} per gap size than others. These deviations are slight nonetheless, and using the value for U_{max}, we have found that the analytical solution can provide an excellent estimate for the point at which device failure occurs for a membrane subjected to Casimir and electrostatic forces. We thus have added a valuable tool to aid in the design of our resonators.

4.5.2. Deflection

The centre deflection is a key parameter in all of our analytical calculations, and its value determines the size of the forces present in our system. We found an analytical approximation for this centre deflection distance by discarding some higher-order terms in equation 2.108. In the previous paragraph, we found the maximum deviation, or centre deflection, to equal $d/4.1$ for our analytical models to resemble COMSOL closely. To determine the accuracy of our analytical expression, we again use COMSOL and calculate the centre deflection of the circular NbTiN membrane for three gap sizes. The sizes are $200\,\mathrm{nm}$, $400\,\mathrm{nm}$, and $600\,\mathrm{nm}$. We use the Casimir effect with $\eta = 1$ and vary the voltage V in both our simulations. We stop at the pull-in voltage V_{PI} for a certain gap size d as given by graph 4.12. The comparison between both models is shown below in figure 4.13.

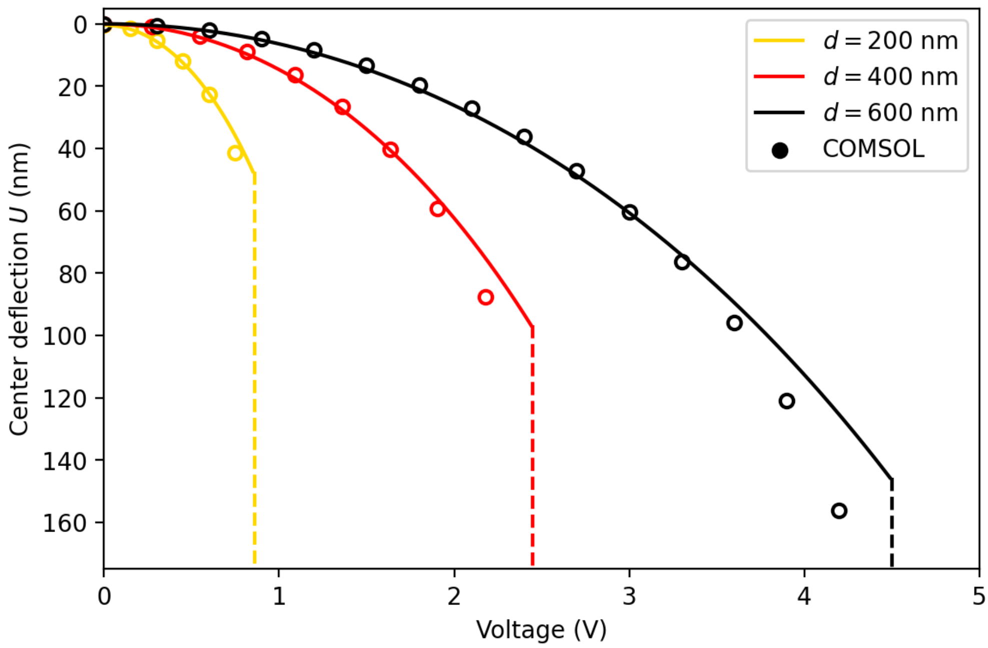

Figure 4.13: Centre deflection of a circular NbTiN membrane as calculated by COMSOL and equation 2.108. The centre deflection is calculated for three different gap sizes and varying voltages, with the Casimir effect present at all times.

The dots indicate the deflections found by COMSOL. Note that the cutoff points, which are indicated with dashed lines, have been added manually. Equation 2.108 does not indicate when this exact moment occurs, and we have chosen the point at which formula 2.107 indicates that the pull-in voltage has been reached for a certain gap size d, using $U_{max} = d/4.1$.

We can make two observations when looking at figure 4.13. The first is that the resonator deflection U as calculated by COMSOL, dips deeper than the maximum deflections U_{max} we found before using analytics. This confirms the notion we made earlier that U_{max} is a handy fitting parameter which aided us in correcting values of V_{PI}. It is not equal to the actual maximum deflection, which is not a constant fraction of the gap size. Secondly, we see that the analytical formula is able to predict the deflections for smaller values quite well. It fails to predict them accurately for larger forces when the deviations grow larger, however, and the deflection distance for which this occurs seems to lie beyond a critical point in between 60 and 80 nm. After this point, it underestimates the actual deviation as calculated by COMSOL.

We provide additional sweeps in figure 4.14 where we swap the dependent and independent variables of figure 4.13 around. We keep the voltage V constant and change the gap size, and calculate the centre deflection using our two models. Again, we do not go further than the pull-in voltage V_{PI} as predicted by our earlier simulations.

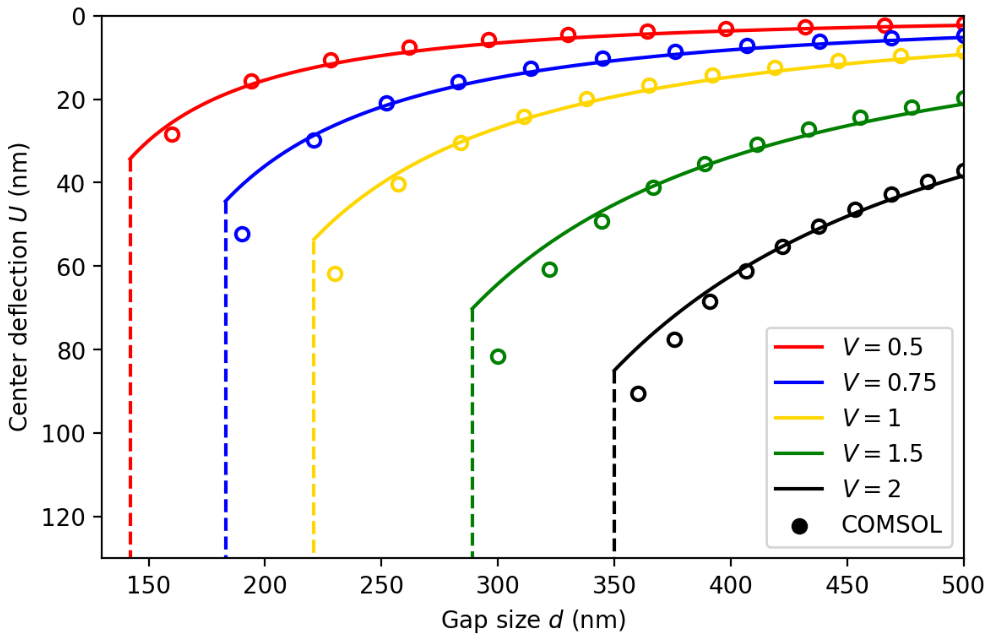

Figure 4.14: Centre deflection of a circular NbTiN membrane as calculated by COMSOL and equation 2.108. The centre deflection is calculated for five different voltages with varying gap sizes, with the Casimir effect present at all times.

The lower voltages show good resemblance, but we see similar trends as before. The analytical solutions fail to value the centre deflection at a correct size when the combination of Casimir forces and electrostatic forces grows large. This deviation is probably due to the higher-order Taylor terms, which we discarded before, growing in size when the force magnitude increases. Additionally, the terms proportional to U^3, which we discarded, could play a major role. To determine the influence of this U^3 term, a root finding algorithm was used on equation 2.106 and its results compared to formula 2.108. The result proved negligible differences between the found values of U, validating our earlier assumptions of the terms proportional to U^3 having little to no role in our system. By extension, it also leaves the higher-order Taylor terms as the possible culprit for the analytical model deviating from COMSOL for larger deflections, which is shown in more detail in Appendix A.

4.6. Resonator Parameter Sweep

Our analysis has been largely based on resonators which have been fabricated or variations of ones that have been fashioned experimentally. The square SiC membranes were fabricated by Xu et. al, and the circular NbTiN membranes were produced in square variants by Xu et. al too. The specific materials offer great insight into the possibilities, but up until now, we have gained little sense of which system parameters play a crucial role in the responsivity boosts that we found.

We wish to gain some understanding on what material and geometric parameters are crucial in these high aspect ratio nonlinearly strained systems. This might aid future fabrication developments as one could more easily select what material to pick for their membrane. We will stick to the circular NbTiN membrane parameters as a base and explore 5 parameters briefly. These are the membrane radius R, the membrane thickness h, the material Young's modulus E, the material density ρ and the material stress σ, which is closely related to the initial tension n_0 by $n_0 = \sigma h$. We must note that in order for these resonators to keep solely to the softening regime, other nonlinear effects such as the geometric nonlinearity must not become significant. This means the deflection should still be negligible compared to the membrane dimensions.

4.6.1. Radius

In these parameter sweeps, we keep all of the other membrane parameters constant and equal to those given in tables 3.1 and 3.2. Furthermore we use $\eta = 1$ and $V = 0.5$. We will start with the radius R. With the radius, we are mainly interested in whether the extreme aspect ratio of this system is necessary in order to leverage our responsivity boosting technique. We know that the aspect ratio is important, but the fabrication of such membranes is difficult, and a reduction in radius with considerable boosts would be highly desirable. We therefore look at two other situations in which $R = 0.2\,\mathrm{mm}$ and $R = 40\,\mu\mathrm{m}$. We first find the pressures at which these membranes shift $1\,\mathrm{Hz}$ under normal free conditions and determine the responsivity when exposed to the Casimir and electrostatic effect. To keep it brief, we only show the Δf_{res} plots similar to figures 4.6 and 4.8.

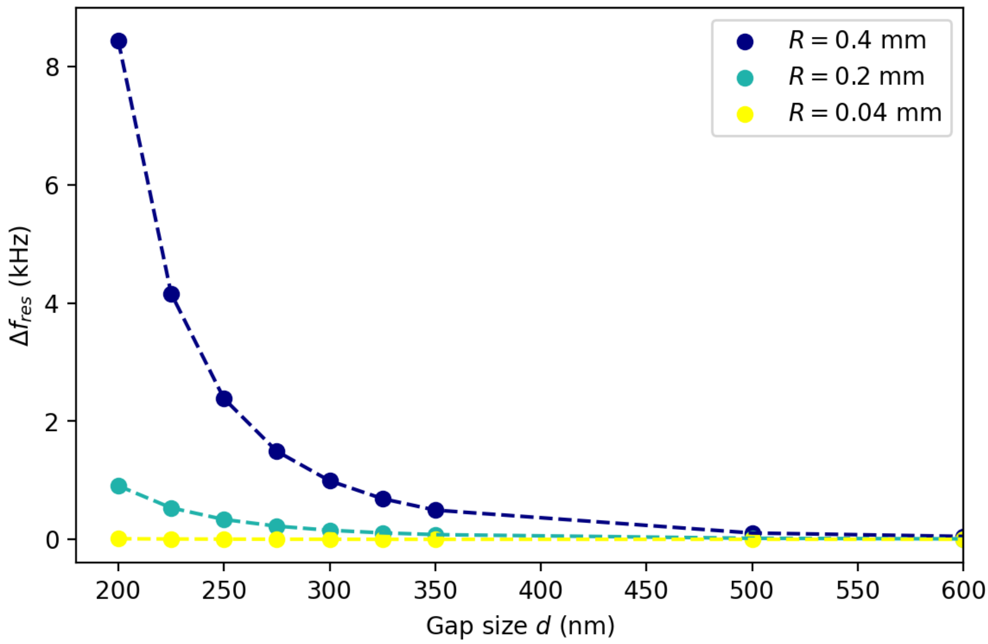

Figure 4.15: Absolute value of the change in eigenfrequency of a circular NbTiN membrane subjected to the Casimir effect for $\eta = 1$ and the electrostatic effect with $V = 0.5$ per gap size d when put under a pressure P_0. The variation in R has a drastic effect on the change in eigenfrequency. The higher values of R show a larger increase in responsivity.

The result is one we could have expected. The material can withstand the forces better the less the big the radius is. A larger membrane is subjected to a larger resultant force, causing it to dip deeper. This deflection is not big enough to increase the geometric nonlinearity notably, but enough to drastically increase the softening effect. The smallest radius shows little to no shift, with a maximum frequency shift of $10\,\mathrm{Hz}$. At this radius size, the geometric nonlinearity is dominant, and the frequency first increases slightly before softening again. This is not visible as the scale of the other graphs washes out this characteristic. The blue navy line shows high values of responsivity increase as it is the biggest radius, which leads to bigger deflections. The material is less able to keep membranes of this size away from the cavity bottom due to the increased forces, which are area-dependent. A more interesting result is seen when the radius is $0.2\,\mathrm{mm}$. The responsivity boost still reaches a thousand Hertz for the lowest gap size. This, paired with the fact that the voltage is low and the fact that the graph is not trending in a vertical direction, means that pull-in is still relatively far away. This means that a higher responsivity boost can be achieved when using higher voltages. These responsivity boosts could then also be worthwhile for gap sizes larger than $200\,\mathrm{nm}$, which would be more easily manageable in terms of engineering.

To examine the role of the radius further, we simulate a $300\,\mathrm{nm}$ gap, $0.5\,\mathrm{V}$ $\eta = 1$ system for 5 different Radii. The responsivity for each radius is shown in figure 4.16

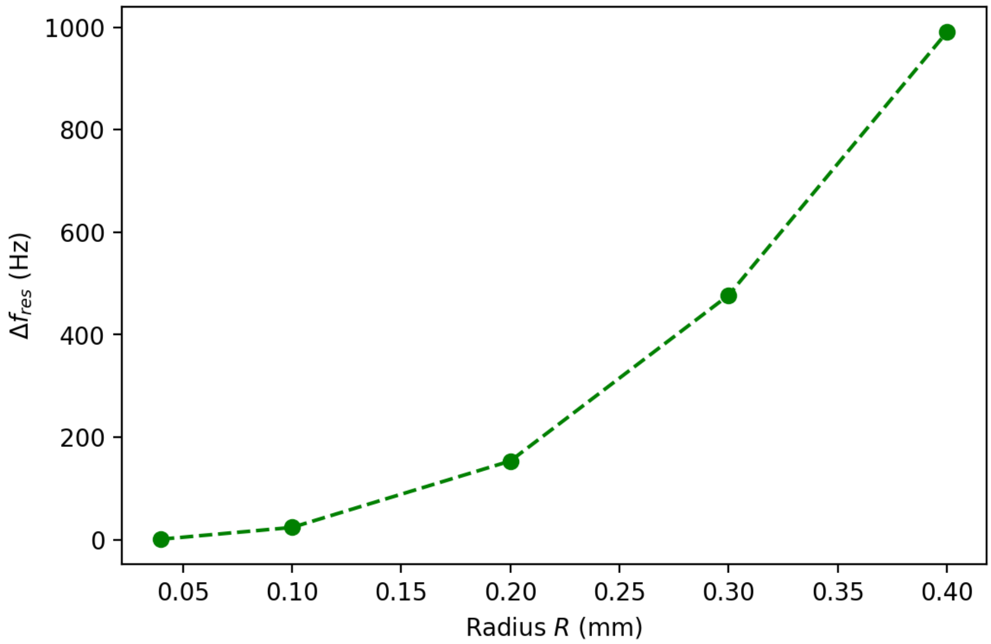

Figure 4.16: Responsivity per radius for a NbTiN membrane above a $300\,\mathrm{nm}$ gap with a voltage of $0.5\,\mathrm{V}$ and $\eta = 1$. A quadratic relationship is seen.

We see a characteristic that one might expect. The force on the membrane is proportional to the area, which is proportional to the radius squared. The bigger the force on the membrane, which itself is bigger too, the larger the deflection will be. This deflection leads to the increased softening effect due to the Casimir and electrostatic forces. The shift grows as a consequence. We therefore see a quadratic relationship which tends to 0 for smaller radii. Note that due to the scale, the radius of $0.04\,\mathrm{mm}$ seems to have reached a value of 0 in its responsivity. This, however, is not the case; it is a mere $1\,\mathrm{Hz}$ which is washed away in comparison to the almost $1000\,\mathrm{Hz}$ for the biggest radius.

4.6.2. Thickness

Next, we look into the role of the membrane thickness. With the radius restored to $0.4\,\mathrm{mm}$ we vary the thickness, testing a thinner membrane $h = 100\,\mathrm{nm}$ and a thicker one $h = 220\,\mathrm{nm}$. Thinner membranes offer less restoring force than thicker ones, as the decrease in material leads to the membrane coping with transverse forces less well. We can therefore expect larger responsivity boosts as the deflections will grow larger, but these will be accompanied by a quicker pull-in occurrence. We see our expectations confirmed in figure 4.17

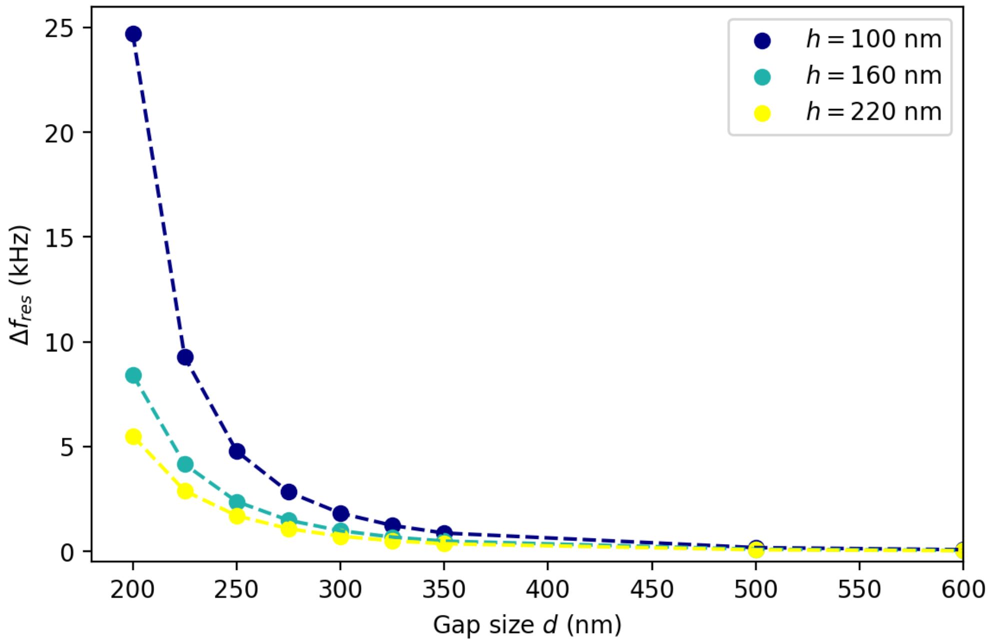

Figure 4.17: Absolute value of the change in eigenfrequency of a circular NbTiN membrane subjected to the Casimir effect for $\eta = 1$ and the electrostatic effect with $V = 0.5$ per gap size d when put under a pressure P_0. The variation in h has a drastic effect on the change in eigenfrequency. The higher value of h shows a lower increase in responsivity.

The thinner membrane indeed shows the highest responsivity boosts, but is dangerously close to pull-in as the graph jumps from a Δf_{res} of 9500 to almost 25000 within $25\,\mathrm{nm}$, displaying a responsivity of $620\,\mathrm{Hz/nm}$. The thicker membrane shows lower boosts, but they are still notably large as they rise above the 5000s for the smallest gap size. At a gap size of $350\,\mathrm{nm}$, the increase is still on the order of a few hundred. This is a promising result, which shows that thicker materials are not excluded from this technique.

The square SiC resonator we visited earlier on boasted a thickness of $81\,\mathrm{nm}$. This is half the thickness of the original NbTiN membrane, which could explain the surprising increase in responsivity we found in figure 4.10 despite the Casimir effect being reduced. We perform a similar sweep as in figure 4.16 in which we only vary h for a NbTiN membrane above a $300\,\mathrm{nm}$ gap with a voltage of $0.5\,\mathrm{V}$ and the Casimir effect with $\eta = 1$ present.

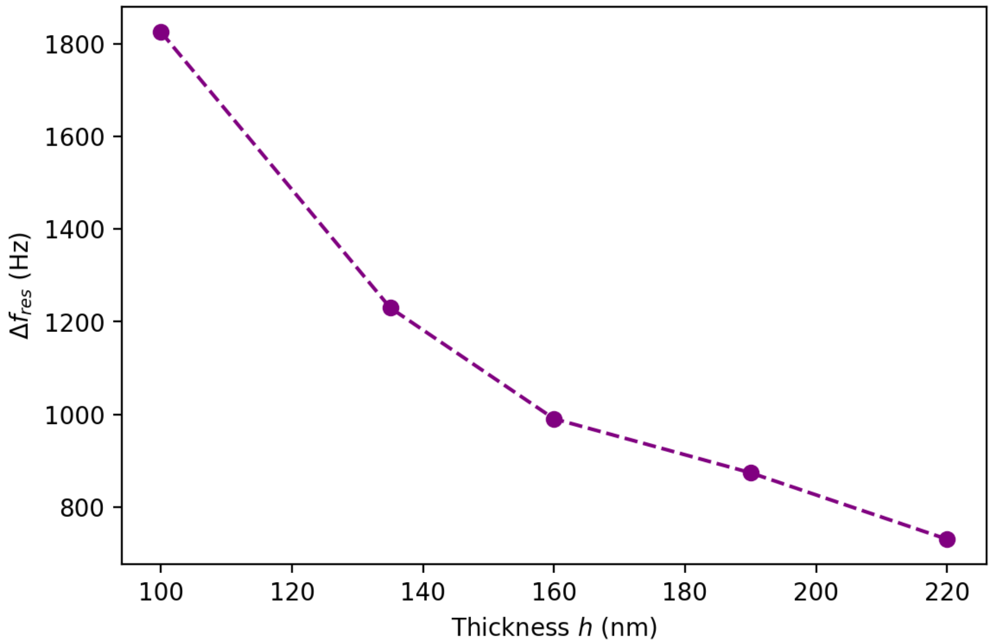

Figure 4.18: Responsivity per thickness for a NbTiN membrane above a $300\,\mathrm{nm}$ gap with a voltage of $0.5\,\mathrm{V}$ and $\eta = 1$. An inverse proportionality to the thickness is seen in the responsivity.

The trend can be understood by looking at the analytical formula we derived for the frequency softening due to nonlinear effects.

$$\omega_{1,1}^2(V,\eta) = \omega_{1,1}^2(0,0)\left(1 - \frac{R^2}{\alpha^2\sigma h}\left(\frac{\varepsilon_0\varepsilon_r}{d^3}V^2 + \eta\frac{\pi^2\hbar c}{60d^5}\right)\right).$$

The difference in the eigenfrequency, or the responsivity, is equal to

$$\frac{R^2}{\alpha^2\sigma h}\left(\frac{\varepsilon_0\varepsilon_r}{d^3}V^2 + \eta\frac{\pi^2\hbar c}{60d^5}\right)$$

which is proportional to the inverse of the thickness. We see this trend in figure 4.18.

4.6.3. Young's Modulus

Leaving the geometric parameters behind, we will now focus on the material parameters instead. We kick off with the Young's modulus, and we will again use a lower value $E = 200\,\mathrm{GPa}$ and a higher value $E = 700\,\mathrm{GPa}$ than the base value of $E = 441\,\mathrm{GPa}$.

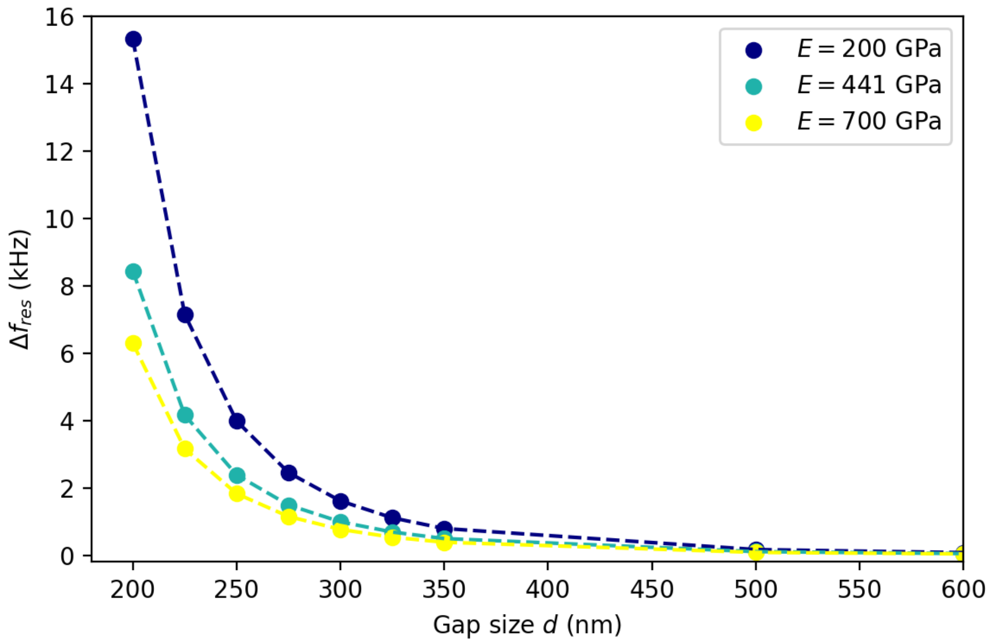

Figure 4.19: Absolute value of the change in eigenfrequency of a circular NbTiN membrane subjected to the Casimir effect for $\eta = 1$ and the electrostatic effect with $V = 0.5$ per gap size d when put under a pressure P_0. The variation in E has a drastic effect on the change in eigenfrequency. The higher value of E shows a lower increase in responsivity.

We see that lower values of E make for a better responsivity boost. The square SiC membrane also boasted a lower value of E compared to the NbTiN membrane, which would have added to the larger responsivity boost in figure 4.10. The lower value of E already achieves boosts in responsivity above 1000 for gap sizes of $350\,\mathrm{nm}$, which is impressive considering the low voltage. The higher value of E does not mean a total reduction of responsivity increase, as we see the boosts rise above a thousand when gap sizes shrink below $275\,\mathrm{nm}$. It seems that, while important, the Young's modulus will not be a limiting factor if one were to design a membrane with this responsivity boosting technique in mind. All three values show high jumps in eigenfrequency for gap sizes that are not unattainable.

Continuing our investigation, we once again research the system previously explored for the geometrical parameters where we only vary the value of the Young's modulus. We know that the Young's modulus is proportional to the inverse of the axial strain of a material. The larger the axial strain, the smaller the modulus becomes. It is therefore no surprise to see a larger responsivity for lower values of the Young's modulus. The lower values mean a larger axial strain, indicating that the membrane is deflected further and thus the effect of the nonlinear attractive forces larger. The increased nonlinear force leads to a bigger frequency softening, and thus a larger responsivity as shown.

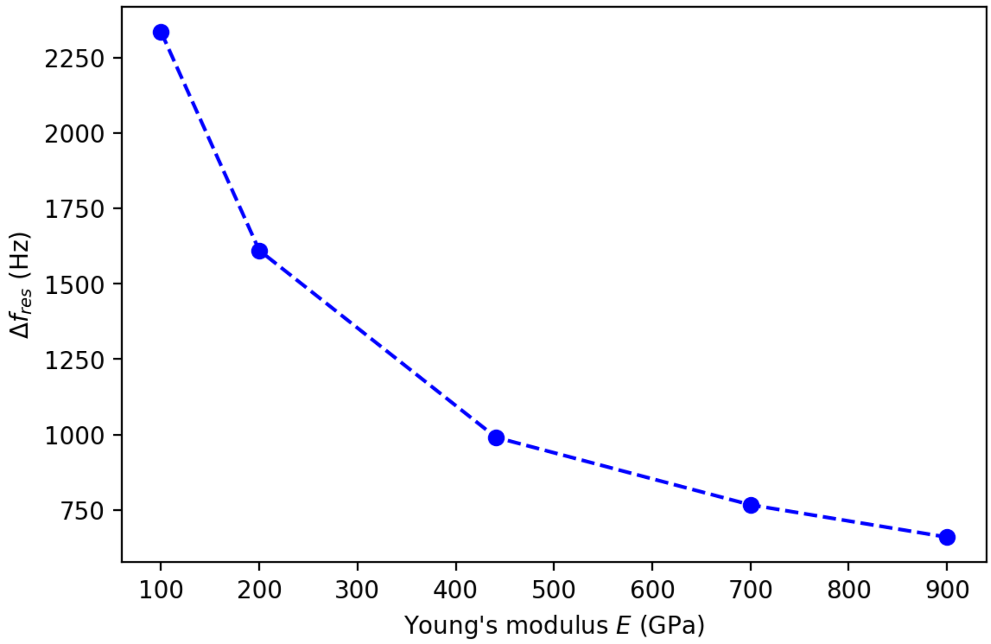

Figure 4.20: Responsivity per Young's modulus for a NbTiN membrane above a $300\,\mathrm{nm}$ gap with a voltage of $0.5\,\mathrm{V}$ and $\eta = 1$. An inverse proportionality to the modulus is seen in the responsivity.

4.6.4. Density

With the role of Young's modulus determined, we find a surprising result in our next endeavour. It is shown in figure 4.21 where we research the role of the density ρ. We again use three values for the density and determine the shift in their eigenfrequencies due to a pressure of P_0 per gap size.

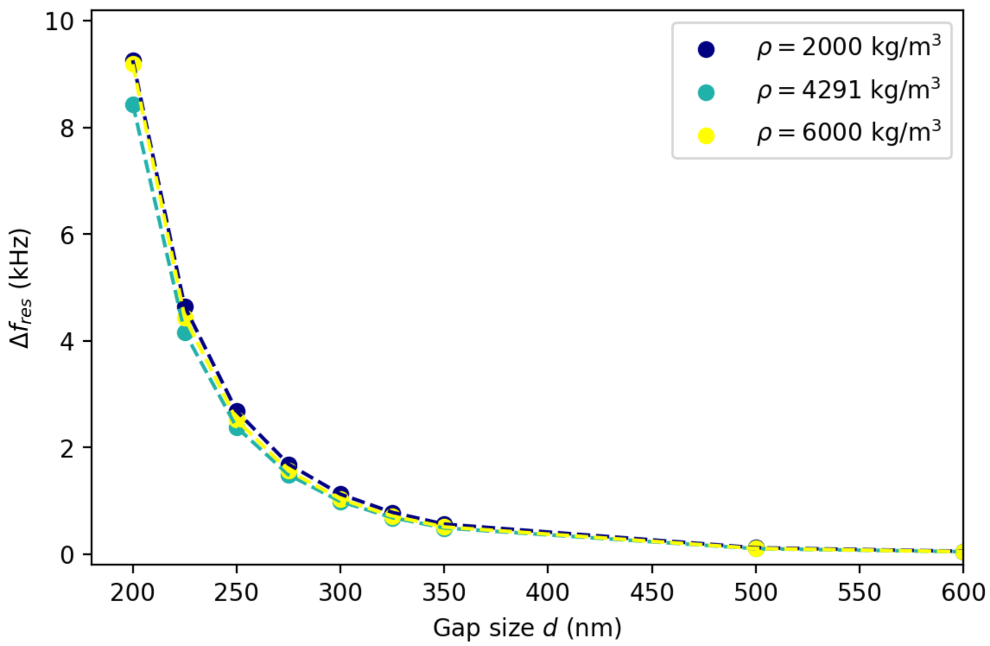

Figure 4.21: Absolute value of the change in eigenfrequency of a circular NbTiN membrane subjected to the Casimir effect for $\eta = 1$ and the electrostatic effect with $V = 0.5$ per gap size d when put under a pressure P_0. The variation in ρ does not affect the change in eigenfrequency.

This result is a strange one indeed, which is not something we suspected beforehand. The value of ρ influences the eigenfrequency directly as it is closely bound to the effective mass of the membrane. For example, the eigenfrequency when the density is equal to $2000\,\mathrm{kg/m^3}$ is equal to $510\,\mathrm{kHz}$ for a gap of $700\,\mathrm{nm}$. This eigenfrequency changes to $293\,\mathrm{kHz}$ when we set the density to $6000\,\mathrm{kg/m^3}$. One would therefore expect the density of the material to be of crucial influence on the responsivity boost. It turns out, however, that the change in the eigenfrequency due to the softening effect is very similar across the three values, with the middle value surprisingly offering the lowest increase by a small margin. If we look back at equation 2.87, we can understand why this result might not be so surprising after all. We see that the decrease in the eigenfrequency is independent of ρ as ρ is a parameter which influences both the eigenfrequency and the softening effect with the same magnitude. We therefore have to conclude that ρ is an unimportant design parameter when looking purely at the responsivity boost.

However, we are again surprised. As shown before in the analysis of the membrane thickness, the inverse proportionality of the responsivity to the thickness can be found when only varying h. We do the same for ρ, whilst looking at our frequency softening formula. The base resonance frequency is proportional to the inverse of the density, but the change should not be. The result is surprising for that reason and not one we have an explanation for.

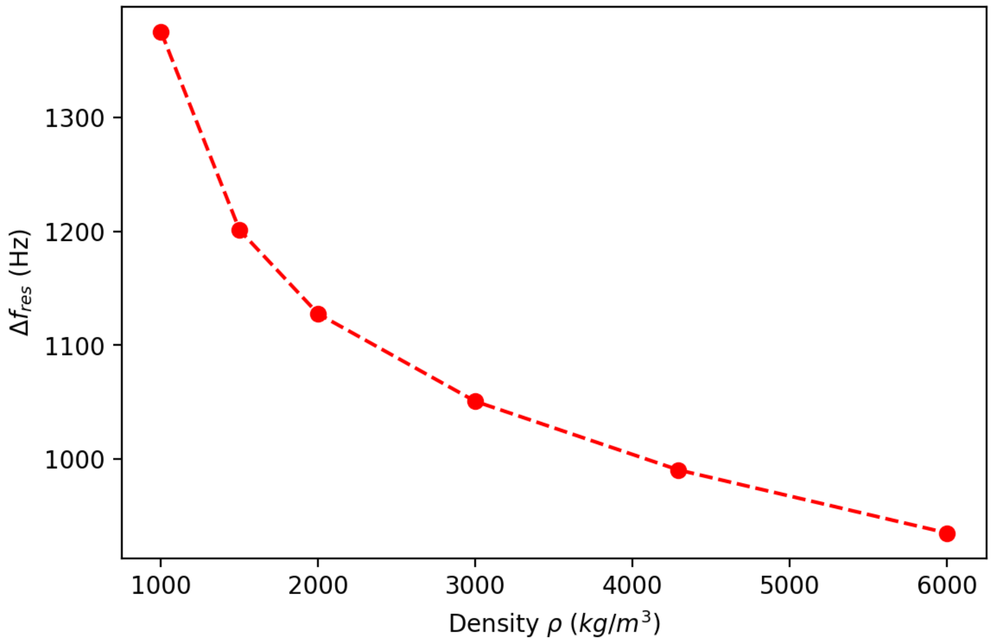

Figure 4.22: Responsivity per density for a NbTiN membrane above a $300\,\mathrm{nm}$ gap with a voltage of $0.5\,\mathrm{V}$ and $\eta = 1$. An inverse proportionality to the density is seen in the responsivity.

We do note that the change in the eigenfrequency for wildly differing densities is quite minimal, but present nonetheless. We can therefore conclude that the responsivity is slightly affected by the density alone and that the earlier results could be explained by the way we have defined our responsivity, as the change due to P_0. This pressure is different for every system, and by coincidence, these values could have overlapped, creating the illusion of a system that is not dependent on ρ.

4.6.5. Pre-stress

We finish our analysis with the material stress σ in figure 4.23. There we see the that for the value of $\sigma = 250\,\mathrm{MPa}$ the onset of pull-in almost occurs at the lowest gap size and is extremely abrupt with an increase in Δf_{res} of 40000 within $25\,\mathrm{nm}$, boasting a record high $1.6\,\mathrm{kHz/nm}$ responsivity. Higher values of stress do not kill the boosting effect straightaway as the $\sigma = 700\,\mathrm{MPa}$ membrane rises above a Δf_{res} of 5000. Lower values of stress make a membrane less stiff and more easily deflectable, which logically increases the responsivity boost, but the pull-in danger seems to be very high here. Lower values of σ thus offer better boosts but suffer from the same issue as thinner membranes, the danger of pull-in. This duality is at the centre of this thesis. Using nonlinear attractive forces is a double-edged sword, offering sensor improvement while at the same time introducing the devices to the dangers of failure. In terms of designing a membrane, a safer bet would probably be a highly stressed membrane which gives more room for error before pull-in destroys the device. The responsivity boosts for these higher values are still respectable.

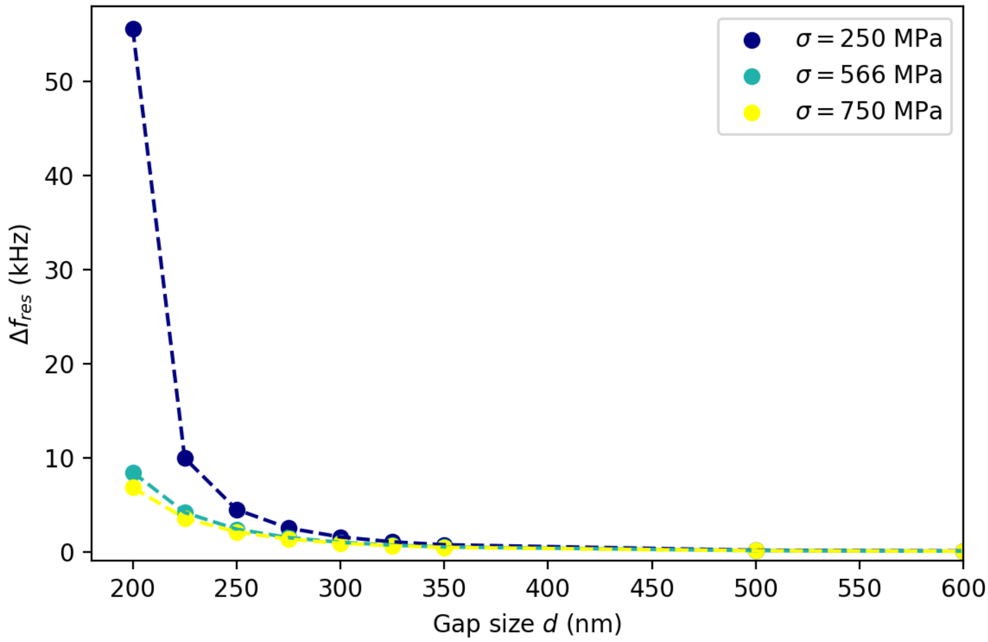

Figure 4.23: Absolute value of the change in eigenfrequency of a circular NbTiN membrane subjected to the Casimir effect for $\eta = 1$ and the electrostatic effect with $V = 0.5$ per gap size d when put under a pressure P_0. The variation in σ has a drastic effect on the change in eigenfrequency when it decreases in magnitude.

Smaller radii, thicker membranes, higher Young's moduli and higher material stresses lead to less of a responsivity increase straightaway, but are interesting avenues to pursue more research. They are further from the pull-in point but still offer notable increases, which can be increased even more with lower gap sizes or higher voltages. Last in line to simulate is once again a sweep of only the value of the pre-stress and the shift in the eigenfrequency as an output.

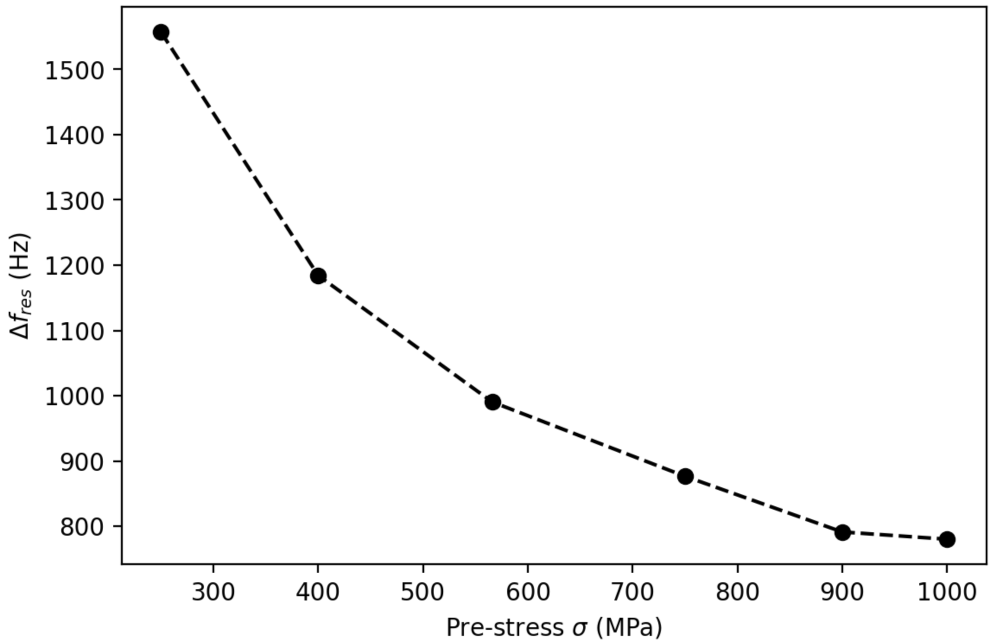

Figure 4.24: Responsivity per value of pres-stress for a NbTiN membrane above a $300\,\mathrm{nm}$ gap with a voltage of $0.5\,\mathrm{V}$ and $\eta = 1$. An inverse proportionality to the stress is seen in the responsivity.

As shown before with the thickness h using the analytical formula for the frequency softening, we expected to see an inverse relationship between the shift and the value of the stress, which is confirmed in figure 4.24.

4.7. Discussion

The principal mechanism behind the responsivity boost lies in the fact that the softening effect can have an unrestricted effect on the resonator, as other nonlinear effects that usually play a role are minimal. Hardening effects, such as the geometrical nonlinear hardening, are of little effect for these huge aspect ratios in which the defections are small compared to the overall membrane sizes. This allows the softening effect to change the eigenfrequency solely, thereby creating the opportunity to use its dramatic effect on the output to our advantage. This responsivity boost is a tunable technique which, in essence, only requires the aspect ratio to be extreme enough. We noted numerous times how these boosts come at a cost, however, namely the danger of device failure due to pull-in and the limitation it has to the dynamic range. Having shown the various instances where the responsivity of the membranes is larger due to the changes in the spring softening, we now briefly discuss the significance of these results. These increases are, first of all, a promising sight. They are possible to realise with a variety of materials and geometries, and forces. The responsivity increase is present for conductors as well as for dielectric-conductor combinations. The technique is possible with a diverse range of geometries and thicknesses, as shown by the impact of some parameter values on the results. One can attain boosts by using the Casimir effect and or the electrostatic effect.. Furthermore, any nonlinear attractive force in principle will do to achieve these boosts, which, as shown, can exceed the state of the art by a significant margin. This makes the technique in principle quite versatile as the only requirements are a high aspect ratio, a nonlinear force, and a stiff membrane.

However, it is necessary to take these results with a pinch of salt. We should realise that we are using an idealised simulation. In our models, be it analytical or FEM, we considered only static loads, no membrane/air damping, a perfect homogenic membrane structure, no charging effects, perfect vacuum and perfect parallelism. Additionally, we did not consider damping created by nonlinear force fields themselves, such as thermoelastic damping [84] or dipole damping due to electrostatics [85]. This does not mean that the results have no significance, but that further research should be conducted into the possible effects of the phenomena we ignored. The boosts presented here should not be seen purely by their numerical values but as a starting point or a possible opportunity to improve resonator operation. The exact magnitude of which shall possibly be decreased by the effects we did not account for.

The extreme aspect ratio sizes do offer limitations in terms of engineering possibilities as they are difficult to fabricate, especially commercially. Furthermore, the possibility of pull-in when subjected to larger forces leading to device failure, makes these sensors relatively fragile compared to those not using nonlinear force fields. The limited range of applicable pressures would make the sensors possibly too fragile for applications such as microphones. Exact estimates on the range of possible pressures depend on the exact parameter values of the system and would have to be determined on a case-by-case basis.

4.7.1. Possible Applications

Despite these considerations, we could imagine using this technique in a variety of different ways. First of all, of course, is the boosting of membrane resonators that are already in existence to enhance their capabilities. This could lead to the sensing of masses or pressures of minimal sizes. For example, in certain areas of fundamental research, the magnitude of the Casimir effect during a superconducting transition is of interest. Sensors to be able to detect these transitions are hypothesised to be able to need to sense pressures on the order of millipascals [86]. Other applications in fundamental research include quantum optomechanics, or microwave resonators in which 2D mechanical resonators have been used [87].

In order to prevent us from covering every type of sensor that our membrane could be, we will highlight two distinct applications instead. The first one is a simple one and it is based on, for example, the results shown in figure 4.23. We see a huge output swing in the resonance frequency due to the softening effect for a lower material stress. One could, in principle, use this as a switch detector. The huge change in the eigenfrequency is dramatic enough to determine a very small change in the value of a system parameter, and it could therefore be useful as such. The resonator could be used as a sensor to detect discrete changes in a system, showing the exact moment when a system parameter steps over a critical value of interest. The sensor would have to operate close to the pull-in point, however.

A second possible application for the membrane resonator would be as a dynamic pressure sensor, such as a microphone. MEMS microphones already utilise 2D flexible membranes to detect sound and are prevalent in modern smartphones. In microphone engineering, the effect mentioned earlier, as squeeze film damping, is present. The air trapped in the cavity damps the movement of the resonator. When the resonator moves due to pressure oscillations, the resonator moves up and down. The air in the cavity between the cavity bottom and the resonator is therefore compressed and extended in an oscillatory fashion. A schematic example of this effect is shown in figures 4.25a and b.

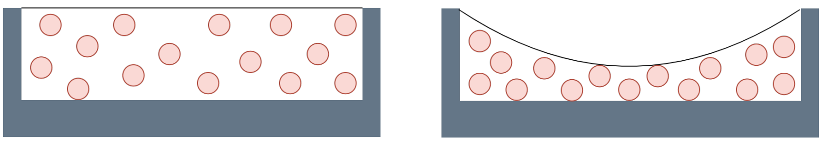

(a) (b)

Figure 4.25: Schematics of the squeeze film effect in a resonator. (a) The membrane is in the equilibrium position, and the air molecules inside the cavity experience the same pressure as the outside atmosphere. If the pressure were different, the membrane would bulge. (b) The membrane oscillates and, when moving downwards, squeezes the air molecules together, creating a damping effect on its motion as the air resists the compression.

The air resists this compression, which leads to the damping of the overall motion of the membrane. The damping, as we saw in the theory, leads to a less pronounced output peak. Engineers try to combat the squeeze film effect by adding perforations to the cavity bottom and the membrane itself. Behind these perforations is a large cavity often called the back cavity [74]. This cavity facilitates the air which is forced out of the cavity through the back plate perforations. The perforations in the membrane itself also facilitate air movement, but one would prefer to keep the perforation count in the membrane to a minimum to keep them from influencing the membrane operation too much. A schematic showing the back cavity is given in figure 4.26.

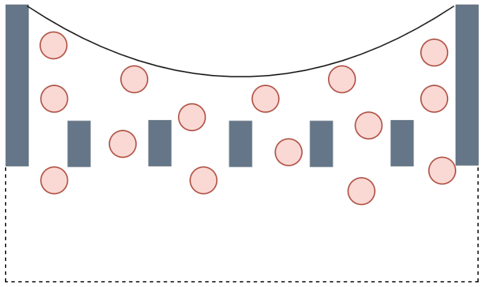

Figure 4.26: Schematic of a MEMS microphone including a back cavity. The back cavity facilitates air movement during operation, which reduces the damping of the membrane significantly.

This technique is successful in reducing the damping, but it does lead to larger microphone structures as the cavity has to be incorporated. This is the point where our discovered responsivity boosting might prove to be a useful addition. Using nonlinear attractive forces for extreme aspect ratio membranes, one could imagine counteracting the damping effect given by squeeze film damping. If those two effects negate each other, then microphones could be produced without the need for back cavities. The microphones would be bigger in the in-plane dimensions, but the out-of-plane dimensions would shrink considerably. Because the amount of voltage one could use is arbitrary, there could also be room for possibly having a tweakable responsivity depending on the voltage input. Do note that the eigenfrequency should not be softened too much, as for microphones in general it is undesirable to have a resonance frequency close to the frequency regime of audible sounds [74].

5 Conclusion

The rapid advancements in technology that have revolutionised human life over the past decades have been possible thanks to devices and sensors that have been created using advanced micro- and nano technologies. However, our imagination causes us to desire smartphones, computers, and technologies that are better, cheaper, and more able than the ones we have right now. This desire to improve is never quenched, and if we wish for our devices to become faster and more compact, then improvements to the next generation of MEMS sensors are mandated. They should become smaller and be able to sense more accurately for the same price.

In this thesis, we set out to investigate a certain type of MEMS sensor, a membrane resonator. These resonators already have widespread applications in technology, but recent advancements in fabrication have enabled them to be fabricated with extreme aspect ratios, where dimensions become smaller than ever before. The introduction of these sensors with unprecedented dimensions brings about new challenges as phenomena such as the Casimir force can play dominant roles in their operation. In order to be able to use these devices effectively, we should therefore understand to what extent they are influenced by these forces. Besides understanding the interplay between the device structure and external forces, we also set out to discover if there were possibilities of exploiting these forces to our advantage.

We started with a broad general coverage on resonators and their defining parameters to get accustomed to them. Shortly afterwards, we diverted our focus to the 2 dimensional membrane resonator kind analytically. We explored the mode shapes in square and circular variations and derived expressions for the defining output characteristic of resonators, their resonance. We introduced the nonlinear attractive forces of our interest and followed up on them by obtaining formulas for their influences on the resonance frequencies of membrane sensors. During this coverage, we found an opportunity to possibly enhance the performance of our sensors by leveraging the nonlinear force field effects. To prove this more concretely, we required more than just analytics, however. To that end, we used our analytics together with experimental data and built, simplified and validated a finite element model in COMSOL, which was able to reproduce real-life experiments. We were then ready to start exploring the possibility of improving extreme aspect ratio membrane resonators with nonlinear force fields. With the finite element COMSOL simulations, we presented a variety of situations in which the responsivity of the membrane resonators was improved. Using a custom definition for the resonator's responsivity, we found that for our NbTiN membrane, the responsivity was boosted up to 280 times for a reduced Casimir effect and up to 570 times when the Casimir was in full force. This boost was even higher for SiC membranes, where the Casimir effect managed a peak of 710 fold the original responsivity. The combination of the Casimir effect and electrostatic voltages proved the highest boosts with a record 14782 fold increase in the responsivity when using a voltage of $1.2\,\mathrm{V}$. The boosts were shown be able to exceed the state of the art by a factor of 6.7 by showing responsivities of $133.2\,\mathrm{kHz/kPa}$ and $37\,360\,\mathrm{kHz}/500\,\mathrm{Pa}$. These increases do not come without cost, however and we presented techniques of predicting the dreaded pull-in effect to define the safe dynamical range, which is drastically reduced when using this technique.

We are therefore ready to return to the research questions that we posed in the introduction of this text. The influence of nonlinear attractive forces on extreme aspect ratio membrane resonators is profound. The extreme aspect ratio allows the nonlinear forces to dominate the resonance frequency of the membranes by softening the membrane stiffness. This effect trumps all other nonlinear force effects, which, due to the extreme aspect ratio, are negligible. The softening effect is potentially harmful as it can cause the membrane to collapse during an event called pull-in when the forces overcome the restoring force of the membrane. However, as we found in the results, there is ample opportunity to use the nonlinear forces to our advantage. Using an electrostatic voltage of $0.15\,\mathrm{V}$, we were able to show a membrane responsivity of $133.2\,\mathrm{kHz/kPa}$. This technique applies not only to conducting surfaces but also to combinations of conductors and dielectrics. We can improve the responsivity of these membranes by allowing the nonlinear forces to be strong enough to pull the membrane down, but not strong enough to destroy it. Within this regime, one can find improved device operation, which can potentially be applied to a variety of resonator sensors.

5.1. Outlook

The idea of boosting the responsivity of membranes by using nonlinear forces such as the Casimir effect is exciting, but at the same time, experimentally unverified. This thesis has concerned itself with simulations and analytical analysis in order to find the scope of the possible improvements. With these new possibilities presented, we would like to finish with recommendations for future research. As eluded to before, the biggest challenge, in our opinion, lies in the implementation in experimental setups. Stepping out of the idealised simulations will always prove a challenge, there are four main directions in which future research may go. These may be pursued after a first and foremost step has been taken, a measurement showing the immense responsivity swings due to a nonlinear attractive field. This measurement should stay as close to the simulation as possible, meaning extremely parallel, vacuum and superconducting in order to facilitate excellent electromagnetic reflections. With this measurement confirming results projected by the simulation, one may proceed in a number of ways and move from the idealised situation.

An important research step would be to confirm the dependence of the Casimir effect on the conductors and to determine the values given by Serry et. al[36] for the values of η. They present a value of $\eta = 0.5$ for a cavity with only one side layered in conducting material, and $\eta = 1$ when both sides are covered. We have taken this value for granted and played around with its consequences, but a confirmation or determination of the actual values in an experiment would greatly aid in the understanding of the impacts that the Casimir effect could have. Even more interesting would be to see the magnitude of the effect between two dielectrics. We used the value of $\eta = 0.2$ without providing any basis for it to show the possibilities of low η systems, but an experimentally determined value would aid in the applications of the Casimir effect in this responsivity boosting technique, as using superconductive temperatures limits the applications severely.

Another direction which is important in order for this technique to be able to find its way in applications outside of fundamental research is a deep dive into the role of various sources of damping on the responsivity boosts. We mentioned in the applications a possible application for microphones in which the squeeze film effect could be countered using this technique. Before any of this is possible, a full-scale investigation into the damping due to the structure, and especially the air damping in the cavity, should be conducted. If this damping does not completely wash away the results proposed by this boosting technique, then applications outside of vacuum setups would be more likely, even though one could still use it in combination with ventilation holes and back cavities. The follow-up would be actively counteracting damping effects using nonlinear responsivity boosting, in which other nonlinear attractive forces might be tried to determine the broadness of this potential scientific discovery. Various sources of damping in MEMS are the subject of active research into preventing or evading them, and this technique could potentially prove a useful tool.

A third direction would be to research the potential applications of this technique into boosting the sensitivity rather than the responsivity. As mentioned in the beginning of the results, we kept to the responsivity for practical reasons. However, the potential change in sensitivity might be possible with this technique and should be experimentally verified. An improved sensitivity would open up new regimes of force detection which could aid significantly in fundamental research. It would also greatly assist in the general scientific interest of this technique as sensitivity is considered the more valuable parameter of the two for resonators.

A final but definitely not less important research direction lies in the biggest negative of this responsivity boosting technique, the pull-in dangers. The prevention of pull-in is paramount to the exploitation of nonlinear attractive force fields. We provided analysis and a technique which combined analytics with FEM in order to predict the occurrence of pull-in. However, this method takes a long time to complete and research into faster, more automated methods to calculate or predict the pull-in effect and the reduced dynamic range would be highly valuable. Other techniques, such as pull-in reversion, in which membranes are 'unstuck', are at the moment not available but would broaden the applications of this effect to a great extent.

The results in this thesis are thus presented as such to provide a starting point for future research, which could follow a variety of directions. The boost in membrane responsivity proves exciting, nonetheless, despite the worries presented above. We therefore believe and hope that the possible applications to microphones, resonator sensors to sense pressure, humidity, electromagnetic waves, mass, temperature, or other effects are inspiring to an extent that future research will continue to look further into this phenomenon.

References

[1] JC Brice. “Crystals for quartz resonators”. In: *Reviews of modern physics* 57.1 (1985), p. 105.

[2] RJ Alfredson and POAL Davies. “The radiation of sound from an engine exhaust”. In: *Journal of Sound and Vibration* 13.4 (1970), pp. 389–408.

[3] Jiri Marek. “MEMS for automotive and consumer electronics”. In: *2010 IEEE International Solid-State Circuits Conference-(ISSCC)*. IEEE. 2010, pp. 9–17.

[4] Marc Fueldner. “Microphones”. In: *Handbook of silicon based MEMS materials and technologies*. Elsevier, 2020, pp. 937–948.

[5] Hua-Bin Fang et al. “Fabrication and performance of MEMS-based piezoelectric power generator for vibration energy harvesting”. In: *Microelectronics Journal* 37.11 (2006), pp. 1280–1284.

[6] Harrie AC Tilmans, Walter De Raedt, and Eric Beyne. “MEMS for wireless communications:‘from RF-MEMS components to RF-MEMS-SiP’”. In: *Journal of Micromechanics and Microengineering* 13.4 (2003), S139.

[7] Bahram Azizollah Ganji and Mojtaba Shams Nateri. “A high sensitive MEMS capacitive fingerprint sensor using slotted membrane”. In: *Microsystem technologies* 19 (2013), pp. 121–129.

[8] Ruize Xu, Shengli Zhou, and Wen J Li. “MEMS accelerometer based nonspecific-user hand gesture recognition”. In: *IEEE sensors journal* 12.5 (2011), pp. 1166–1173.

[9] Sadhana Tiwari et al. “Zinc oxide nanorods functionalized paper for protein preconcentration in biodiagnostics”. In: *Scientific reports* 7.1 (2017), p. 43905.

[10] HB Peng et al. “Ultrahigh frequency nanotube resonators”. In: *Physical review letters* 97.8 (2006), p. 087203.

[11] Michael Roukes. “Nanoelectromechanical systems face the future”. In: *Physics World* 14.2 (2001), p. 25.

[12] Silvan Schmid, Luis Guillermo Villanueva, and Michael Lee Roukes. *Fundamentals of nanomechanical resonators*. Vol. 49. Springer, 2016.

[13] Ron Lifshitz and Michael C Cross. “Nonlinear dynamics of nanomechanical and micromechanical resonators”. In: *Reviews of nonlinear dynamics and complexity* 1.1 (2008).

[14] Ata Keşkekler. “Nonlinear coupling and dissipation in two-dimensional resonators”. PhD thesis. TU Delft, 2023.

[15] TU Delft. *Classical Mechanics and Special Relativity, Harmonic Oscillator*. `https://qiweb.tudelft.nl/mecharela/harmonic_oscillator/`. Accessed: 23-4-2025.

[16] Zurich Instruments. *Ring-down method for rapid determination of high Q-factor resonators*. `https://www.zhinst.com/ch/en/blogs/ring-down-method-rapid-determination-high-q-factor-resonators`. Accessed: 9-5-2025.

[17] Nils Johan Engelsen, Alberto Beccari, and Tobias Jan Kippenberg. “Ultrahigh-quality-factor micro- and nanomechanical resonators using dissipation dilution”. In: *Nature Nanotechnology* 19.6 (2024), pp. 725–737.

[18] Zhili Hao, Ahmet Erbil, and Farrokh Ayazi. “An analytical model for support loss in micromachined beam resonators with in-plane flexural vibrations”. In: *Sensors and Actuators A: Physical* 109.1-2 (2003), pp. 156–164.

[19] Xinxin Li et al. “Ultrathin single-crystalline-silicon cantilever resonators: Fabrication technology and significant specimen size effect on Young’s modulus”. In: *Applied Physics Letters* 83.15 (2003), pp. 3081–3083.

[20] Abbas Abbaspour-Tamijani, Laurent Dussopt, and Gabriel M Rebeiz. “Miniature and tunable filters using MEMS capacitors”. In: *IEEE Transactions on Microwave Theory and Techniques* 51.7 (2003), pp. 1878–1885.

[21] QP Wang et al. “Design of a novel RF MEMS square resonator”. In: *Microsystem Technologies* 21 (2015), pp. 1805–1810.

[22] Dumitru I Caruntu and Reynaldo Oyervides. “Voltage response of primary resonance of electrostatically actuated MEMS clamped circular plate resonators”. In: *Journal of Computational and nonlinear dynamics* 11.4 (2016), p. 041021.

[23] Gayathri Pillai and Sheng-Shian Li. “Piezoelectric MEMS resonators: A review”. In: *IEEE Sensors Journal* 21.11 (2020), pp. 12589–12605.

[24] Linlin Wang et al. “A review on coupled bulk acoustic wave MEMS resonators”. In: *Sensors* 22.10 (2022), p. 3857.

[25] Reza Abdolvand et al. “Micromachined resonators: A review”. In: *Micromachines* 7.9 (2016), p. 160.

[26] R.J. Dolleman. “Graphene Based Pressure Sensors: Resonant Pressure Transduction Using Atomically Thin Materials”. MA thesis. Technical University, Delft, 2014.

[27] Richard Haberman. *APPLIED PARTIAL DIFFERENTIAL EQUATIONS with Fourier Series and Boundary Value Problems*. 5th ed. Pearson, 2013.

[28] Singiresu S Rao. *Vibration of continuous systems*. John Wiley & Sons, 2019.

[29] Milton Abramowitz and Irene A Stegun. *Handbook of mathematical functions: with formulas, graphs, and mathematical tables*. Vol. 55. Courier Corporation, 1965.

[30] JWS Lord Rayleigh. “The theory of sound”. In: *Aufl. von 1894. Reprint: Dover Publications, New York 1945* (1945).

[31] Hendrik BG Casimir and Dirk Polder. “The influence of retardation on the London-van der Waals forces”. In: *Physical Review* 73.4 (1948), p. 360.

[32] Steven K Lamoreaux. “Demonstration of the Casimir force in the 0.6 to 6 μ m range”. In: *Physical Review Letters* 78.1 (1997), p. 5.

[33] Michael Bordag et al. *Advances in the Casimir effect*. Vol. 145. OUP Oxford, 2009.

[34] Evgenni Mikhailovich Lifshitz, M Hamermesh, et al. “The theory of molecular attractive forces between solids”. In: *Perspectives in theoretical physics*. Elsevier, 1992, pp. 329–349.

[35] Basma Elsaka et al. “Casimir Effect in MEMS: Materials, Geometries, and Metrologies—A Review”. In: *Materials* 17.14 (2024), p. 3393.

[36] F Michael Serry, Dirk Walliser, and G Jordan Maclay. “The role of the Casimir effect in the static deflection and stiction of membrane strips in microelectromechanical systems (MEMS)”. In: *Journal of Applied Physics* 84.5 (1998), pp. 2501–2506.

[37] korkmazgil. “Nonlinear Dynamics of Nanomechanical Drum Resonators due to Casimir Force”. MA thesis. Aalto University, 2024.

[38] César D Fosco, Fernando C Lombardo, and Francisco D Mazzitelli. “Proximity force approximation for the Casimir energy as a derivative expansion”. In: *Physical Review D—Particles, Fields, Gravitation, and Cosmology* 84.10 (2011), p. 105031.

[39] Michael Hartmann, Gert-Ludwig Ingold, and Paulo A Maia Neto. “Plasma versus Drude modeling of the Casimir force: Beyond the proximity force approximation”. In: *Physical Review Letters* 119.4 (2017), p. 043901.

[40] Boris Vladimirovich Derjaguin et al. *Surface forces*. Vol. 1. Springer, 1987.

[41] Vasyl Michael Harik and Li-Shi Luo. *Micromechanics and nanoscale effects: MEMS, multi-scale materials and micro-flows*. Vol. 10. Springer Science & Business Media, 2004.

[42] John A Pelesko and David H Bernstein. *Modeling mems and nems*. CRC press, 2002.

[43] Miko Elwenspoek and Remco J Wiegerink. *Mechanical microsensors*. Springer Science & Business Media, 2001.

[44] Benjamin Reichert and Zoran Ristivojevic. “Analytical results for the capacitance of a circular plate capacitor”. In: *Physical Review Research* 2.1 (2020), p. 013289.

[45] Gustav R Kirchhoff. “Zur theorie des condensators”. In: (1879).

[46] William E Boyce and Richard C DiPrima. *Elementary differential equations*. Vol. 9. Wiley New York, 2009.

[47] Paul CP Chao, CW Chiu, and CY Tsai. “A novel method to predict the pull-in voltage in a closed form for micro-plates actuated by a distributed electrostatic force”. In: *Journal of Micromechanics and microengineering* 16.5 (2006), p. 986.

[48] Chandan Samanta, Nishta Arora, and AK Naik. “Tuning of geometric nonlinearity in ultrathin nanoelectromechanical systems”. In: *Applied Physics Letters* 113.11 (2018).

[49] Danilo Karličić et al. “Nonlocal mass-nanosensor model based on the damped vibration of single-layer graphene sheet influenced by in-plane magnetic field”. In: *International Journal of Mechanical Sciences* 96 (2015), pp. 132–142.

[50] Xingyin Xiong et al. “Using electrostatic spring softening effect to enhance sensitivity of MEMS resonant accelerometers”. In: *IEEE Sensors Journal* 21.5 (2020), pp. 5819–5827.

[51] Yiqiu Zhang et al. “A novel design of a MEMS resonant accelerometer with adjustable sensitivity”. In: *Sensors and Actuators A: Physical* 379 (2024), p. 115859.

[52] Banafsheh Sajadi et al. “Static and dynamic pull-in of electrically actuated circular micro-membranes”. In: *ASME International Mechanical Engineering Congress and Exposition*. Vol. 50541. American Society of Mechanical Engineers. 2016, V04AT05A030.

[53] JA Pelesko and XY Chen. “Electrostatic deflections of circular elastic membranes”. In: *Journal of Electrostatics* 57.1 (2003), pp. 1–12.

[54] Wen Zhang et al. “Pull-In Analysis of the Flat Circular CMUT Cell Featuring Sealed Cavity”. In: *Mathematical Problems in Engineering* 2015.1 (2015), p. 150279.

[55] Maryam Shokravi. “Dynamic pull-in and pull-out analysis of viscoelastic nanoplates under electrostatic and Casimir forces via sinusoidal shear deformation theory”. In: *Microelectronics Reliability* 71 (2017), pp. 17–28.

[56] R Soroush et al. “Investigating the effect of Casimir and van der Waals attractions on the electrostatic pull-in instability of nano-actuators”. In: *Physica scripta* 82.4 (2010), p. 045801.

[57] Xiao Li Jia, Jie Yang, and Sritawat Kitipornchai. “Pull-in instability of geometrically nonlinear micro-switches under electrostatic and Casimir forces”. In: *Acta mechanica* 218.1 (2011), pp. 161–174.

[58] Sazzadur Chowdhury, Majid Ahmadi, and William C Miller. “Nonlinear effects in MEMS capacitive microphone design”. In: *Proceedings International Conference on MEMS, NANO and Smart Systems*. IEEE. 2003, pp. 297–302.

[59] BD Hauer et al. “A general procedure for thermomechanical calibration of nano/micro-mechanical resonators”. In: *Annals of Physics* 339 (2013), pp. 181–207.

[60] Ali Sarafraz et al. “Pressure-induced nonlinear resonance frequency changes for extracting Young’s modulus of nanodrums”. In: *Nonlinear Dynamics* 111.16 (2023), pp. 14751–14761.

[61] Dieter Maier-Schneider, J Maibach, and Ernst Obermeier. “A new analytical solution for the load-deflection of square membranes”. In: *Journal of microelectromechanical systems* 4.4 (1995), pp. 238–241.

[62] Zichao Li et al. “Strain engineering of nonlinear nanoresonators from hardening to softening”. In: *Communications Physics* 7.1 (2024), p. 53.

[63] Peter G Steeneken et al. “Dynamics of 2D material membranes”. In: *2D Materials* 8.4 (2021), p. 042001.

[64] Minxing Xu et al. “Measuring Casimir Force Across a Superconducting Transition”. In: *arXiv preprint arXiv:2504.10579* (2025).

[65] Minxing Xu et al. “High-Strength amorphous silicon carbide for nanomechanics”. In: *Advanced Materials* 36.5 (2024), p. 2306513.

[66] L Zhang et al. “Superconducting properties and chemical composition of NbTiN thin films with different thickness”. In: *Applied Physics Letters* 107.12 (2015).

[67] Anita Lloyd Spetz et al. “High temperature sensors based on metal–insulator–silicon carbide devices”. In: *physica status solidi (a)* 162.1 (1997), pp. 493–511.

[68] Gang Liu, Blair R Tuttle, and Sarit Dhar. “Silicon carbide: A unique platform for metal-oxide-semiconductor physics”. In: *Applied Physics Reviews* 2.2 (2015).

[69] Wen-Teng Chang and Christian Zorman. “Electrical characterization of microelectromechanical silicon carbide resonators”. In: *Sensors* 8.9 (2008), pp. 5759–5774.

[70] S Frederico et al. “Silicon sacrificial layer dry etching (SSLDE) for free-standing RF MEMS architectures”. In: *The Sixteenth Annual International Conference on Micro Electro Mechanical Systems, 2003. MEMS-03 Kyoto. IEEE*. IEEE. 2003, pp. 570–573.

[71] MEMS and Nanotechnology Exchange. *Lift off: Page 1 of 1*. `https://www.mems-exchange.org/catalog/lift_off/`. Accessed: 13-5-2025.

[72] Dejan Davidovikj et al. “Visualizing the motion of graphene nanodrums”. In: *Nano letters* 16.4 (2016), pp. 2768–2773.

[73] Amal Z Hajjaj et al. “Highly tunable electrothermally and electrostatically actuated resonators”. In: *Journal of Microelectromechanical Systems* 25.3 (2016), pp. 440–449.

[74] Mikko Suvanto. “The MEMS microphone book”. In: *MOSOMIC, Kangasala, Finland* 1 (2022), pp. 978–9529456604.

[75] Robin J Dolleman et al. “Amplitude calibration of 2D mechanical resonators by nonlinear optical transduction”. In: *Applied Physics Letters* 111.25 (2017).

[76] Frieder Lucklum, Erwin K Reichel, and Bernhard Jakoby. “Miniature density–viscosity measurement cell utilizing electrodynamic-acoustic resonator sensors”. In: *Sensors and Actuators A: Physical* 172.1 (2011), pp. 75–81.

[77] Patrick A Truitt et al. “Efficient and sensitive capacitive readout of nanomechanical resonator arrays”. In: *Nano letters* 7.1 (2007), pp. 120–126.

[78] Saber Azizi et al. “Tuning the primary resonances of a micro resonator, using piezoelectric actuation”. In: *Nonlinear dynamics* 76 (2014), pp. 839–852.

[79] Ewald Benes et al. “Sensors based on piezoelectric resonators”. In: *Sensors and Actuators A: Physical* 48.1 (1995), pp. 1–21.

[80] Victor Fiore et al. “Storing optical information as a mechanical excitation in a silica optomechanical resonator”. In: *Physical review letters* 107.13 (2011), p. 133601.

[81] Minhang Bao and Heng Yang. “Squeeze film air damping in MEMS”. In: *Sensors and Actuators A: Physical* 136.1 (2007), pp. 3–27.

[82] Chenxi Wei and Yin Zhang. “The ultra-high sensitivity of mass resonator achieved by the beam with variable thickness”. In: *Results in Physics* 49 (2023), p. 106483.

[83] Swapnil More and Akshay Naik. “Graphene resonant pressure sensor with ultrahigh responsivity-range product”. In: *Journal of Micromechanics and Microengineering* 34.7 (2024), p. 075006.

[84] Ardeshir Karami Mohammadi and Nassim Ale Ali. “Effect of high electrostatic actuation on thermoelastic damping in thin rectangular microplate resonators”. In: *Journal of Theoretical and Applied Mechanics* 53.2 (2015), pp. 317–329.

[85] Johannes Rieger et al. “Frequency and Q factor control of nanomechanical resonators”. In: *Applied Physics Letters* 101.10 (2012).

[86] Giuseppe Bimonte. “Casimir effect between superconductors”. In: *Physical Review A* 99.5 (2019), p. 052507.

[87] RW Andrews et al. “Quantum-enabled temporal and spectral mode conversion of microwave signals”. In: *Nature communications* 6.1 (2015), p. 10021.

A

Analytical Model Deviation compared to COMSOL

In figure 3.9, the analytical model for a circular membrane subjected to an electrostatic potential is compared to the results given by COMSOL and experimental results. The results show a promising match, especially between the analytical formula 2.87 and COMSOL. This match is surprising considering we only used the first-order Taylor term when deriving the formula. The calculation of ω_0 is surprisingly accurate when comparing it to the value found by COMSOL, with a deviation of less than 0.3%. However, this match does not hold for eigenfrequencies under larger voltages at which the graph deviates from the results that COMSOL provides, as we show in figure A.1

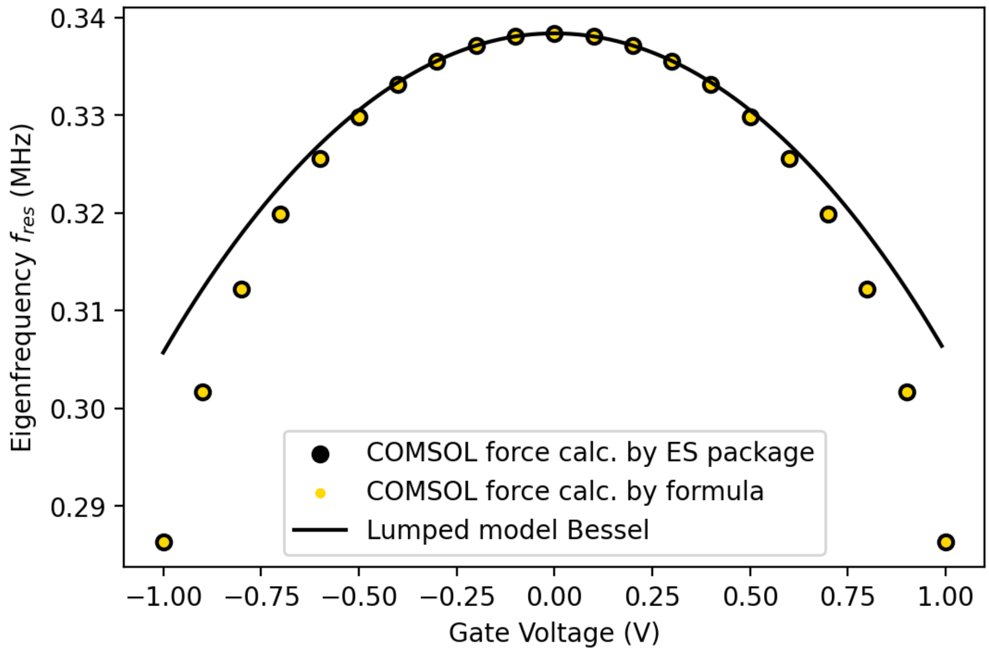

Figure A.1: Comparison of equation 2.87 with our COMSOL model. The COMSOL data of the frequency softening, which was presented in figure 3.8, was used. The models show a good match for lower voltages, however, the analytical model loses its accuracy for larger voltages. Most likely, this is due to the fact that only one Taylor term was used.

The analytical formula loses its accuracy when the voltages grow too large. This is to be expected as we only used the first Taylor term. Its performance is still impressive since we see a reasonable match in the softened frequency up to ± 0.5V. The electrostatic field at a gap distance of $300\,\mathrm{nm}$ at that voltage is 1.66 million V/m strong. The deviation of the analytical formula is probably mainly responsible for the deviations shown in figures 4.14 and 4.13 as it lies at the basis for the pull-in calculations. The analytical calculations for the centre deflections show an underestimation of the actual deflection given by COMSOL, which is comparable to the underestimation of the frequency softening shown in figure A.1.

B

Responsivity Boost of a Reduced Casimir NbTiN Membrane

We present a few more simulations of the frequency softening induced by electrostatic and Casimir forces. These are similar to figures 4.7 and 4.8, but instead of using $\eta = 1$, we use $\eta = 0.5$ to examine the case of only the cavity bottom being layered in a conductive layer. They are presented below.

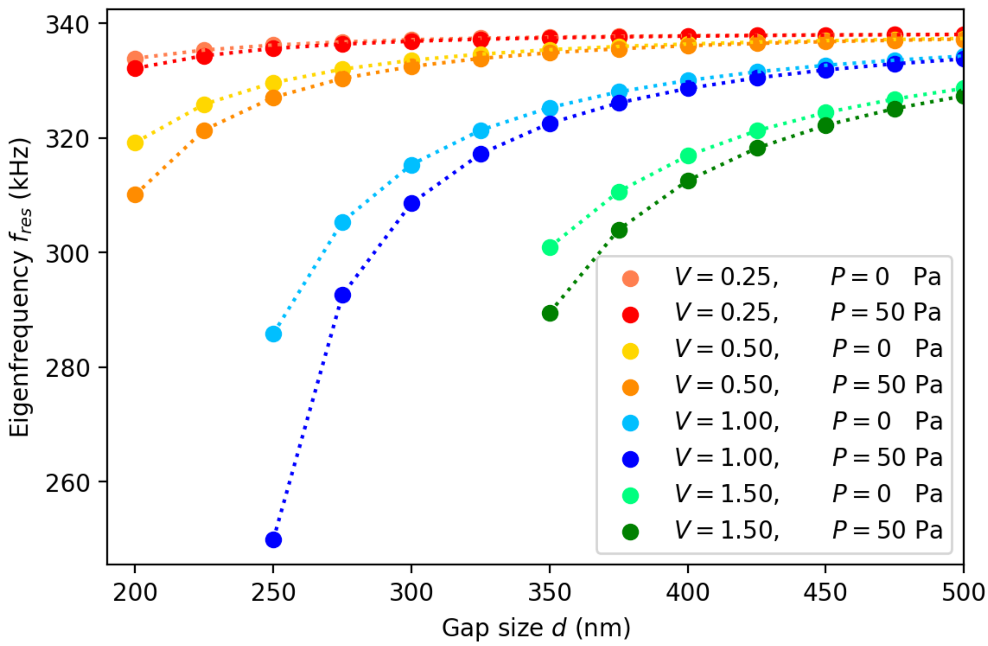

Figure B.1: Eigenfrequencies of a circular NbTiN resonator subjected to the reduced Casimir effect ($\eta = 0.5$) and varying electrostatic potentials. For each case, two simulations, which are grouped by colours, have been performed. One for a static pressure of $P = 0\,\mathrm{Pa}$ and one for $P = P_0 = 50\,\mathrm{Pa}$.The eigenfrequencies are calculated for different gap sizes.

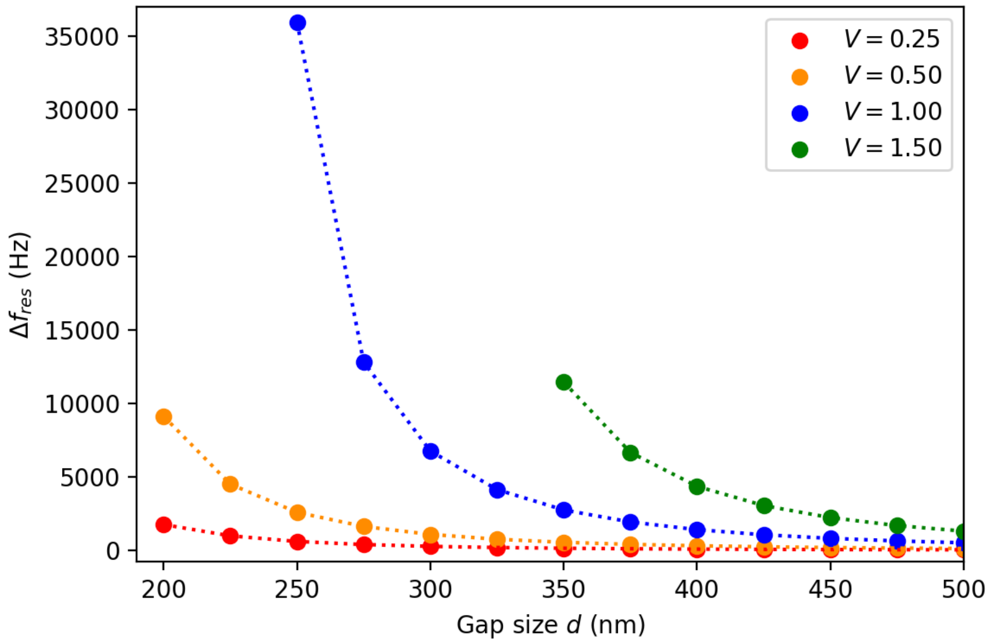

Figure B.2: Absolute value of the change in eigenfrequency of a circular NbTiN membrane subjected to the reduced Casimir effect ($\eta = 0.5$) and varying electric potentials per gap size d when put under a pressure P_0. The higher values of V show a larger increase in responsivity due to the magnitude of the force being larger.

The responsivities are boosted significantly due to the electrostatic voltage, despite the Casimir force being reduced, which is a welcome sight. Boosts of almost ten thousand are seen for relatively low voltages for gap sizes at which the Casimir effect becomes a dangerous pull-in factor. One interesting observation to be made in figure B.2 is the fac that for a voltage of 1 V, the simulation can find eigenfrequencies for gaps of $250\,\mathrm{nm}$, whereas this size was unreachable when $\eta = 1$ in figure 4.8. The reduced Casimir effect is not powerful enough to create a pull-in when it is halved in size for those gap sizes when the voltage is 1. We see that for a voltage of 1.5 V, the graph does not show larger responsivity boosts and only reaches gap sizes of $350\,\mathrm{nm}$. The large voltage, despite the Casimir force being reduced, initiates a pull-in for these gap sizes, which is so abrupt that it is not possible to find eigenfrequencies for smaller gaps such as $325\,\mathrm{nm}$. This is despite the eigenfrequency not being as softened as we have seen before when pull-in occurs. This means that the pull-in effect happens between these gap sizes and happens quickly, as the softening effect will reduce the eigenfrequency to 0 before pull-in happens.

C

Responsivity Boosting of a Fictitious Membrane

We used the material parameters shown in tables 3.1 and 3.2 to simulate our results, which we presented in the results chapter. We even swept some parameters to study their influence on the eigenfrequencies and the responsivity boosts. However, earlier on, before these results were obtained, entirely different material parameters were used to simulate the NbTiN membranes due to a misunderstanding. These parameter values were taken from uncharacterized SiN resonators instead of characterised NbTiN ones. These values are therefore mostly fictitious, and to our knowledge, no material possesses these exact material parameters when used in a thin film configuration. The parameter values that were incorrectly assumed to be those of NbTiN films are given in table C.1.

Table C.1: Incorrect NbTiN film material parameters used in COMSOL to determine responsivity boosts. The parameter values match no other material to our knowledge.

Parameter	Symbol	Unit	Fictitious material
Young's modulus	E	GPa	238
Density	ρ	$\mathrm{kg/m^3}$	6500
Poisson's ratio	ν	-	0.252
Material stress	σ	MPa	800
Thickness	h	nm	150

The truthfulness of these values was discovered only after the simulations had been run and the results had been plotted. We still show them here, as they might prove useful in future research, perhaps when some parameter values of materials match. The case for only the (reduced) Casimir effect and the case for the combined Casimir and electrostatic effects are given. The material parameters were those used for the circular membranes.

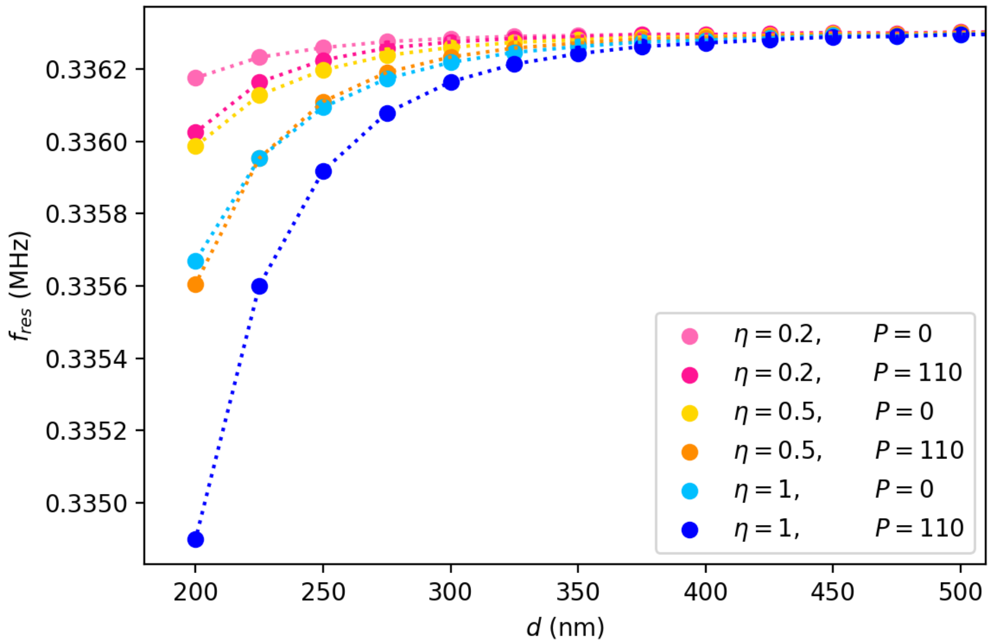

Figure C.1: Eigenfrequencies of a circular resonator using fictitious material values shown in table C.1 subjected to reduced Casimir effects. For each case, two simulations, which are grouped by colours, have been performed. One for a static pressure of $P = 0\,\mathrm{Pa}$ and one for $P = P_0 = 110\,\mathrm{Pa}$.The eigenfrequencies are calculated for different gap sizes.

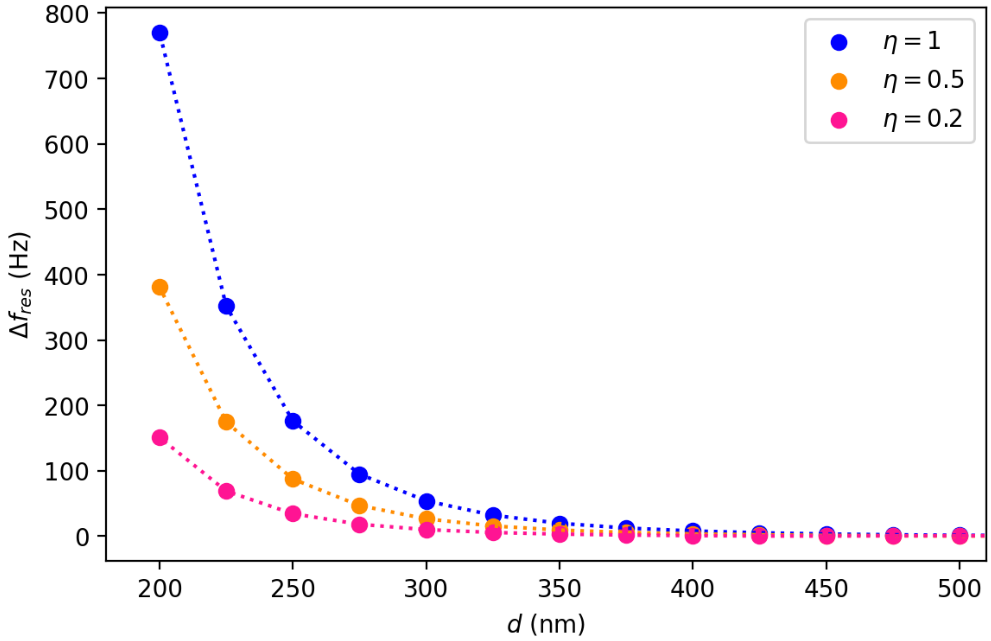

Figure C.2: Absolute value of the change in eigenfrequency of a circular resonator using fictitious material values shown in table C.1 subjected to reduced Casimir effects per gap size d when put under a pressure P_0. The higher values of η show larger increases in responsivity due to the magnitude of the force being larger.

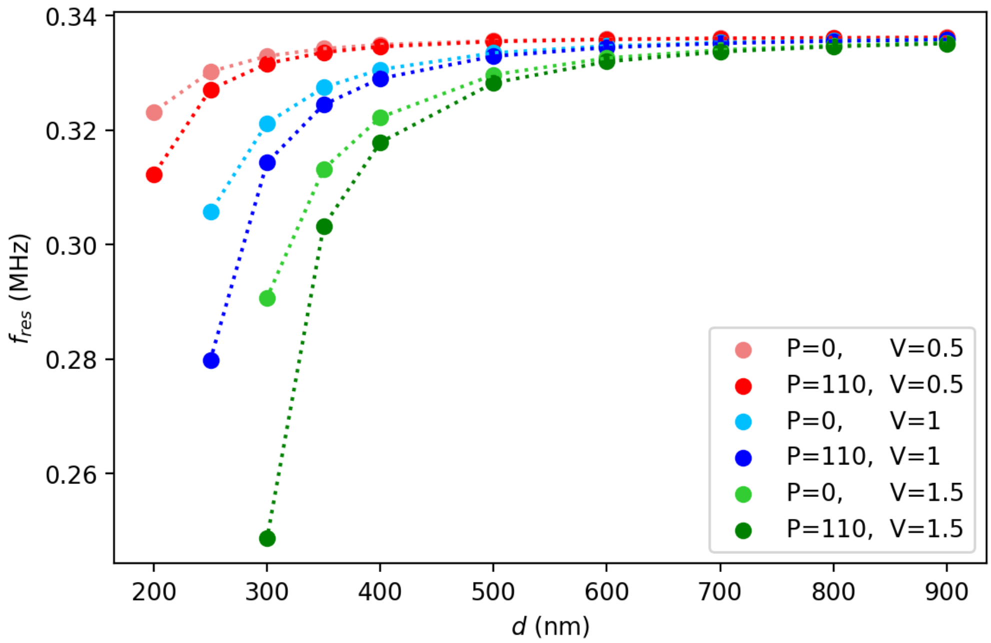

Figure C.3: Eigenfrequencies of a circular resonator using fictitious material values shown in table C.1 subjected to the Casimir effect and varying electrostatic potentials. For each case, two simulations, which are grouped by colours, have been performed. One for a static pressure of $P = 0\,\mathrm{Pa}$ and one for $P = P_0 = 110\,\mathrm{Pa}$.The eigenfrequencies are calculated for different gap sizes.

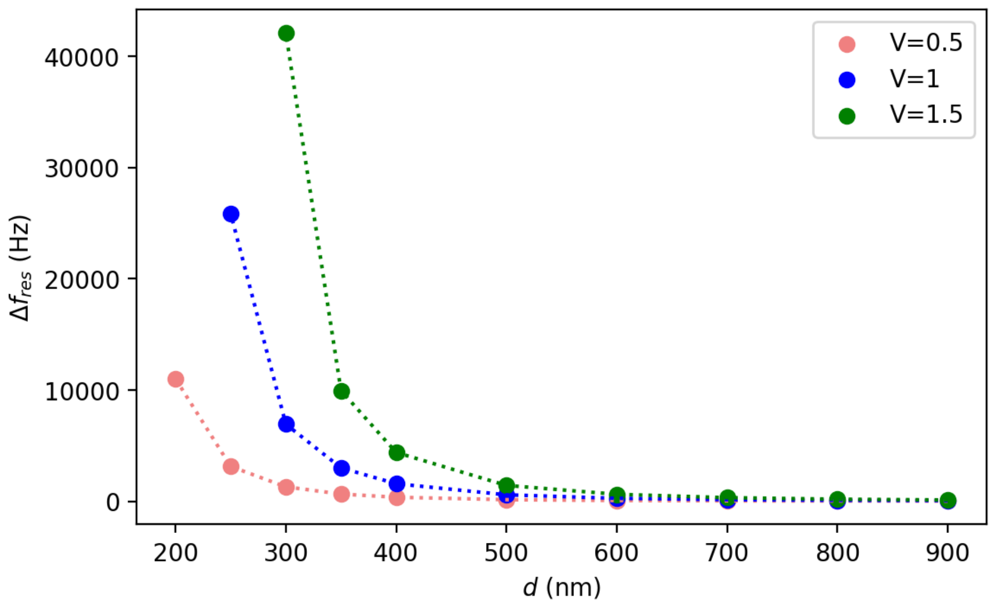

Figure C.4: Absolute value of the change in eigenfrequency of a circular resonator using fictitious material values shown in table C.1 subjected to the Casimir effect and varying electric potentials per gap size d when put under a pressure P_0. The higher values of V show a larger increase in responsivity due to the magnitude of the force being larger.